

¹ Supplementary materials for ‘Canaries of the Arctic: the collapse of
² eastern Bering Sea snow crab’

³

⁴ **Contents**

⁵ Supplementary materials	¹
Methods overview	1
Population dynamics model	1
Survey selectivity	3
Objective function	3
Penalties and priors	4
Population dynamics model sensitivities	4
Does allowing mortality or catchability to vary over time improve model fits?	4
How well can the model estimate mortality and selectivity with simulated data?	5
How do the assumptions about weighting and priors influence the estimated quantities?	6
Covariate construction	6
Temperature	7
Predation	7
Disease	8
Cannibalism	8
Fisheries data	9
Crab density	9
Generalized additive models	9
Sensitivities to model assumptions in GAMs	11
Error structure	11
Does incorporating the uncertainty in the estimates of mortality change model outcomes?	11
Shape of estimated relationships	12
How could temperature relate to mortality mechanistically?	12
A word on methods	14
Frequently asked questions	14
Are you sure the collapse wasn’t a result of cod predation?	14
Are you sure the collapse wasn’t a result of trawling?	15
What do crab eat? If they starved, did there appear to be large declines in their prey base? . .	15

33	If it was a large mortality event, did you see large numbers of empty carapaces in the survey?	15
34	Were that many crab really in the eastern Bering Sea to begin with? Was the ‘collapse’ an	
35	artifact of some survey error?	15

36 Supplementary materials

37 Methods overview

38 We used an integrated population model to estimate variation in mortality over time for snow crab in the
 39 eastern Bering Sea and generalized additive models (GAMs) to relate the estimated variation in mortality
 40 to potential stressors in the environment. The population dynamics model was fit to abundance and size
 41 composition data from the National Marine Fisheries Service (NMFS) summer bottom trawl survey on the
 42 eastern Bering Sea shelf to estimate total mortality by maturity state and year for male snow crab. We
 43 then developed indices for temperature occupied, disease prevalence, cannibalism, and crab density from the
 44 NMFS survey to test as covariates in GAMs. Cod predation indices were developed using stomach content
 45 data collected on NMFS surveys in addition to cod size composition and abundances. Indices for fishery
 46 related effects were collated from fisheries statistics from the Alaska Department of Fish and Game and also
 47 included in the GAMs.

48 Ecological detective work in the marine environment is hampered by the difficulty of observation and this is
 49 particularly so on the eastern Bering Sea shelf. The waters in which snow crab reside range from 50-200 meters
 50 deep and are seasonally covered by ice, making data collection only feasible in the summer. Consequently,
 51 the survey based portions of our analyses are derived from a yearly snapshot of the population over an
 52 approximately 30 year period. Each of the hypotheses explored here clearly result in some mortality. We
 53 know that millions of crab are eaten by cod every year, the directed and bycatch fisheries kill crab, larger
 54 crab eat smaller crab, and crab die from bitter crab disease each year. The goal of our analysis is to place
 55 each of these processes in a historical context to try to understand the relative impact of each and what
 56 was different about the recent collapse. More than one way exists to analyse the available data on this
 57 issue. Below we describe our approach, including a description of each of the components of our analysis,
 58 a discussion of the rationale behind our modeling decisions, and sensitivities and simulation tests of our
 59 models, all of which provide what we think is sound reasoning for our analysis.

60 Population dynamics model

61 The population dynamics model presented here incorporated the best available information on relevant
 62 population processes to estimate total mortality for male snow crab on the eastern Bering Sea shelf and is
 63 similar in structure to the model used to assess eastern Bering Sea snow crab for management (Szuwalski,
 64 2021). The model tracked numbers of male crab at size at maturity state over time with size bins ranging
 65 from 30-95 mm carapace width with 5 mm bin widths. Only male crab were modeled because male and
 66 female crab appear to have somewhat different dynamics and the male crab in the modeled size range are
 67 better selected by the survey gear (Szuwalski, 2021). Snow crab are sexually dimorphic, with male snow crab
 68 growing to nearly twice the size of females, which accounts for the better selection in the survey. Only crab
 69 smaller than 95 mm were modeled for two reasons: 1) to attempt to isolate the effect of the directed fishery
 70 (crabs of >101 mm carapace width are targeted in the fishery; discussed further below) and 2) almost all of
 71 the crab that disappeared since 2018 are in this size range. The population dynamics model operates on a
 72 half year time step, starting in July at the time of the NMFS survey. Total mortality (Z) is estimated by
 73 year (y) and maturity state (m). Other estimated parameters include the initial numbers at size by maturity
 74 state, yearly log recruitments, a vector of scalars that determine the proportions of estimated recruitment
 75 split into the first two size bins, and a variance component for the penalty on total mortality. Parameters
 76 determining growth, maturity, and survey selectivity were estimated outside of the model and specified when
 77 estimating mortality and catchability. Mortality is the only population process that occurs in the first half
 78 of a given year:

$$N_{t=y+0.5,s,m} = N_{t=y,s,m} e^{-Z_{t,s,m}/2} \quad (1)$$

79 Growth occurs at the beginning of the second half of the year for immature crab and is represented in the
 80 model by multiplying the vector of immature crab at size by a size-transition matrix $X_{s,s'}$ that defines the
 81 size to which crab grow given an initial size. Snow crab are observed to undergo a ‘terminal molt’ to maturity
 82 after which growth ceases (Tamone et al., 2005). Accordingly, all immature crab are assumed to molt and no
 83 mature crab molt in our model. The newly molted crab are assigned to a maturity state based on observed
 84 ogives of the proportion of mature new shell males by size calculated from chelae height measured in the
 85 NMFS survey data (Otto, 1998), which varies over time ($\rho_{y,s}$; Figure 5). The average probability of having
 86 undergone terminal molt is used in years during which data were not collected. This process results in two
 87 temporary vectors of numbers at size:

$$n_{t=y+0.5,s,m=1} = \rho_{y,s} X_{s,s'} N_{t=y+0.5,s,m=1} \quad (2)$$

$$n_{t=y+0.5,s,m=2} = (1 - \rho_{y,s}) X_{s,s'} N_{t=y+0.5,s,m=2} \quad (3)$$

89 The size transition matrix $X_{s,s'}$ was constructed using growth increment data collected over several years (see
 90 Szuwalski [2021] for a summary) to estimate a linear relationship between pre- and post-molt carapace width
 91 (Figure 6), ($\hat{W}_{s,w}^{pre}$ and $\hat{W}_{s,w}^{post}$, respectively) and the variability around that relationship was characterized by
 92 a discretized and renormalized normal distribution with a size-varying standard deviation, $Y_{s,w,w'}$ (Figure 6).

$$X_{s,w,w'} = \frac{Y_{s,w,w'}}{\sum_{w'} Y_{s,w,w'}} \quad (4)$$

$$Y_{s,w,w'} = (\Delta_{w,w'})^{\frac{L_{s,w} - (\bar{W}_w - 2.5)}{\beta_s}} \quad (5)$$

$$\hat{L}_{s,w}^{post} = \alpha_s + \beta_{s,1} \text{hat}W_{s,w}^{pre} \quad (6)$$

$$\Delta_{w,w'} = \bar{L}_{w'} + 2.5 - W_w \quad (7)$$

93 It is important to note that crab can ‘outgrow’ this model, which is represented by the pre-molt-carapace
 94 widths (e.g. 87.5 and 92.5 mm carapace width in Figure 6) that have low probability of molting to any of
 95 the sizes that are included in the population dynamics model.
 96 Recruitment by year, τ_y , was estimated as a vector in log space and added to the first two size of classes of
 97 immature crab based on another estimated vector δ_y that determines the proportion allocated to each size
 98 bin.

$$n_{t=y+0.5,s=1,m=1} = n_{t=y+0.5,s,m=1} + \delta_y e_y^\tau \quad (8)$$

$$n_{t=y+0.5,s=2,m=1} = n_{t=y+0.5,s,m=1} + (1 - \delta_y) e_y^\tau \quad (9)$$

100 Finally, the last half of the year of mortality is applied to the population after growth, molting, and recruit-
 101 ment occurs. Note that this allows a crab to experience two different mortalities within a given year as it
 102 undergoes terminal molt.

$$N_{t=y+1,s,m=1} = n_{t=y+0.5,s,m=1} e^{-Z_{t,s,m}/2} \quad (10)$$

$$N_{t=y+1,s,m=2} = (N_{t=y+0.5,s,m=2} + n_{t=y+0.5,s,m=2}) e^{-Z_{t,s,m}/2} \quad (11)$$

104 **Survey selectivity**

105 The observed numbers of crab at size by year in the NMFS survey reflect the ability of the trawl gear to
 106 capture the crab, also known as ‘selectivity’. The selectivity of trawl gear can change according to size, and
 107 consequently needs to be accounted for in the population dynamics model when fitting to the survey data.
 108 Values for survey selectivity at size were specified using data from experimental *Nephrops* trawls (a small
 109 trawl net designed to maintain bottom contact), operated by the Bering Sea Fisheries Research Foundation
 110 in collaboration with the NMFS summer survey. The experimental trawls were performed at the same time
 111 and location as the NMFS summer survey tows to evaluate the efficiency of the NMFS survey trawl gear
 112 at capturing snow crab (Somerton et al., 2013). The *Nephrops* gear used by the BSFRF was assumed to
 113 capture all crab in its path given strong bottom contact. The resulting area-swept estimates of numbers of
 114 crab at size from the BSFRF and NMFS surveys ($\hat{N}_{y,s,NMFS}$ and $\hat{N}_{y,s,BSFRF}$, respectively) can be used to
 115 infer the selectivity of the NMFS gear in year y as:

$$S_{y,NMFS} = \frac{\hat{N}_{y,s,NMFS}}{\hat{N}_{y,s,BSFRF}} \quad (12)$$

116 The experimental trawls captured snow crab in the years 2010, 2011, 2016, 2017, and 2018, but the spatial
 117 foot print and sample sizes varied by year (Figure 7). The calculated selectivities by size and by year were
 118 fairly consistent for snow crab of carapace widths 40 - 95 mm, but the signal was less consistent for crab
 119 larger than ~100 mm carapace width (Figure 8). The selectivity of large crab determines the estimated scale
 120 of the population in a population dynamics model, but the information we have on selectivity of large crab is
 121 poor and different assumptions about selectivity lead to very different inference about the stock (Szuwalski,
 122 2021b). The lack of clear information on the scale of the population exploited by the fishery is one of the
 123 key reasons we used the range of sizes included in this model and excluded the directed fishery data from
 124 the analysis. A GAM was fit through the estimates of selectivity and the resulting estimates by size were
 125 directly specified in the population dynamics model.

126 ‘Catchability’ represents the fraction of the population available to the survey gear (either as a result of
 127 spatial mis-match or the inability of the gear to come in contact with the animals as a result of burrowing
 128 or hiding in untrawlable habitat). The capability for modeling time-varying catchability was built into the
 129 model in the form of a vector of parameters equal to the length of the time series of data. When time-
 130 varying catchability was estimated, the yearly catchability parameters were used to scale the selectivity
 131 curve described above up or down.

132 **Objective function**

133 The objective function for the population dynamics model consists of likelihood components (representing
 134 the fit of the model to the data) and penalty components (which incorporate constraints in the fitting based
 135 on prior information) that are summed and minimized in log space to estimate parameters within the model.
 136 Several data sources were fit to using the following likelihoods. Observed size composition data for immature
 137 and mature males were fit using multinomial likelihoods and were implemented in the form:

$$L_x = \lambda_x \sum_y N_{x,y} \sum_l p_{x,y,l}^{obs} \ln(\hat{p}_{x,y,l} / p_{x,y,l}^{obs}) \quad (13)$$

138 L_x was the likelihood associated with data component x , where λ_x represented an optional additional weight-
 139 ing factor for the likelihood, $N_{x,y}$ was the sample sizes for the likelihood, $p_{x,y,l}^{obs}$ was the observed proportion
 140 in size bin l during year y for data component x , and $\hat{p}_{x,y,l}$ was the predicted proportion in size bin l during
 141 year y for data component x . Sample sizes were input as 50.

142 Observed indices of abundance for immature and mature males were fit with log normal likelihoods imple-
 143 mented in the form:

$$L_x = \lambda_x \sum_y \frac{(\ln(\hat{I}_{x,y}) - \ln(I_{x,y}))^2}{2(\ln(CV_{x,y}^2 + 1))} \quad (14)$$

¹⁴⁴ L_x was the contribution to the objective function of data component x , λ_x was any additional weighting
¹⁴⁵ applied to the component, $\hat{I}_{x,y}$ was the predicted value of quantity I from data component x during year y ,
¹⁴⁶ $I_{x,y}$ was the observed value of quantity I from data component x during year y and $CV_{x,y}$ was the coefficient
¹⁴⁷ of variation for data component x during year y .

¹⁴⁸ Penalties and priors

¹⁴⁹ Smoothing penalties were placed on estimated vectors of deviations for immature and mature natural mor-
¹⁵⁰ tality (and immature and mature catchability in the simulation analyses aimed at understanding the es-
¹⁵¹ timability of mortality and catchability) using normal likelihoods on the second differences of the vectors.
¹⁵² Normal priors were also placed on the mean value of natural mortality and catchability and the deviation
¹⁵³ of the estimated mortality from that mean. A prior value of 0.27 is used for the average natural mortality
¹⁵⁴ based on assumed maximum age of 20 and Hamel's (2015) empirical analysis of life history correlates with
¹⁵⁵ natural mortality. The priors used for catchability were derived from the selectivity experiments described
¹⁵⁶ above. The normal priors were of the form:

$$P_x = \lambda_x \sum_y \frac{((\hat{I}_{x,y}) - (I_{x,y}))^2}{CV_{x,y}^2} \quad (15)$$

¹⁵⁷ P_x was the contribution to the objective function of the penalty associated with model estimate x , λ_x was
¹⁵⁸ any additional weighting applied to the component, $\hat{I}_{x,y}$ was the predicted value of population process I
¹⁵⁹ relevant to penalty x during year y , $I_{x,y}$ was the prior value of process I relevant to penalty x during year y
¹⁶⁰ and $CV_{x,y}$ was the input coefficient of variation for penalty x during year y .

¹⁶¹ An example of the way in which these equations were implemented can be seen in lines 132-218 of
¹⁶² 'snow_down.TPL' in our github repo 'snow_down/models/model_vary_m'.

¹⁶³ Population dynamics model sensitivities

¹⁶⁴ Modeling decisions are necessarily made in the process of writing population dynamics models and it is
¹⁶⁵ possible for these decisions to influence the outcome of an analysis. Within the context of our model, these
¹⁶⁶ decisions include what processes to allow to vary over time, the weights assigned to different data sources
¹⁶⁷ and penalties in the objective function, which parameters to place priors or penalties on, and what those
¹⁶⁸ priors or penalties should be. We ran several sensitivity analyses to understand the implications of these
¹⁶⁹ modeling decisions on the outcome of our analysis.

¹⁷⁰ Does allowing mortality or catchability to vary over time improve model fits?

¹⁷¹ Catchability and mortality are somewhat confounded within population dynamics models (Thompson, 1994).
¹⁷² Fewer crab observed in a given year can be attributed to either crab dying or by crab moving out of the
¹⁷³ surveyed area either by walking out of the boundaries or burying themselves into the substrate. At the same
¹⁷⁴ time, it is also clear that catchability and mortality likely vary over time in reality in spite of the fact that
¹⁷⁵ they are often assumed to be time-invariant in population dynamics models (Johnson et al., 2014). Somerton
¹⁷⁶ et al. (2013) showed that catchability varied somewhat by substrate and depth for snow crab in the EBS.
¹⁷⁷ The spatial distribution of snow crab varies over time and substrate and depth vary over space, so it follows
¹⁷⁸ that catchability should also vary over time.

179 We started exploring the impacts on model output of including time-variation in mortality and catchability
180 by fitting a model with no time-variation in mortality or catchability. Then we compared the output of
181 this model to models that allow time-variation in mortality, catchability, and both processes simultaneously
182 (Figure 9 & Figure 10). The model with no time-variation in mortality or catchability was able to capture the
183 general trend in immature and mature survey abundance solely through estimating variability in recruitment.
184 Allowing time-variation in catchability improved the fits to immature survey abundances more than time-
185 varying mortality, but time-variation in either process improved fits in a similar manner for mature survey
186 abundances. Mature size composition data were fit similarly for all models, but immature size composition
187 data were better fit by the models that allowed time-varying catchability (Figure 9). Part of the reason
188 this difference in fits to immature size composition data occurs is the variability in the first several size bins
189 resulting from the poor selectivity of the survey for small animals. Sometimes the peaks seen in larger size
190 classes are reflected in the preceding years' data for the smallest size classes, sometimes those peaks are not
191 reflected (compare Figure 11 to Figure 12). As a consequence, positive residuals occur in the smallest size
192 classes when a pseudocohort is consistently seen in large size classes, but not observed in the smallest size
193 bins (e.g. 1991 vs. 1992; 1997 vs 1998).

194 The model without time-variation in mortality or catchability explained 67% of the deviation in the abun-
195 dance indices, time-varying mortality explained 77%, time-varying catchability explained 94%, and both
196 processes varying explained 99% of the historical deviance. Model selection based on information criteria
197 (e.g. AIC; Akaike, 1974) are often used to identify a model within a suite of models that most parsimoniously
198 fits the data. Adding time-variation in natural mortality or catchability alone improved model fits parsimo-
199 niuously (AIC of 3434.15 for base model vs. 1593.836 and 1321.486 for time-varying mortality and catchability,
200 respectively). However, adding time-variation in both processes resulted in a higher AIC (1449.275) than
201 implementing time-variation in catchability, owing to the large number of parameters estimated. While
202 catchability and mortality are somewhat confounded, catchability is also confounded with other sorts of
203 error (e.g. observation) and allowing a relatively unconstrained estimation of catchability over time resulted
204 in over-fitting the data, the consequences of which will be seen in simulations below. Even with this paring of
205 potential models, there are several assumptions that could influence the output of our models. The following
206 sensitivities are aimed at exploring the impacts of those assumptions on model output.

207 How well can the model estimate mortality and selectivity with simulated data?

208 One of the most essential exercises to perform with a population dynamics model before using its output is
209 to perform a 'self-test' in which data are simulated from the population dynamics model with appropriate
210 error and then fit to by the model. The goal of this test is to determine whether or not a model can return
211 the parameter values underlying the simulated data with the available quantity and quality of data. For our
212 analysis, the ability of the model to estimate mortality and catchability are of particular interest because
213 they are candidates for use as input into GAMs to attempt to link the estimates to environmental stressors.
214 Recruitment is also of interest because of its confounding with the other processes.

215 Log-normal error was added to the true underlying abundance from the simulation model with three different
216 coefficients of variation: 0.01, 0.10, and 0.30. Simulated data sets were generated 100 times under each
217 observation error scenario and the population dynamics models were fit to them. Two population dynamics
218 models were fit: one in which time-varying natural mortality was estimated and one in which time-varying
219 natural mortality and time-varying catchability were estimated. Estimates of mortality were closer to the
220 true underlying values than estimates of catchability (compare Figure 13 to Figure 14). Mature mortality was
221 better estimated than immature mortality regardless of data quality or model configuration. The correlation
222 between estimated and simulated mortality was 0.65 and 0.96 for immature and mature mortality for the
223 0.01 observation error scenarios, respectively. The ability of the models to estimate mortality became more
224 similar as data quality decreased. Overall, the model was best able to estimate mature mortality and this is
225 likely a consequence of its separation from estimated recruitment in time. In general, estimates of catchability
226 for both maturity states were unreliable.

227 As a result of these simulation analyses, two modeling decisions arose. First, we used estimated variation in
228 mortality from models that only estimate time-variation in mortality because the estimates of mortality from

229 models that estimated time-variation in both mortality and catchability were less reliable. This precludes
230 attempts to identify relationships between estimated catchability and environmental variables. Second, the
231 inability of the model to capture the scale of the population (Figure 15) underscores the need to relate
232 mortality to the environmental covariates outside of the model, rather than attempting to build them into
233 the model (similar to Dorn and Barnes, 2022). The covariates described below are indices of a particular
234 environmental stressor, not absolute quantities that could provide scale to the model.

235 **How do the assumptions about weighting and priors influence the estimated quantities?**

236 Some aspects of the model that may influence the outcome of the fitting are specified by the user with no
237 clear ‘correct’ value. These include the weights assigned to the size composition data, some priors placed
238 on population processes, and the weights assigned to the smoothness penalties. We performed sensitivity
239 analyses for these parameters to check how different specifications changed the fits to the data and the
240 estimates of mortality and catchability. We input a range of values for the size composition weights (25, 50,
241 100), the prior on the mean natural mortality in log space (-1.6, -1.2, -0.8), the input standard deviation for
242 the penalties on natural mortality (0.01, 0.1, 0.2) and the smoothness penalty on the estimated time series’
243 of mortalities and catchabilities (0.001, 0.1, 0.5, 0.1).

244 Differences among sensitivity scenarios resulted in very small changes in the fits to the data (Figure 16), but
245 larger changes in estimated mortalities and catchabilities (Figure 17). The smoothness penalty placed on
246 mortality over time appeared to be the largest driver of changes in estimates of M and q, so we looked at a
247 wider range of smoothness penalties (i.e. 0.001, 0.1, 0.25, 0.5, 1, 5, 10, 1000). Trajectories of mortalities were
248 roughly preserved across this range. The prior on mean natural mortality predictably scaled the estimated
249 time series up or down. The best available information suggests natural mortality should be approximately
250 0.27 given an assumed (but based on a range of studies; see Szuwalski, 2021 for a summary) maximum
251 age of 20 years for wild snow crab. Based on these analyses, we elected to use small smoothing penalties
252 because there is no evidence to suggest that mortality should be particularly smooth from year to year and
253 relatively tight priors on the mean mortality given outside information to support an average mortality value
254 based on longevity. These analyses also underscore the fact that the scale of the population is difficult to
255 estimate with the data available and the need to relate mortality to the environmental covariates outside of
256 the population dynamics model. This likely comes from the fact that recruitment and immature mortality
257 are confounded (i.e. fewer immature crab in a given year can be because of increased immature mortality or
258 because of lower recruitment).

259 **Covariate construction**

260 A wide range of factors could potentially influence mortality of snow crab on the eastern Bering Sea shelf,
261 including temperature, predation, disease, cannibalism, and fisheries effects. The NMFS summer trawl
262 survey provides a rich spatio-temporal data set to develop time series of temperature occupied, predation,
263 disease, and cannibalism (Zacher et al., 2022). The fisheries-dependent observer data provide spatio-temporal
264 information on bycatch (AKFIN, 2022). The main text notes that more than 10 billion crab have gone missing
265 since 2018. This number is derived from the input total numbers observed in the survey to the assessment,
266 which decreased from 11.7 billion animals in 2018 to 940 million animals in 2021. However, this figure does
267 not account for the selectivity of the survey gear and includes both sexes. If survey selectivity is accounted
268 for, the number of missing crab increases dramatically, with the most recent assessment estimating a decline
269 from ~47 billion in 2017 to 2.58 billion in 2022. Regardless of the metric used, the number of crab missing
270 from the Bering Sea survey was exceptionally large.

271 Currently, estimating spatially-explicit, time-varying mortality is not computationally feasible, nor are data
272 on movement available to inform such a model. Consequently, our analysis aggregates the spatial data
273 for snow crab into time-series. The end goal is to use these time-series in predictive models to identify
274 relationships between estimated mortality and stressors, so attention has to be paid to creating appropriate
275 comparisons. For example, a predation index needs to consider not only the total consumption of crab by

276 cod, but also the total number of crab in the ocean of the size that can be consumed by cod to be comparable
277 to changes in estimated mortality rates (discussed more below).

278 Another important point for consideration in covariate construction is the estimation of mortality by maturity
279 state. Snow crab in the EBS undergo an ontogenetic migration in which juvenile crab settle on the northeast
280 portion of the shelf after their pelagic phase, then migrate southwest into deeper and (usually) warmer
281 waters (Ernst et al., 2005; Parada et al., 2010). This means that the conditions and stressors experienced
282 by immature crab can be different than those by mature crab. To address this issue, the spatial data sets
283 for temperature, disease, and cannibalism were split based on the size above which half of the population
284 was mature in a given year. The size at which more than half of the population is mature changes by year,
285 depending on recruitment dynamics and other demographic processes (Figure 18). After the survey data
286 were split at the 50% at maturity size, time series of maturity-specific environmental stressors (Figure 19)
287 were created as described below.

288 Temperature

289 Temperature is one of the key physical variables that structures the benthic ecosystem of the EBS (Mueter
290 and Litzow, 2008). The cold pool, a mass of water <2 degrees Celsius, can act as a barrier to species
291 interaction based on temperature preferences of different species. Snow crab are a stenothermic species,
292 preferring cold water and juvenile snow crab in particular are rarely found outside of the cold pool (Dionne,
293 2003). The cold pool is directly related to the winter ice extent in the Bering Sea and has varied dramatically
294 over time as the ecosystem moves between cool and warm stanzas (e.g. 2006-2010 vs. 2014-2019; Figure 1b
295 of the main text and Figure 20). As the cold pool changes from year to year, so does the spatial distribution
296 of snow crab (Figure 21). The ontogenetic migration of snow crab results in crab of different sizes and
297 maturity states experiencing different temperatures in a given year (Figure 22). The ‘temperature occupied’
298 for different sizes of crab by year $T_{s,y}$ was calculated here as an average of the observed bottom temperatures
299 at the stations at which crab of a given size were captured t_i , weighted by the area-swept density of crab at
300 a given station d_i :

$$T_{s,y} = \frac{\sum_i d_i t_i}{\sum_i d_i} \quad (16)$$

301 The resulting time series of temperatures occupied by size were then split by maturity state by identifying a
302 cutoff beyond which half of the population was mature and aggregating the temperatures above and below
303 the cutoff to represent immature and mature temperature occupied (Figure 23).

304 Predation

305 Pacific cod (*Gadus macrocephalus*) are the most important predator of snow crab based on stomach content
306 data collected in the NMFS bottom trawl survey (Long and Livingston, 1998), with 16.5% of cod stomachs
307 containing snow crab (Burgos et al., 2010). Crab ranging from 8-57 mm carapace width constitute 95% of the
308 crab consumed by cod in the Bering Sea, but crab up to 106 mm carapace have been observed in cod stomachs
309 (Burgos et al., 2010). An index of summer daily consumption (tons/day) of snow crab between 30-95mm
310 carapace width eaten by Pacific cod in the eastern Bering Sea was developed using cod stomach content
311 data from the survey to estimate the proportion by weight of crab in cod diets and the size composition of
312 crab by carapace width of prey found in cod stomachs, stratified by year, survey stratum, and cod length
313 (collection and analysis methods described in Livingston et al. 2017). Cod total consumption rate (metabolic
314 demand) was calculated using a cod bioenergetics model (Holsman and Aydin 2015) to estimate laboratory-
315 measured maximum consumption rates adjusted for bottom water temperatures and cod abundance-at-length
316 measured at each haul location (following methods described in Barbeaux et al. 2020), and summed to an
317 eastern Bering Sea ecosystem-wide total.

318 Changes in the cold pool can alter the interaction between snow crab and Pacific cod over time. Decreases in
319 the size of the cold pool coincide with more northerly positions of the centroids of abundance of cod (e.g. 2003

320 and 2018-2019; Figure 24 & Figure 25). This increased interaction coincided with increased numbers of crab
 321 consumed by cod in the last several years (Figure 4). The estimated number of cod greater than 50 cm was
 322 also near all-time highs around the period during which crab collapsed (Figure 26). However, this period of
 323 time also coincided with the appearance of the largest pseudo-cohort of snow crab ever seen in the Bering
 324 Sea. Given the generalist nature of Pacific cod, one would expect to see an increase in the amount of crab
 325 consumed by cod during this period of time even if there weren't differences in the interactions between
 326 the species as a result of changes in the cold pool or increases in abundance of large cod. To evaluate
 327 the possibility cod consumption has influenced the mortality of snow crab over time, the relative impact
 328 of consumption with respect to the population size must be considered. Predation indices were calculated
 329 for crab by year $P_{m,y}$ by calculating the ratio of the extrapolated biomass of crab consumed by cod to the
 330 estimated biomass of crab, $N_{y,m,s} * w_s$:

$$P_{m,y} = \frac{cod_{y,m}}{\sum_s N_{y,m,s} * w_s} \quad (17)$$

331 The exact amount of crab eaten cannot be calculated from the available diet data because they are a
 332 snapshot of consumption at one point during the year and consumption would be expected to change with
 333 spatial overlap and temperature-driven changes in metabolism occurring throughout the year. Consequently,
 334 removals due to predation cannot be directly incorporated into the model as fishery removals might be. The
 335 index of consumption described above incorporates the most available data on cod predation, but some
 336 strong assumptions are made (e.g. summer diet is representative of the entire year). As a sensitivity to these
 337 assumptions, we also tested the ratio of the number of cod greater than 50 cm to crab abundance in a given
 338 year as an alternative index of predation in the GAMs. Ultimately, changing the index of predation did not
 339 impact the results of the fitting of the GAMs; temperature and mature population size were still the only
 340 significant covariates and the estimated shapes of relationships and deviance explained were very similar
 341 between models with the different predation indices. Consequently, the models presented in the main text
 342 use the index of consumption as the predation index because it uses the most available information on cod
 343 predation (i.e. stomach contents and the abundance and size composition of cod).

344 Disease

345 Bitter crab syndrome is a fatal disease in snow crab caused by a parasitic dinoflagellate (Meyers et al. 1996).
 346 The presence of disease is recorded in the NMFS summer trawl survey data for the subset of crab that are
 347 individually measured based on a visual inspection. Diseased crab are visually detected by a pink-orange
 348 discoloration of the carapace and opaque hemolymph. The spatial distribution of bitter crab disease is
 349 predominantly on the northeastern shelf where smaller immature animals are found (Figure 27). For this
 350 analysis, disease prevalence was calculated simply as the number of infected individuals identified in the
 351 survey divided by the total number of individuals caught in the survey for the respective maturity states
 352 (Figure 19).

353 Cannibalism

354 Cannibalism has been proposed as a potential driver of the dynamics of snow crab in eastern Canada (Lovrich
 355 et al., 1997). In laboratory studies, crab smaller than 55 mm carapace width were at high risk of being
 356 cannibalized when housed with larger crab (Lovrich et al., 1997). Crab larger than 55 mm carapace width
 357 were much less likely to be cannibalized, but the frequency of injury could be high. Here we developed an
 358 index of cannibalism based on two aspects of the spatial distribution of snow crab: the overlap of crab smaller
 359 than 55 mm carapace width with crab larger than 95 mm carapace width (Figure 28) and the density of
 360 crab larger than 95 mm carapace width within the shared space. The proportion of 55 mm carapace width
 361 crab in the overlapping area represents the 'exposure' of the smaller population to cannibalism and the
 362 density of crab larger than 95 mm carapace width within that area represents the potential 'intensity' of
 363 cannibalism in the shared area. We calculated an index of cannibalism over time as the product of exposure
 364 and intensity. Consequently, a scenario in which there was large overlap, but low densities of large crab

would result in a low cannibalism index value. Similarly, a scenario in which there was low overlap, but high densities would result in a low cannibalism index value. This produces an index that is comparable with estimated mortality—a higher cannibalism index would be expected to be associated with higher mortality if cannibalism is a strong driver of mortality in the size ranges of crabs modeled here.

The proportion of smaller than 55 mm carapace width crab overlapping with larger than 95 mm carapace width crab was calculated by finding the intersection of the station IDs at which at least one crab of both size classes was observed. The density of crab larger than 95 mm carapace width was calculated as the number of >95 mm carapace width crab observed at those stations multiplied by the area swept. This exercise was also done by 5 mm size bins to show the overlap of small crab of different sizes with large crab (Figure 29). The final index aggregated all crab smaller than 55 mm carapace width (Figure 30). Indices of cannibalism were only included in the immature models given laboratory observations indicate cannibalism is rare among crab of similar sizes, though molting crab can be vulnerable.

Fisheries data

Snow crab are caught both in a directed fishery (i.e. a fishery aimed at capturing snow crab) and non-directed fisheries (i.e. fisheries with targets other than snow crab). In the directed fishery, under-sized and/or dirty shelled male crab are often discarded and all females are discarded. Snow crab are discarded from non-directed fisheries using a variety of gear types (including trawl, pots, hook-and-line) and targeting a variety of species (e.g. Pacific cod, walleye pollock, and yellowfin sole) that operate over a wide fraction of the Bering Sea shelf (Figure 31). Figure 31 is plotted in log space, so it appears that the bycatch is spread widely over the shelf, but in normal space, the bycatch is more concentrated (e.g. Figure 32). The location of the centroids of the bycatch have moved over time and increases in latitude correspond with warm years in which reduced ice extent allowed for fishing farther north (Figure 33). Bycatch in trawl fisheries are by far the largest sources of bycatch mortality (Figure 34). Data on discards and bycatch of snow crab are collected by at-sea observers on fishing boats and the percent observer coverage ranges from 10% to 100%, depending on the fishery. Some fraction of the mortality imposed by non-directed fleets is likely unobserved due to crab being struck by the gear and not captured. Consequently, indices of the relative mortality imposed by fisheries discards and bycatch were calculated here as the ratio of the observed numbers of crab discarded or bycaught in a given year divided by the estimated population numbers in a given year. Only discard mortality is considered for the directed fishery in our models because the range of sizes modeled exclude the largest males, which are the targets of the commercial fishery for snow crab.

Crab density

The numbers of crab estimated from the population dynamics models were also used as covariates in the GAMs. Changing densities of crab could capture aspects of intraspecific competition not captured in other covariates. Each respective model of mortality incorporates the population size of the corresponding maturity state given their spatial co-occurrence. Immature mortality also incorporates mature population size because crab are thought to move more extensively after maturing in the pursuit of mates, which suggests that their overlap with the immature portion of the population could be larger than the snapshot the survey provides. This increased overlap could result in impacts on mortality, hence the inclusion of mature population size in the immature mortality models.

Generalized additive models

Generalized additive models (GAMs) were used in the R programming language (package mgcv; Wood, 2011) to relate changes in estimated mortality by maturity state and year, $m_{m,y}$, to environmental covariates by maturity state and year, $\phi_{m,y}$, because of their flexibility in fitting potential non-linear relationships. Models were first fitted in which all potential relevant covariates were included in the model of the form:

$$m_{p,y} = s(\phi_{m,y}) + \epsilon_i \quad (18)$$

409 where ‘ $s()$ ’ is a smoothing function based on thin-plate splines, ϕ is a matrix of environmental covariates
 410 scaled to mean 0 and standard deviation 1, and ϵ is normally distributed error. The number of knots allowed
 411 in the thin-plate splines were restricted to 3 given the relatively short time series and number of potential
 412 stressors. Significance of covariates for the full models can be seen in Table 1 and Table 2 and the resulting
 413 smooths in Figure 35 and Figure 36. Model diagnostics were acceptable given relatively short time series
 414 (Figure 37 & Figure 38). Leave-one out cross validation was performed for the models by systematically
 415 excluding a year of data, refitting the model, and recording the deviance explained and significance of the
 416 covariates. The consistent significance of specific covariates in this exercise lends some credence that those
 417 covariates’ influence in the model was not the result of outliers (Figure 2e). Some collinearity existed among
 418 covariates (Figure 39 & Figure 40), but none of the collinear variables were significant in the models.

A. parametric coefficients	Estimate	Std. Error	t-value	p-value
(Intercept)	0.6035	0.0439	13.7531	< 0.0001
B. smooth terms	edf	Ref.df	F-value	p-value
$s(\text{temperature})$	2.0477	2.4391	3.6011	0.0334
$s(\text{disease})$	1.0000	1.0000	0.5203	0.4786
$s(\text{discard})$	1.0000	1.0000	1.6726	0.2100
$s(\text{bycatch})$	1.0000	1.0000	0.9665	0.3367
$s(\text{mat_pop})$	1.8919	1.9799	6.7981	0.0086
$s(\text{predation})$	1.0000	1.0000	2.9442	0.1009

Table 1: GAM output for full model predicting mature mortality. Deviance explained = 72.04 %

A. parametric coefficients	Estimate	Std. Error	t-value	p-value
(Intercept)	0.1719	0.0105	16.4407	< 0.0001
B. smooth terms	edf	Ref.df	F-value	p-value
$s(\text{disease})$	1.0000	1.0000	1.5639	0.2263
$s(\text{temperature})$	1.8837	1.9841	10.7801	0.0006
$s(\text{mat_pop})$	2.0000	2.0000	13.2472	0.0002
$s(\text{imm_pop})$	1.6241	1.8564	1.6100	0.1681
$s(\text{predation})$	1.0000	1.0000	0.1759	0.6796
$s(\text{bycatch})$	1.0000	1.0000	0.0006	0.9808
$s(\text{cannibalism})$	1.7298	1.9252	2.5843	0.1385

Table 2: GAM output for full model predicting immature mortality. Deviance explained = 77.6 %

419 Models that excluded insignificant variables from each full model were used in out-of-sample prediction and
 420 randomization tests (see Table 3 & Table 4 for covariate significance and deviance explained and Figure 41
 421 & Figure 42 for model diagnostics). One thousand iterations of a randomization test were performed in
 422 which the covariate time series were randomized, the models refit, and the deviance explained recorded.
 423 This test was aimed at understanding if the explanatory power of the model was a result of the number of
 424 covariates considered and the flexibility of the model or if the results were an indication of some underlying
 425 signal in the data. If the deviance explained by the model using the non-randomized data exceeded the 95th
 426 quantile of the randomization trials, the deviance explained from the fitted model is less likely to be a result
 427 of over-fitting resulting from too many covariates or too flexible smooths. The deviance explained from both
 428 of the trimmed models exceeded the 95th quantile of deviance explained from the randomization (Figure 43
 429 & Figure 44). Out-of-sample predictions were made by excluding the last 1,2, and 3 years of data, refitting
 430 the model, then attempting to predict the held out data based on the covariates observed in those years (see
 431 figure 2 of the main text for a discussion and Figure 45 for a larger version of figure 2).

A. parametric coefficients	Estimate	Std. Error	t-value	p-value
(Intercept)	0.6035	0.0467	12.9274	< 0.0001
B. smooth terms	edf	Ref.df	F-value	p-value
s(temperature)	1.9300	2.3189	4.6542	0.0183
s(mat_pop)	1.8887	1.9763	7.8385	0.0019

Table 3: GAM output for trimmed model predicting mature mortality. Deviance explained = 62.16 %

A. parametric coefficients	Estimate	Std. Error	t-value	p-value
(Intercept)	0.1719	0.0121	14.1816	< 0.0001
B. smooth terms	edf	Ref.df	F-value	p-value
s(temperature)	1.7797	1.9506	9.5779	0.0006
s(mat_pop)	1.9813	1.9988	7.4968	0.0031

Table 4: GAM output for trimmed model predicting immature mortality. Deviance explained = 59.5 %

432 Sensitivities to model assumptions in GAMs

433 Modeling decisions are also necessarily made in the process of fitting GAMs and it is possible for these
 434 decisions to influence the outcome of an analysis. Within the context of our model, these decisions include
 435 the assumed error structure, the treatment of the uncertainty associated with the estimates of mortality, and
 436 the allowed shape of the smooths estimated in the GAMs. The following sensitivities address the implications
 437 of these modeling decisions on the outcome of our analysis.

438 Error structure

439 Impacts of assumptions about error structure were explored by assuming beta distributed data in the GAM
 440 and transforming the continuous total mortality rates to an exploitation rate ranging from 0 to 1. This
 441 transformation still resulted in mature population and temperature being the most important variables
 442 related to mortality, however the deviance explained decreased to 60% and 68% for mature and immature
 443 mortality, respectively, compared to 72% and 78% for the model presented in the main text. A potential
 444 shortcoming of the method presented in the main text is that predicted mortality could be less than zero.
 445 This was not the case in any of the model fittings, and would present a problem primarily if the model was
 446 extrapolated to data beyond the observed ranges. A potential fix to this issue is to log the response variable,
 447 but this resulted in unacceptable patterns in the residuals, so this model was not used.

448 Does incorporating the uncertainty in the estimates of mortality change model outcomes?

449 The models presented in the main text use the maximum likelihood estimates of mortality from the popu-
 450 lation dynamics models as response variables in the GAMs. However, each of those estimates of mortality
 451 have associated uncertainty estimated in the fitting process. One way of evaluating the impact of incorpo-
 452 rating the estimated uncertainty from the population dynamics model into the GAM fitting process can be
 453 accomplished in 4 steps:

- 454 1. Invert the Hessian matrix produced from fitting the population dynamics model to calculate a covari-
 ance matrix describing the relationships between each of the estimates of mortality,
- 455 2. Simulate time series of the estimated mortality from a multivariate normal distribution with a mean
 of the point estimates of mortality deviations and the product of step 1 as the covariance matrix,
- 456 3. Refit the GAMs to these simulated mortality time series and record the deviance explained and p-values
 for each covariate,
- 457 4. Repeat these steps many times.

461 A similar methodology can be seen in Johnson et al. (2022). Each of these steps were taken in the R
462 programming language. Inverting the Hessian was accomplished by using the function ‘solve()’; simulating a
463 time series of mortality deviations was accomplished using the function ‘mvrnorm()’. The resulting simulated
464 time series of mortality were very similar to the maximum likelihood estimates of mature and immature
465 mortality, reflecting relatively precise estimates of mortality (Figure 46). The deviance explained across
466 simulated time series were also similar to that produced with the MLE time-series of mortality. Temperature
467 and mature population remained the most important variables in predicting mortality across GAMs fitted
468 to simulated time-series of mortality (Figure 47). Given this outcome, the model presented in the main text
469 does not consider the uncertainty associated with treating the estimates of mortality as ‘data’ in the fitting
470 of the GAMs.

471 **Shape of estimated relationships**

472 The model presented in the main text constrains the number of knots available to the GAM to fit the data for
473 each covariate to 3, but the shapes of GAM-estimated smooths are not constrained. This modeling choice was
474 made because it is not immediately clear a priori what the shape of the smooths should be. For example,
475 the relationship between immature population size and immature mortality could conceivably be linear
476 positive (e.g. higher populations result in higher mortality due to intraspecific competition), linear negative
477 (e.g. larger population sizes dilute the impact of external stressors like predation and fishery effects), dome-
478 shaped (somewhat harder to interpret, but perhaps different processes are important at different population
479 sizes), or monotonic in either direction (e.g. population size modulates external stressors to a point, after
480 which other processes are more important).

481 The model in the main text is unconstrained with respect to the shape of the estimated relationships between
482 mortality and covariates. However, the relationship between immature mortality and mature population size
483 was markedly dome-shaped and a satisfying biological explanation for this shape is not immediately apparent.
484 To explore the impacts of unconstrained estimation of this relationship, we refit the models using shape
485 constrained additive models in the R package ‘scam’ (based on Pya and Wood, 2015). This allows the user
486 to specify constraints on the shape of relationships between model variables (e.g. monotonically increasing or
487 decreasing). We refit our model for immature mortality with the assumption that the relationship between
488 immature mortality and mature population size can only be monotonically increasing. The rest of the
489 covariates were specified as linear predictors, except temperature, which remained non-linear. Given the
490 importance of temperature in the hypotheses we present, we were particularly interested to understand how
491 the assumptions about the shape of other significant covariates influence the estimated relationship between
492 temperature and mortality.

493 Temperature and mature population size were still significant covariates within the shape constrained additive
494 model and immature population size became significant (Table 5). The estimated relationship between
495 mortality and temperature was still strongly positive, but became more linear with the shape constraints
496 imposed on mature population size (Figure 48). The relationship between immature population size and
497 immature mortality was negative (i.e. all other things considered, more immature crab were associated with
498 lower mortality). While the immature population relationship is potentially interesting, the most important
499 outcome of this exercise is that temperature still returned positive relationship with estimated mortality.
500 Using temperature as the only covariate in an unconstrained GAM explained 37% and 38% of the deviance
501 in immature and mature mortality (not shown). All of these points suggest temperature is a key covariate
502 in the estimated mortality dynamics for snow crab in the eastern Bering Sea.

503 **How could temperature relate to mortality mechanistically?**

504 Increased temperature was consistently correlated with increased estimated mortality in our models, but the
505 range of temperatures observed were not beyond the thermal tolerances of snow crab. Foyle et al. (1989)
506 captured 20 snow crab of carapace size 85-95 mm in 1986 and raised them in the lab in a range of thermal
507 regimes to understand the impacts of increased temperatures on mortality and caloric requirements for snow
508 crab. In addition to identifying the thermal tolerances of snow crab (crab stop eating around 12 degrees

A. parametric coefficients	Estimate	Std. Error	t-value	p-value
(Intercept)	-0.0325	0.1850	-0.1757	0.8623
disease	0.0236	0.0162	1.4561	0.1607
imm_pop	-0.0374	0.0174	-2.1454	0.0442
predation	0.0002	0.0169	0.0137	0.9892
bycatch	-0.0003	0.0147	-0.0194	0.9847
cannibalism	-0.0090	0.0153	-0.5887	0.5626
B. smooth terms	edf	Ref.df	F-value	p-value
s(temperature)	1.0005	1.0009	6.7766	0.0167
s(mat_pop)	1.7664	2.0738	3.5320	0.0466

Table 5: GAM output for trimmed model predicting immature mortality. Deviance explained = 59.53 %

509 C), Foyle et al. observed a doubling of caloric requirements for snow crab held in 3 degrees Celsius water
 510 as compared to those in 0 degree waters. Here we calculated an index of the caloric requirements for the
 511 modeled fraction of the population of snow crab in the eastern Bering Sea over time using the abundance
 512 at size of snow crab observed in the NMFS survey, the temperature occupied of crab at size calculated from
 513 observations of bottom temperature in the NFMS survey, and the observations of caloric requirements of
 514 snow crab by temperature produced by Foyle et al. (1989). The relationship between temperature and the
 515 caloric requirements of snow crab ($kCal_t$) reported by Foyle et al. was:

$$kCal_{s=90mm,t} = 2.2 * e^{\frac{-(t-5.2)^2}{30.7}} \quad (19)$$

516 Snow crab numbers at size (s) by year (y) ($N_{s,y}$) and the temperature occupied at size by year ($T_{s,y}$) were
 517 calculated as described above. The caloric requirements reported in Foyle et al. were based on observations
 518 of crab that were 85-95 mm carapace width, so these results need to be extrapolated to the range of sizes
 519 used in this analysis. Kleiber's law (Kleiber, 1947) states there is a consistent relationship between the body
 520 mass and metabolic requirements of organisms ($kCal$). The relationship has been generalized as:

$$kCal_m = mass^{0.75} \quad (20)$$

521 Calculating the metabolic requirements for snow crab at size by year, $kCal_{s,y}^{snow}$, can be calculated by
 522 evaluating the caloric requirements of 90mm carapace width crab at a given temperature were calculated,
 523 then scaling that up or down based on Kleiber's law:

$$kCal_{s,y}^{snow} = \frac{2.2 * e^{\frac{-(t-5.2)^2}{30.7}}}{300^{0.75}} w_s^{0.75} \quad (21)$$

524 Caloric requirements increased sharply in 2018 and to explore potential impacts of this increase, we analyzed
 525 the weight at size data available (Figure 49). A GAM was used to predict observed weights at size $w_{i,s,y}$
 526 using the bottom temperature in which the crab was collected, t_i , measured carapace width cw_i , and year
 527 as a factor:

$$w_{i,s,y} = s(cw_i) + s(t_i) + year + \epsilon \quad (22)$$

528 The GAM explained 97.4% of the deviance in the weights of snow crab and all covariates were significant
 529 (Table 6).

530 In general, higher temperatures were associated with higher weight at size (Figure 50). The weight at size
 531 curves for 2015 and 2017 were scaled significantly higher than the base year of 2011, whereas the year 2018
 532 was marginally significantly lower ($p=0.057$). The marginal significance likely resulted from the relatively
 533 small sample size of weight at size available in 2018 ($N=27$), but the effect size was large (the coefficient

A. parametric coefficients	Estimate	Std. Error	t-value	p-value
(Intercept)	218.5199	2.2252	98.2019	< 0.0001
as.factor(AKFIN_SURVEY_YEAR)2015	6.4525	3.1690	2.0361	0.0419
as.factor(AKFIN_SURVEY_YEAR)2017	12.6093	2.4840	5.0763	< 0.0001
as.factor(AKFIN_SURVEY_YEAR)2018	-11.9217	6.2536	-1.9064	0.0568
as.factor(AKFIN_SURVEY_YEAR)2019	4.0886	2.7473	1.4882	0.1369
B. smooth terms	edf	Ref.df	F-value	p-value
s(WIDTH)	6.4225	7.5862	6340.9617	< 0.0001
s(GEAR_TEMPERATURE)	1.9362	2.3359	17.0800	< 0.0001

Table 6: GAM output for model predicting male snow crab weight. Deviance explained = 97.4%

associated with 2017 was 12.60; the coefficient associated with 2018 was -11.92) which translated to large differences in estimated weight at size between the years reported in the main document. Previous studies looking at the impacts of starvation on the weight at size of snow crab (e.g. Hardy et al., 2000) reported small changes in weight at size (roughly 2.6% of weight lost over 5 months), but larger changes in the weight of the hepatopancreas. However, there are some key differences between these studies and the field observations we report. First, the maximum observed mortality was 20% in the starvation studies; the mortality levels estimated in the Bering Sea exceeded 90% in some years. Second, the starvation experiments were in laboratory environments where no foraging occurred. Seventy crab were confined in containers measuring 122 x 183 x 40 cm in Hardy et al. (2000), which greatly restricted movement and would presumably impact caloric expenditure and the initiation of catabolism of muscle tissue.

544 A word on methods

Attribution of changes in population processes in ecology is a difficult problem, particularly for wild populations that are difficult to directly observe and impossible to experiment on in situ. There are a large range of methodologies that claim to identify causality in observational data (structural equation modeling, empirical dynamic modeling, etc.). Some of the difficulties in determining causality in ecological time series are related to the generally short time series that are available, non-linear dynamics, and departures of populations or covariates into unexplored parameter space. These issues can present issues for any modeling framework and we have tried to address these the best of our ability with the models used here. The use of p-values has been (rightfully) criticized in the literature and the explanatory power of our models are likely overstated. Ultimately, the numerous sensitivities and simulation tests performed here were undertaken to try to understand if a suite of covariates appear to be important under different modeling decisions and considerations of uncertainty, in spite of the potential short-comings of the data available and models selected. Temperature and population density proved to be these covariates.

557 Frequently asked questions

558 Are you sure the collapse wasn't a result of cod predation?

The predation index (i.e. the crab consumed by cod divided by the crab available; Figure 19) was near the time series average during the collapse in 2018 and 2019. If predation were a strong driver of the mortality during the collapse, it is difficult to explain why estimated mortality was not high when the predation indices were much higher in the late 1990s and mid-2010s. Furthermore, the distribution of the cod population during 2018 and 2019 extended much farther north, beyond the portion of the snow crab population that is included in this analysis. Movement north can happen in particularly warm years and would serve to reduce the relative predation pressure on the portion of the population of crab in this analysis because the cod that moved north would be consuming crab outside of our study area. Finally, a large fraction of the missing crab from the recent collapse were not of the sizes typically eaten by cod (Figure 51).

568 Although our predation indices incorporate the best available information about cod diet and abundance,
569 these indices are snapshots taken during the summer survey. It is possible that the consumption of crab was
570 different in other times of the year and, if this were true, knowing how predation changed throughout the
571 year could alter our results.

572 **Are you sure the collapse wasn't a result of trawling?**

573 The bycatch index steadily declined since the beginning of our study, with the relative impact of trawling
574 in 2018 and 2019 below the historical average (Figure 19). It is difficult to reconcile the idea that trawling
575 could have contributed to the collapse with the relatively low mortality rates estimated during the periods
576 when the bycatch index was many times higher in the 1990s. Furthermore, if trawling is a large source
577 of mortality for snow crab, it is difficult to understand how the largest pseudocohort ever observed could
578 have established and survived for ~8 years on the Bering Sea shelf, during which the trawling pressure was
579 relatively consistent.

580 However, not all of the mortality associated with non-directed fleets is observed. The index used in this
581 analysis is a reliable indicator of the trend in bycatch mortality provided the ratio of observed to non-
582 observed mortality is consistent over time. If this is not the case, that could change the outcome of our
583 analysis, but there is no clear methodology for determining that ratio.

584 **What do crab eat? If they starved, did there appear to be large declines in their prey base?**

585 Snow crab have a wide-ranging diet of bivalves, polychaetes, crustaceans, and gastropods in the northern
586 Bering Sea (Kolts et al., 2013). They appear to be a generalist, consuming whatever they can capture and
587 crush with their claws. Kolts et al. (2013) reported that most prey items were consumed in proportion to
588 their estimated abundances, except polychaetes, which seemed to be preferentially selected. The prey items
589 are relatively poorly sampled in the Bering Sea survey, so time series of prey quantity are unreliable.

590 Even if there were abundant forage for snow crab in warm years, the metabolic trade-off between the
591 energy required to obtain, handle, and digest their prey and the energy derived from prey would need to be
592 considered when trying to understand if metabolic demands could be met. This would be a useful area of
593 further research, particularly if reliable time series of benthic forage could be started and maintained.

604 **If it was a large mortality event, did you see large numbers of empty carapaces in the survey?**

595 Hundreds of millions of carapaces are discarded by molting crab each year even when there are no mortality
596 events and these are rarely seen in the survey nets. So, even with a massive mortality event, one might not
597 expect to see the carapaces remaining from the event. Why the carapaces are not seen in the survey nets is
598 not completely clear, but potential hypotheses include relatively fast disintegration on the sea floor or poor
599 selectivity by the survey gear. Discarded carapaces may sit flat on the bottom and be passed over by the
600 net.

601 **Were that many crab really in the eastern Bering Sea to begin with? Was the 'collapse' an
602 artifact of some survey error?**

603 The NMFS summer survey was designed to estimate crab abundances (REFERENCE). Snow crab are widely
604 distributed on the shelf and consequently well sampled by the survey. There are 375 survey locations in the
605 NMFS eastern Bering Sea trawl survey, of which 349 are on a 40 square nautical mile grid. The remaining
606 stations are in high density sampling areas around islands in the Bering Sea implemented to better estimate
607 crab abundances around those islands. On average, snow crab are observed at 233 of the 349 survey stations
608 on the standard grid. In 2018 a large number of stations returned estimated high densities of crab (see Fig.
609 1 of main text), which means that the large estimates of abundance in 2018 were not driven by one or two

610 large survey tows. Further, the recent survey methodology has been repeatedly verified as a useful tool for
611 estimating crab abundance (see Somerton et al., 2013, for example).

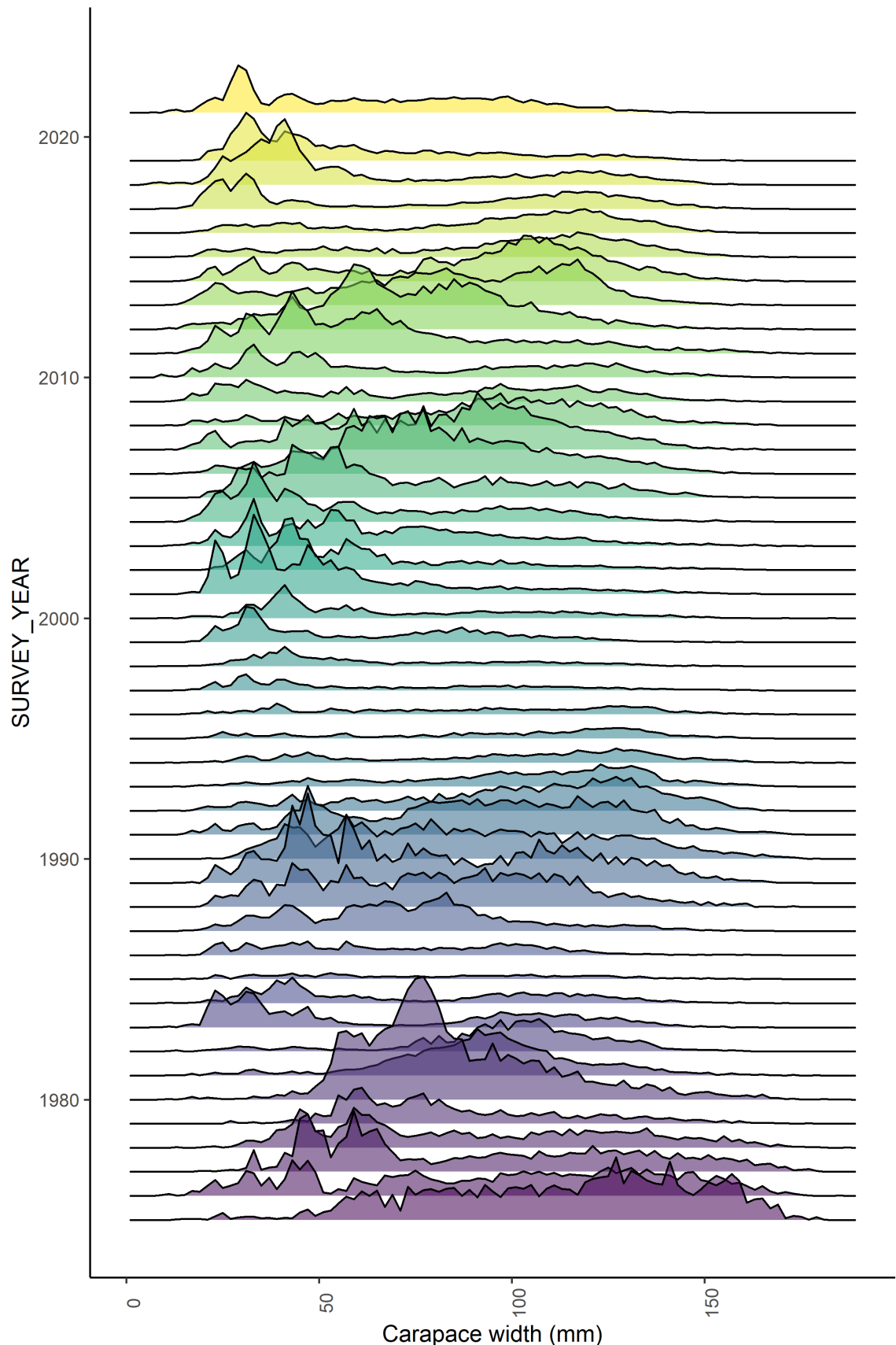


Figure 1: Observed abundance by carapace width of Tanner crab in the NMFS summer survey.



Figure 2: Map of eastern Bering Sea slope habitat (colors). Reproduced from HERE.

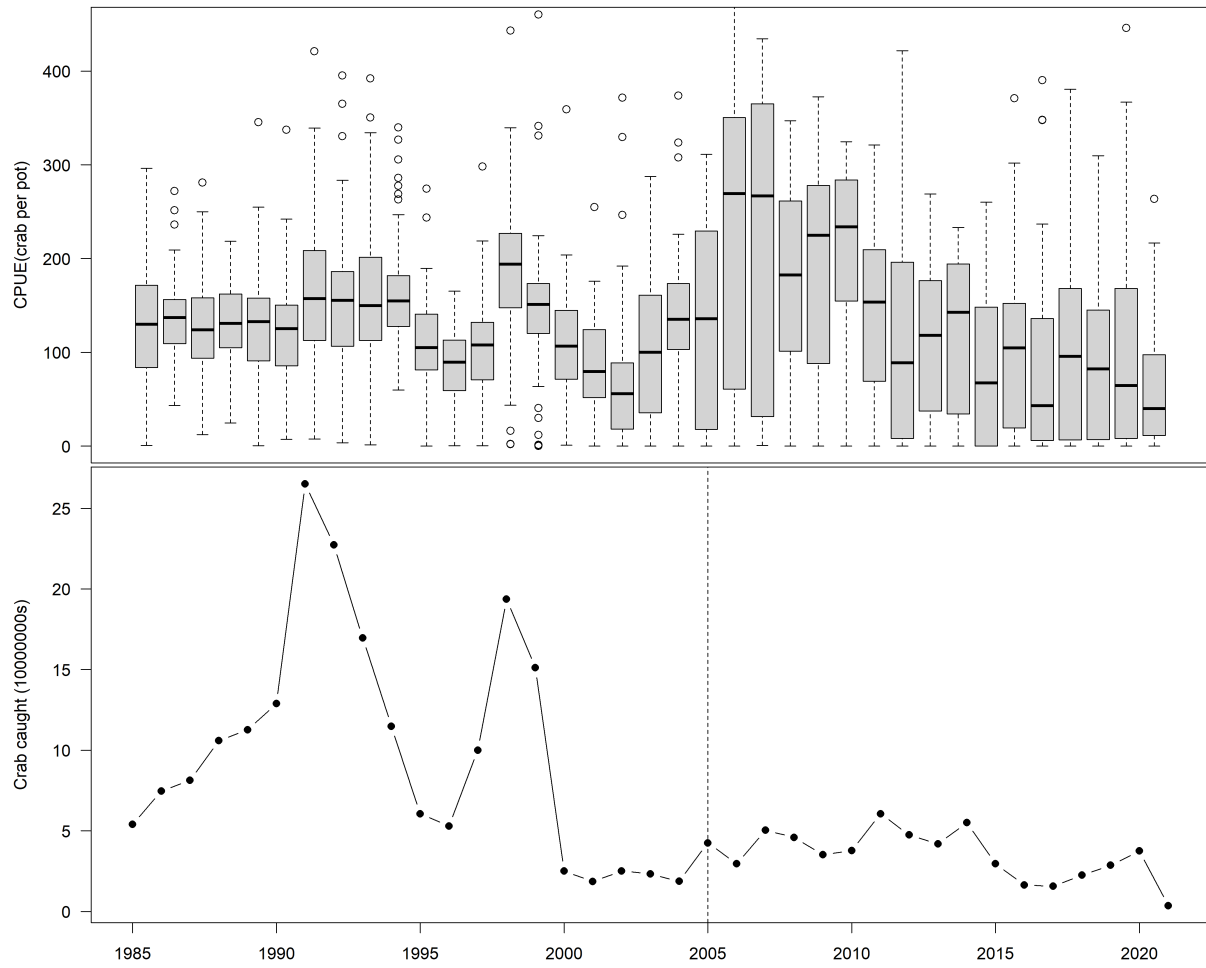


Figure 3: Fishery cpue (top; black lines are median, grey box represents 25-75th quantiles, circles are outliers) and number of crab caught in the directed snow crab fishery (bottom). Vertical dashed line represents the introduction of individual transferrable quota management.

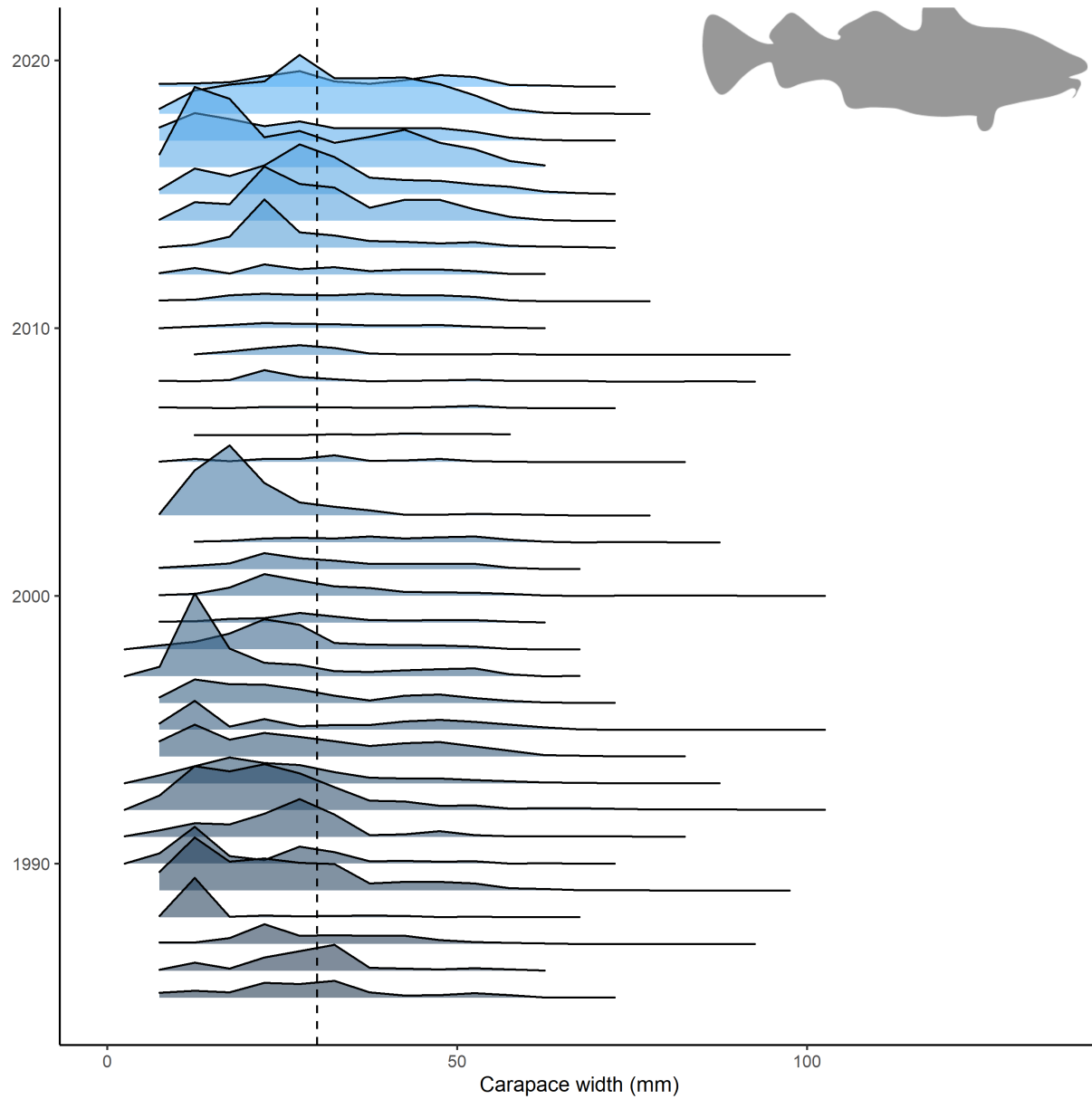


Figure 4: Consumption of crab by Pacific cod at size over time. Dashed line represents the size at which crab enter the population dynamics model presented in the text.

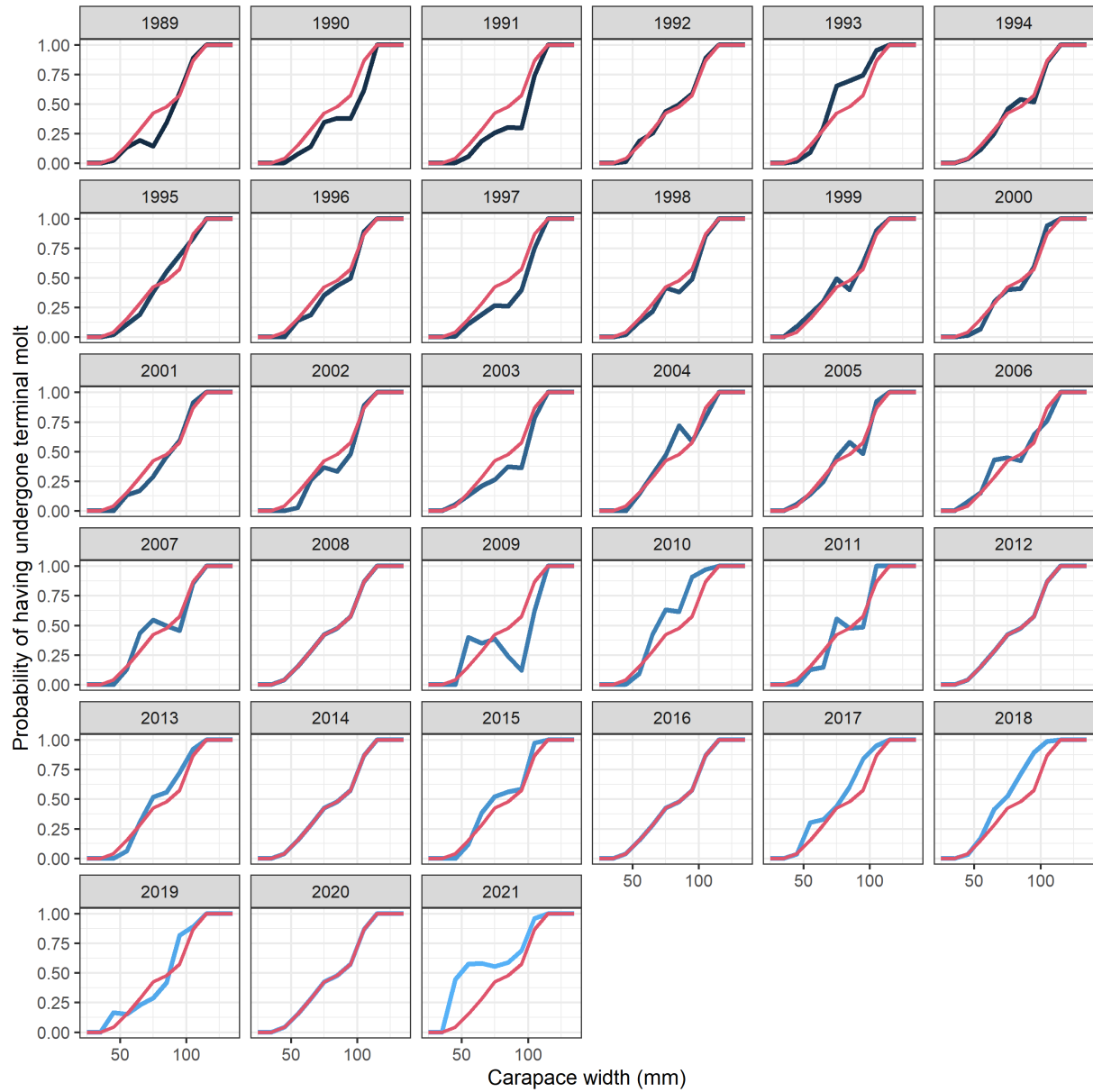


Figure 5: Observed proportion of mature new shell crab in the NMFS summer survey. Red line represents the median over years and the blue lines are the observed data. Chela height data were not collected in years without a blue line. These data are used to separate the numbers at size into mature and immature states for the input data to the population dynamics model.

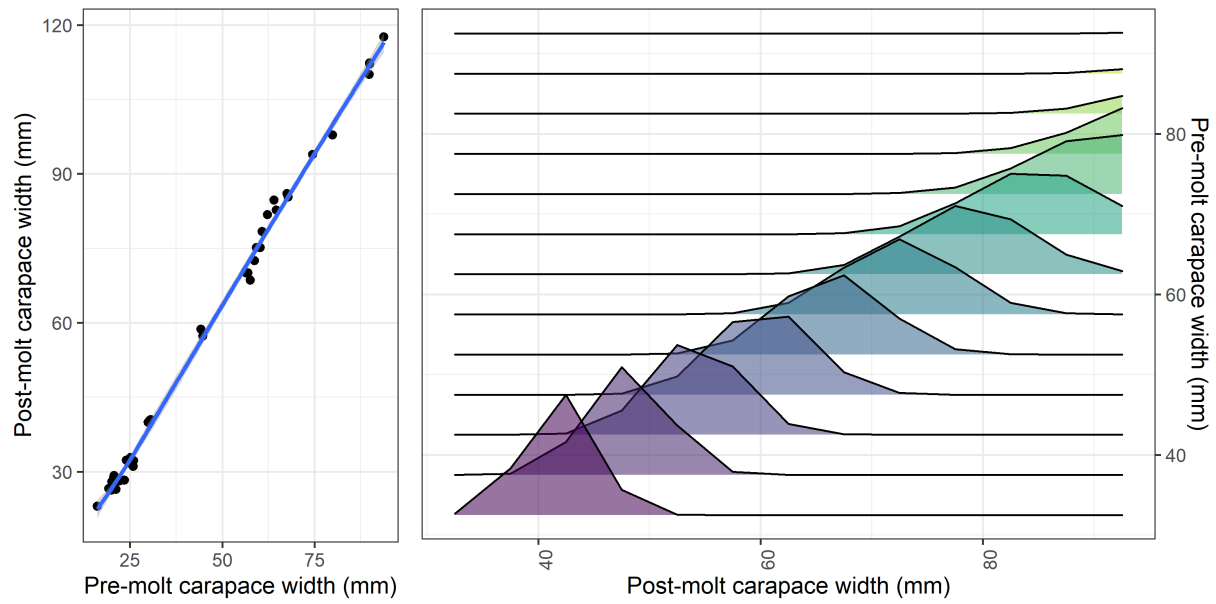


Figure 6: Empirical relationship between pre- and post-molt size (left) derived from crab captured in the wild pre-molt and observed to molt in the lab. Calculated size-transition matrix used in the population dynamics model (right).

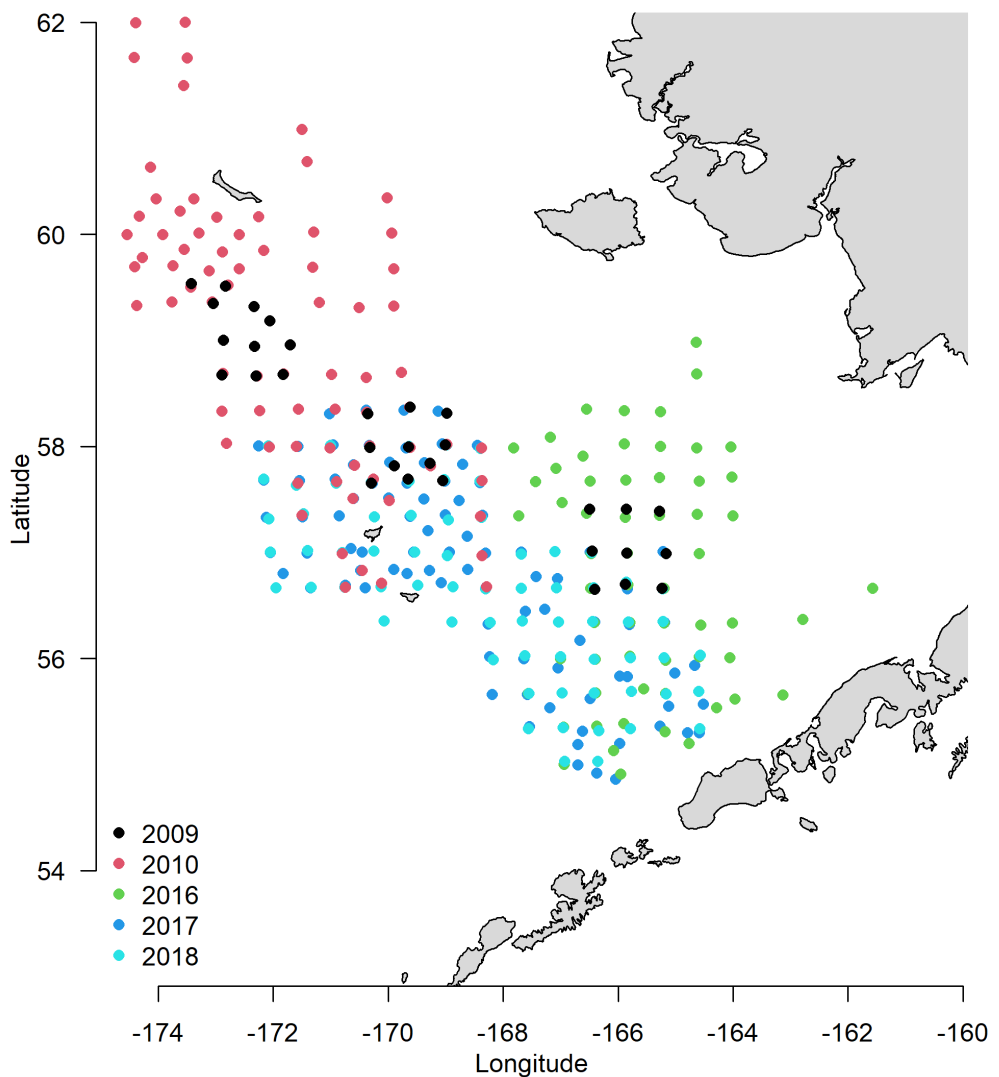


Figure 7: Locations of the BSFRF experimental trawls to evaluate the capture efficiency of the NMFS summer trawl survey for snow crab in the eastern Bering Sea.

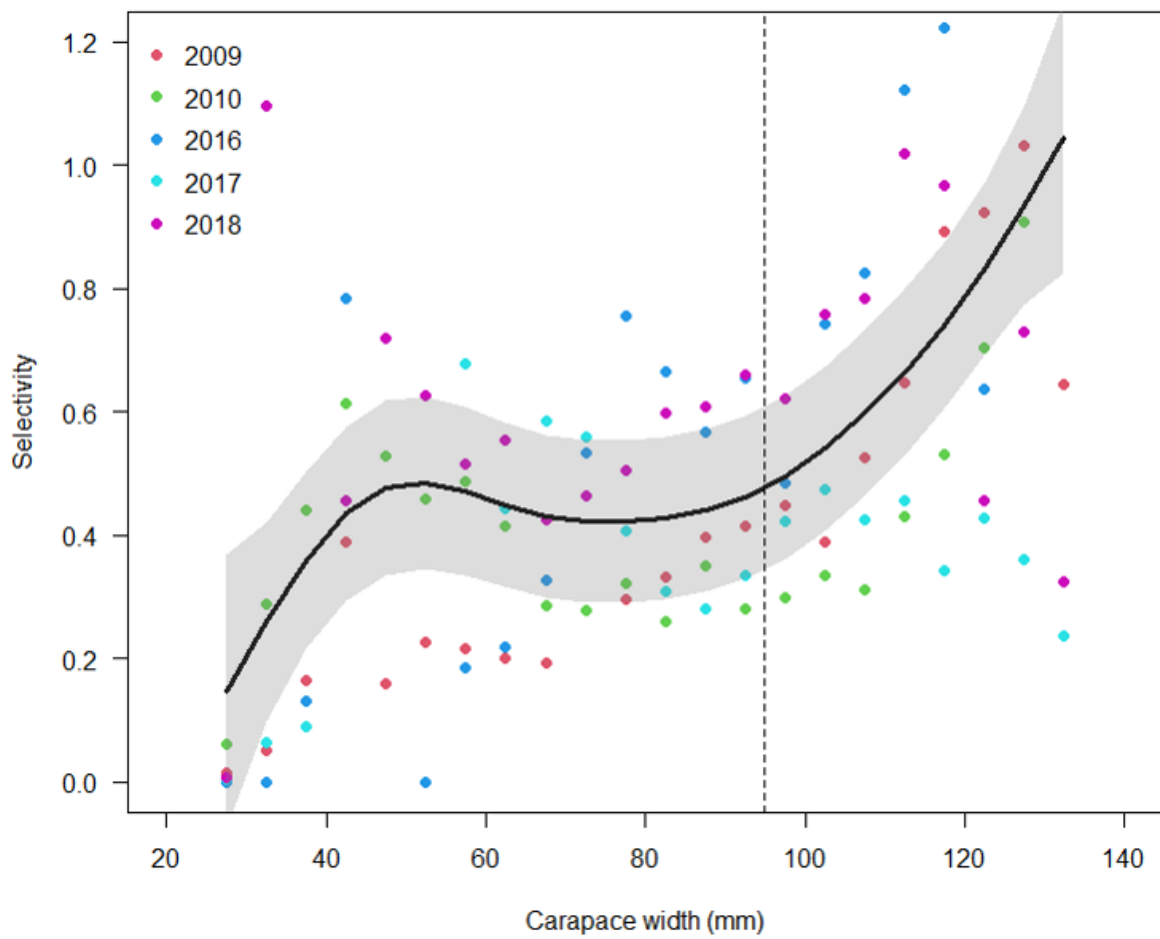


Figure 8: Inferred selectivity from the BSFRF experimental trawls.

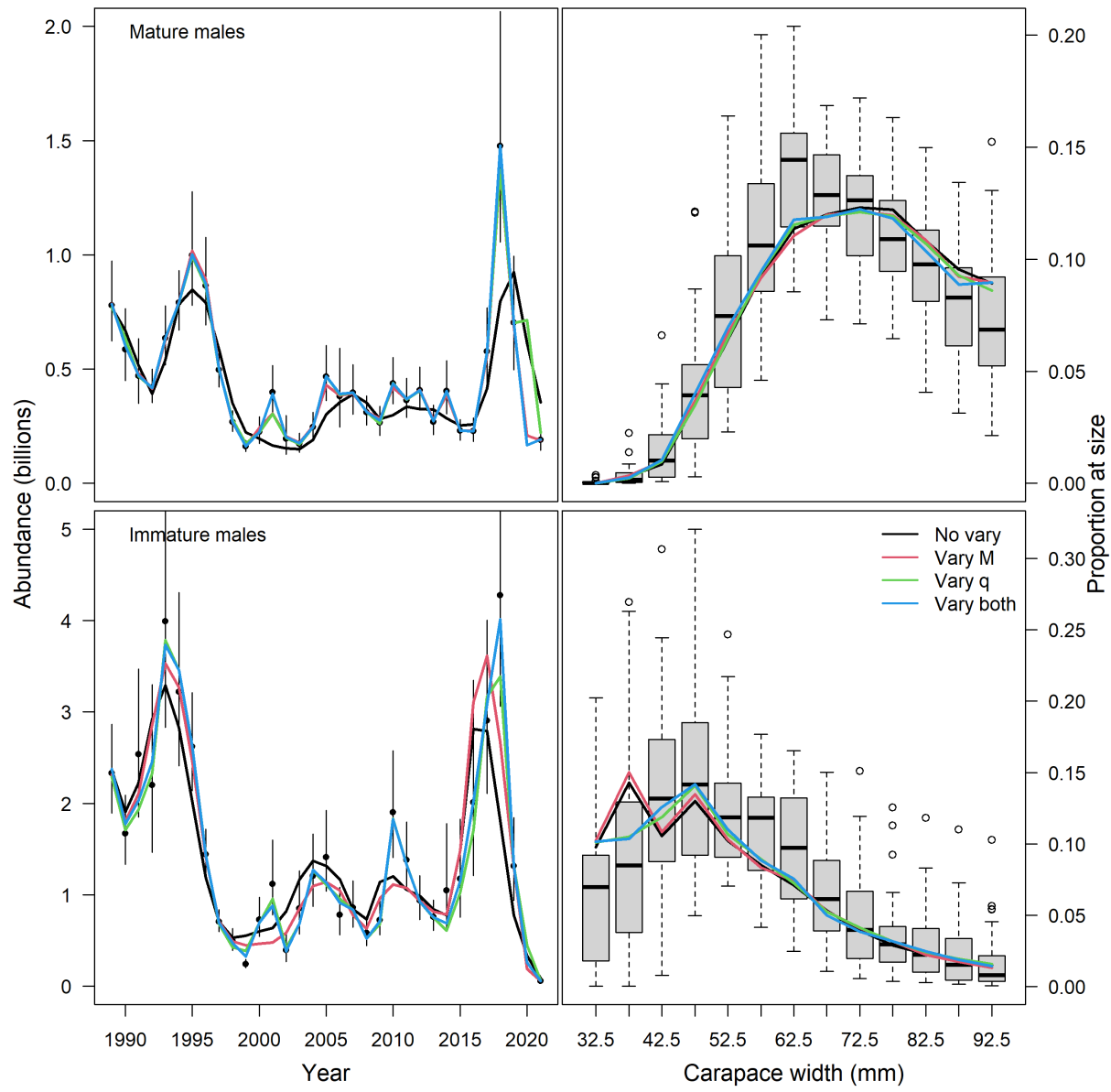


Figure 9: Fits of models with increasing complexity in mortality and catchability. Index of abundances are on the left with observations in black dots with 95% confidence intervals; colored lines are model fits. Size composition data are at the right with observations in box plots (aggregated over year; black lines are median, grey box represents 25-75th quantiles, circles are outliers) and colored lines are model fits.

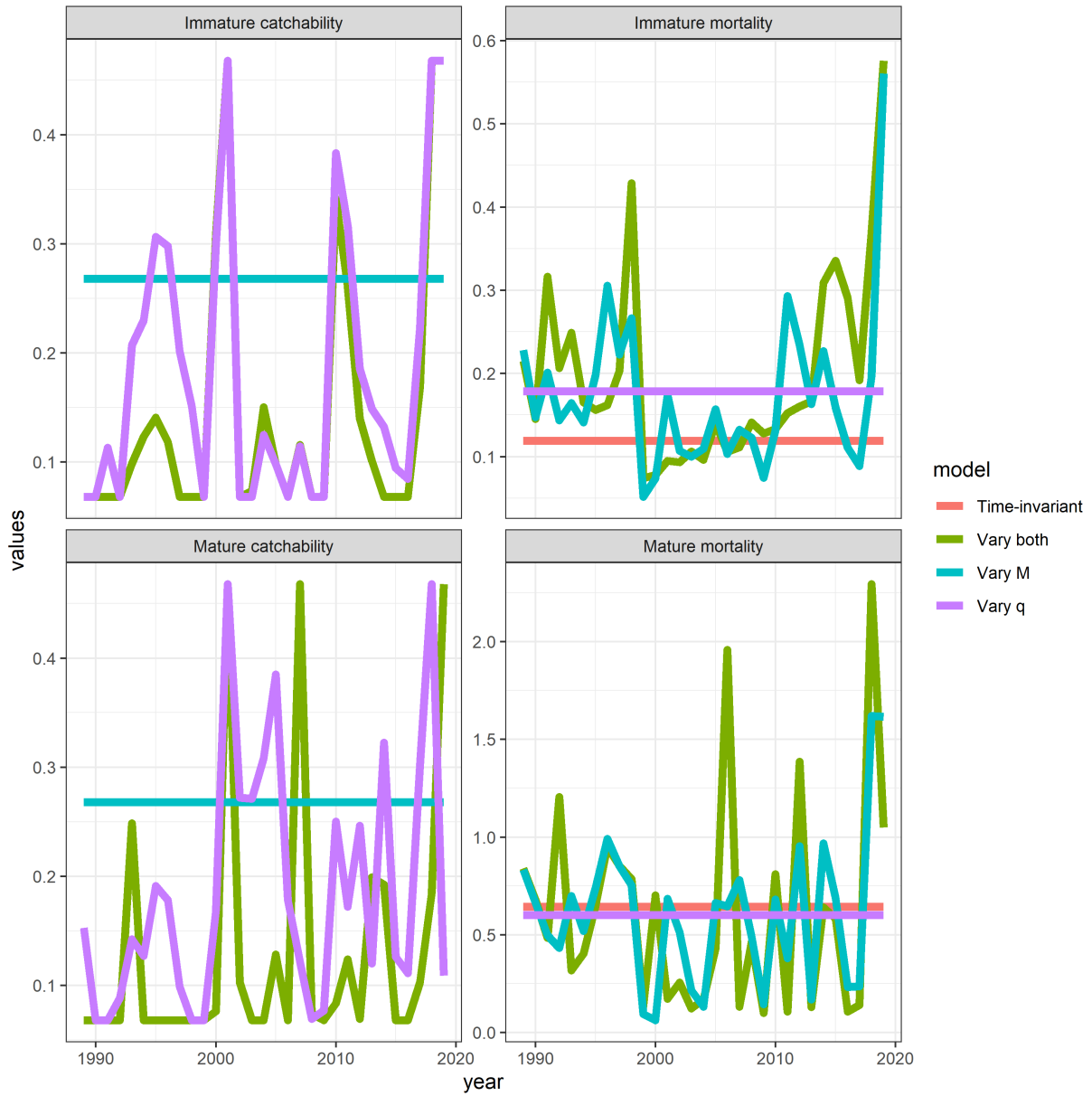


Figure 10: Estimated processes from model with increasingly complex time-variation in mortality and catchability.

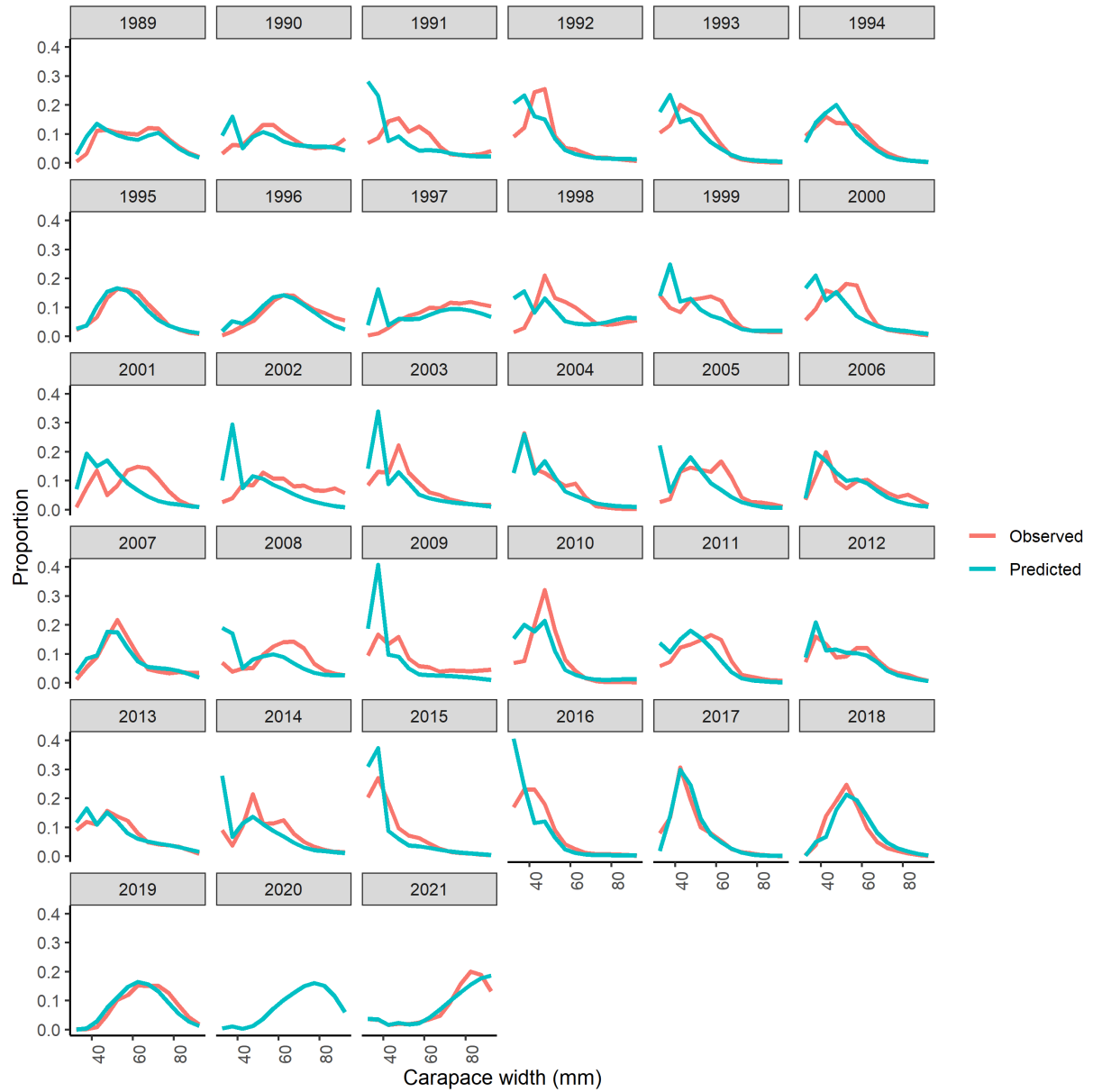


Figure 11: Fits for individual years to immature size composition data from a model in which mortality varied over time.

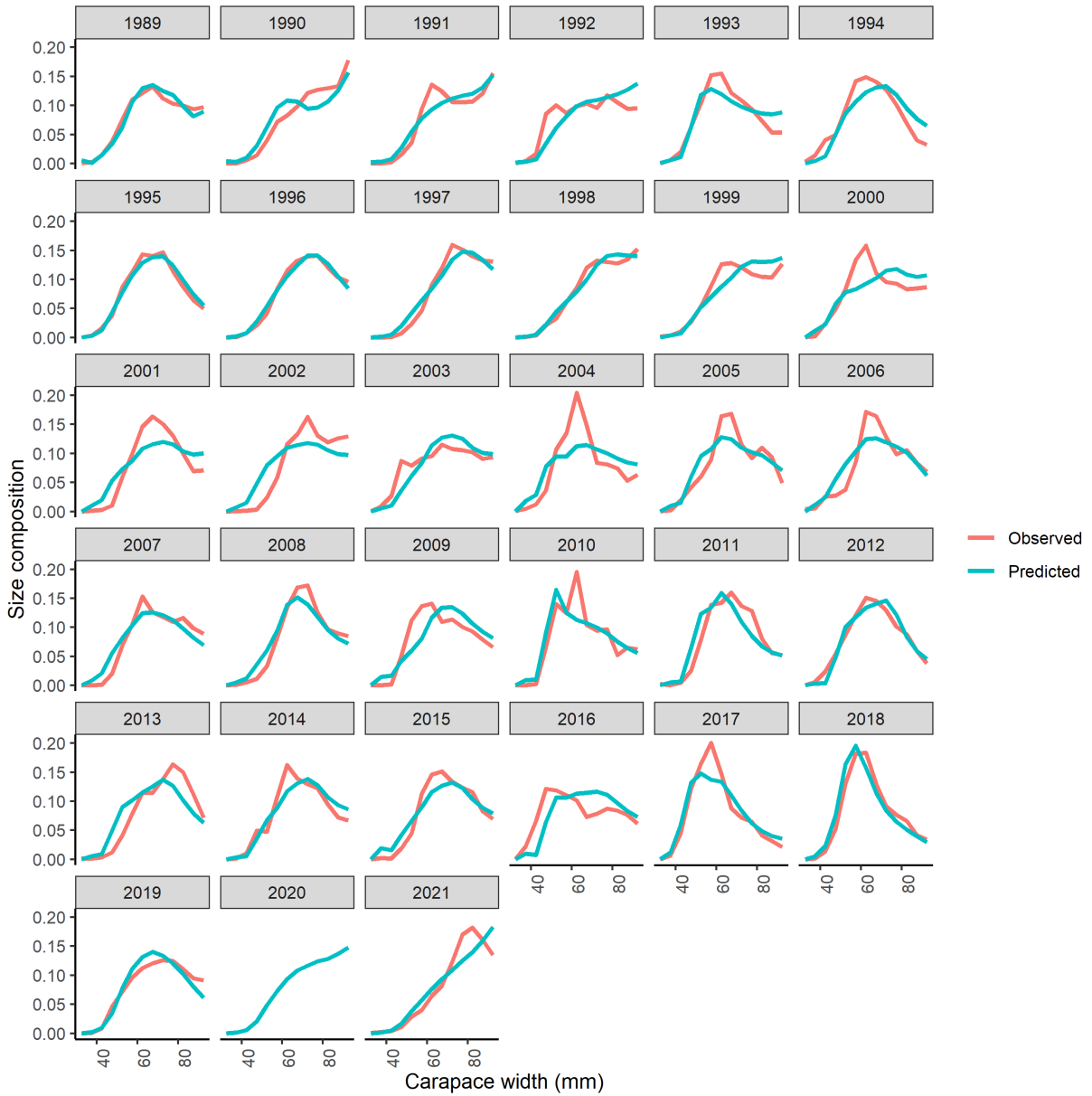


Figure 12: Fits for individual years to mature size composition data from a model in which mortality varied over time.

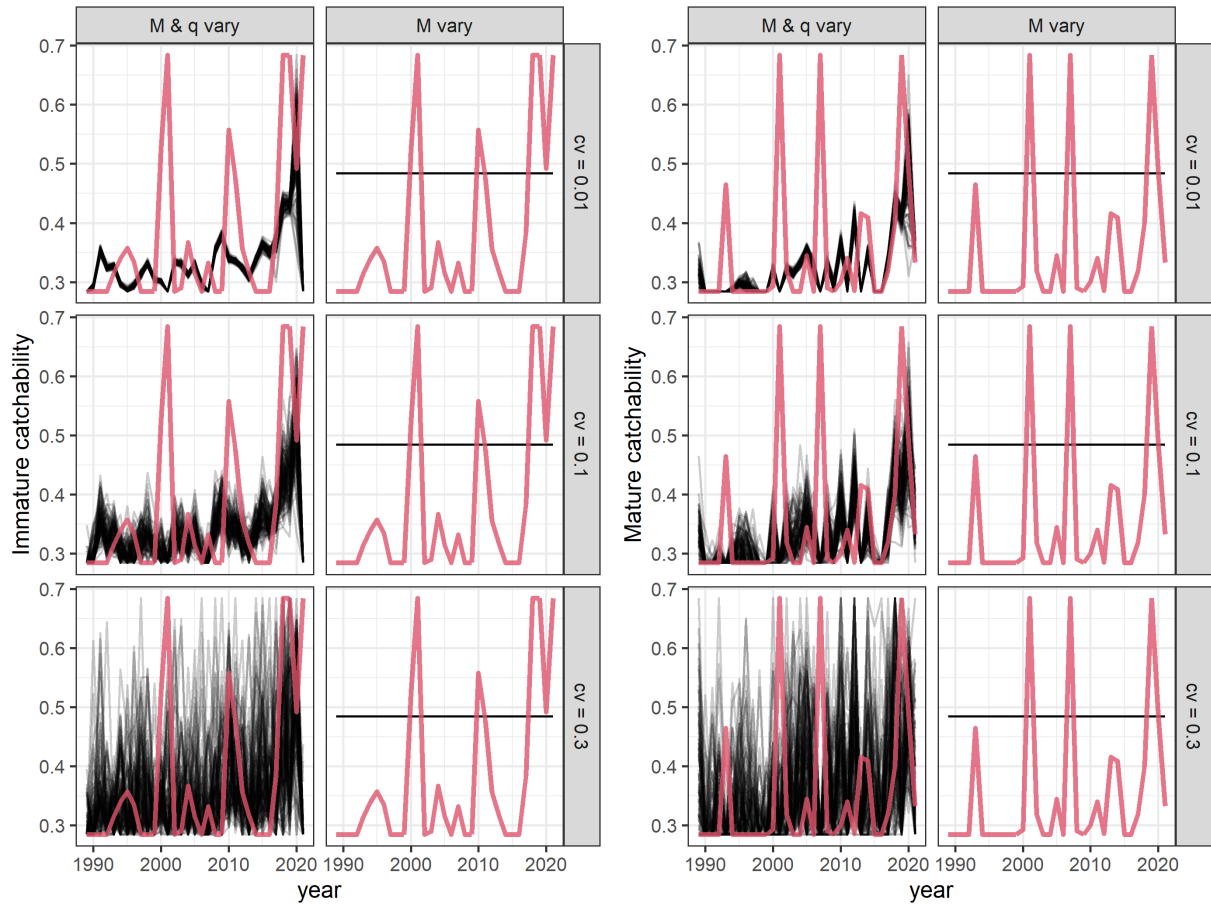


Figure 13: Estimates of catchability by maturity state (black lines) compared to the underlying values (red line) from simulations testing the estimation ability of the population dynamics models.

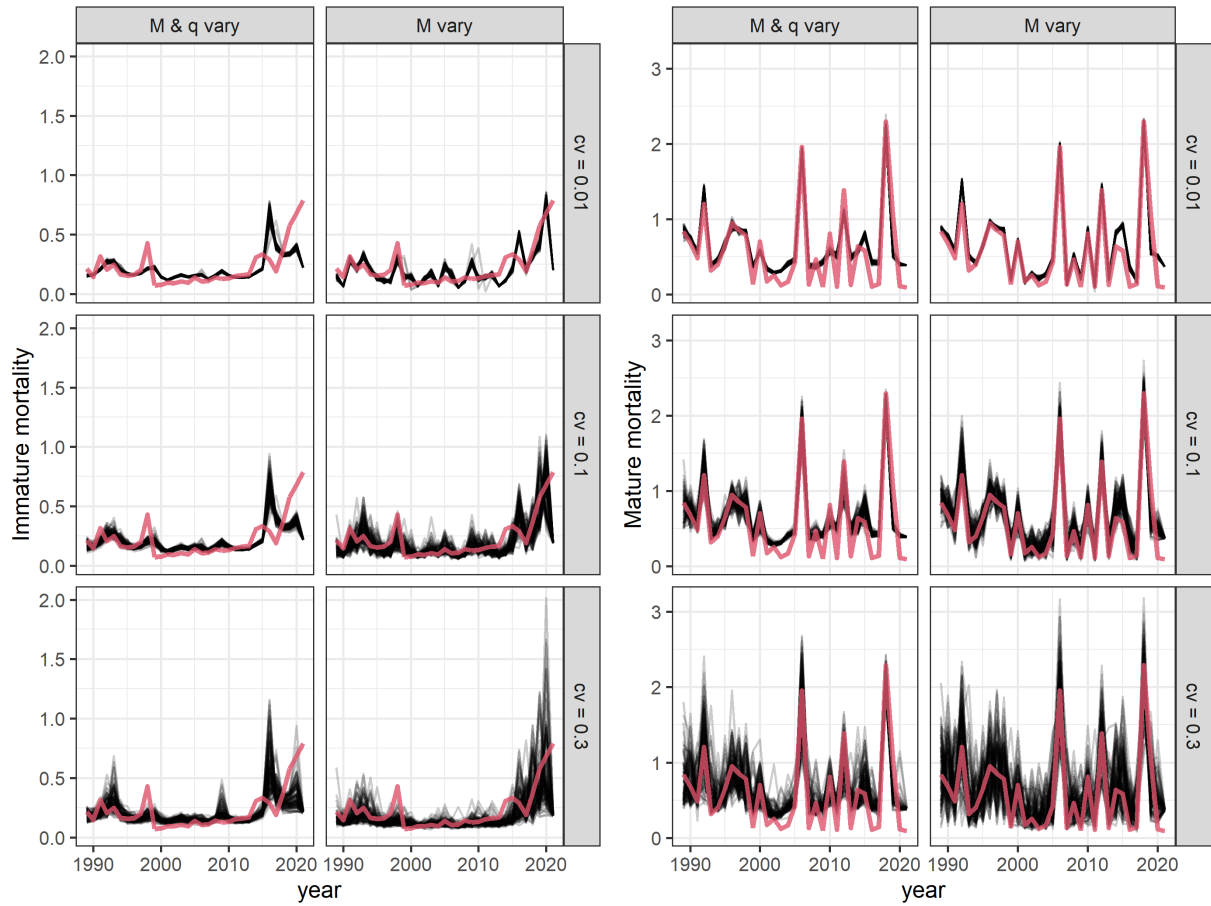


Figure 14: Estimates of mortality by maturity state (black lines) compared to the underlying values (red line) from simulations testing the estimation ability of the population dynamics models.

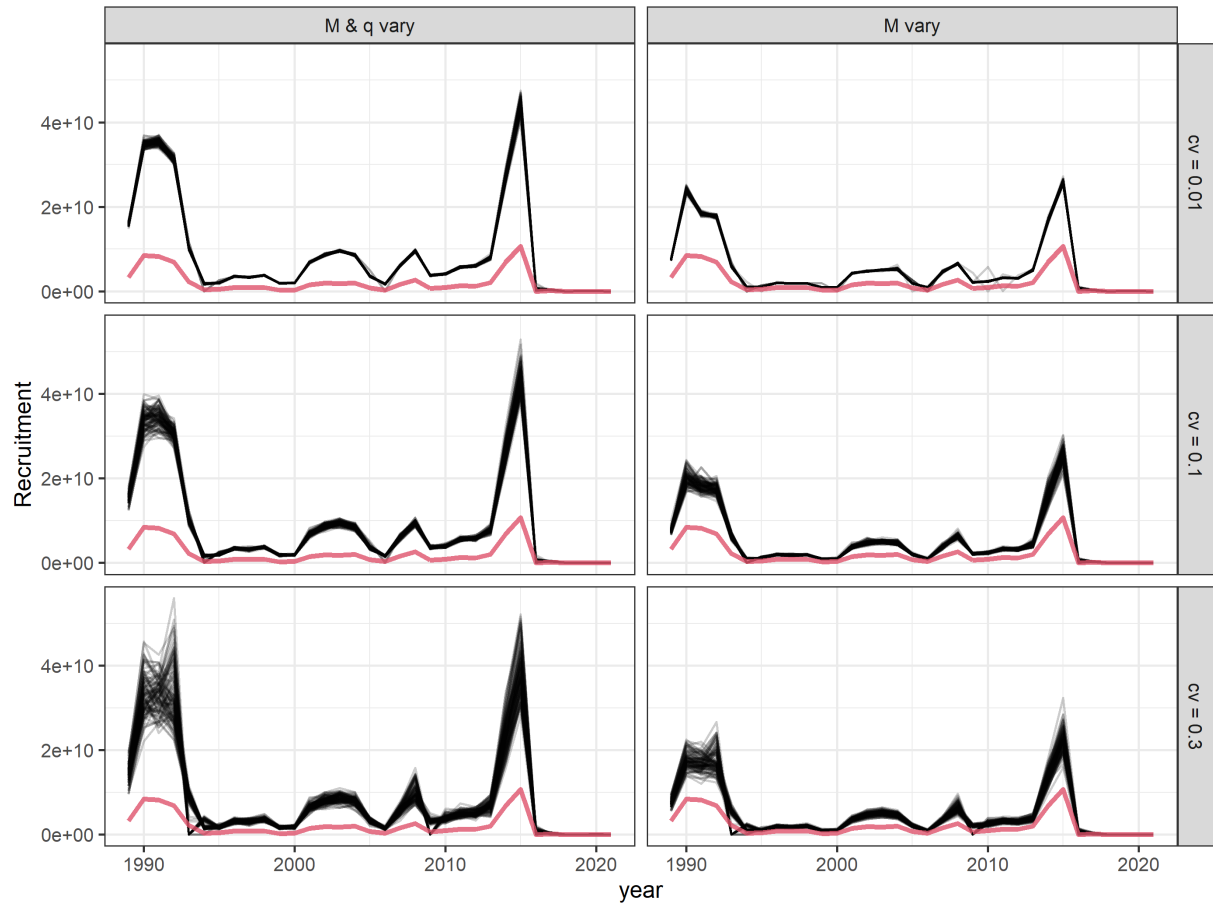


Figure 15: Estimates of recruitment (black lines) compared to the underlying values (red line) from simulations testing the estimation ability of the population dynamics models.

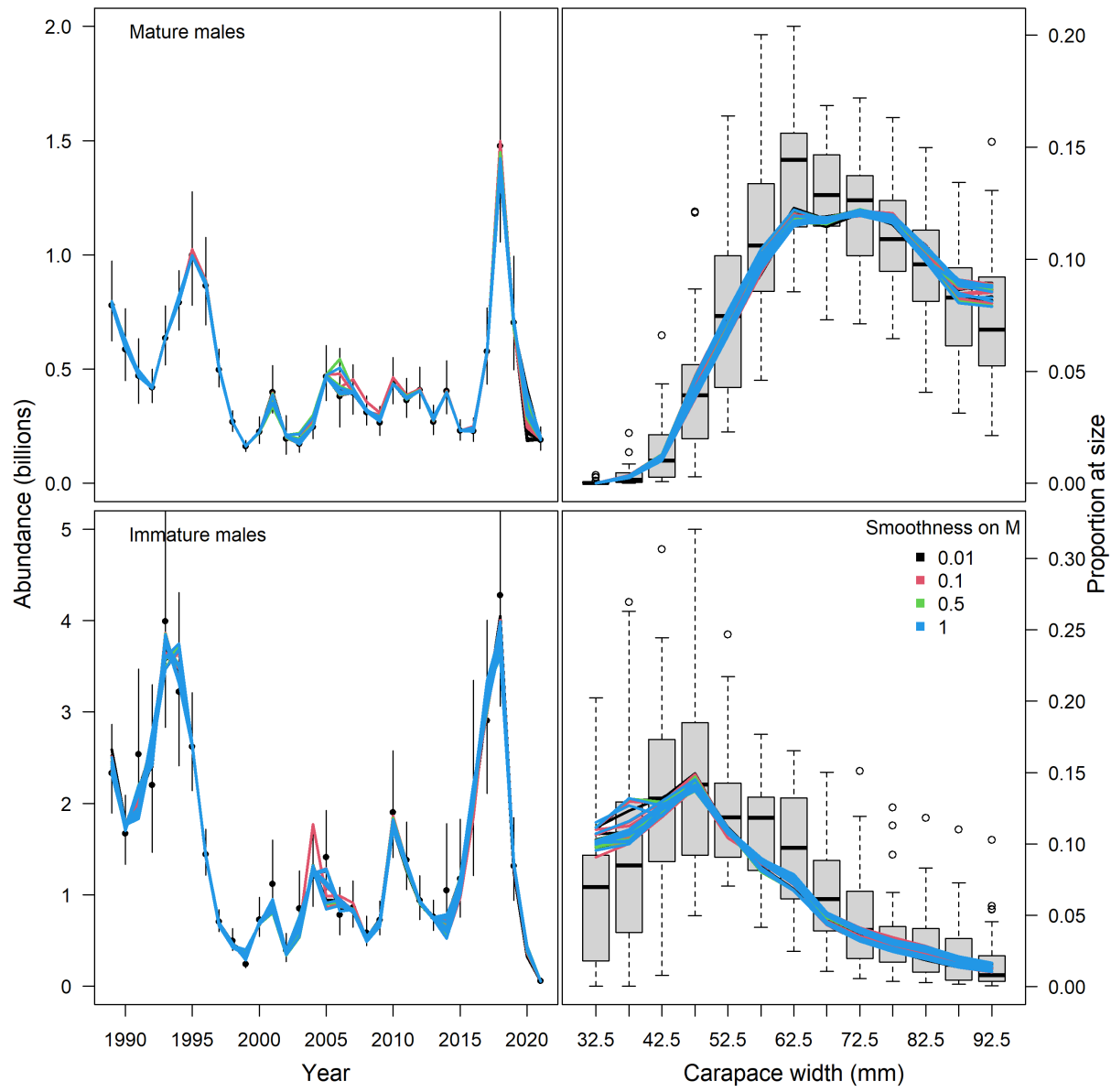


Figure 16: Model fits from sensitivity tests. Indices of abundances are on the left with observations in black dots with 95% confidence intervals; colored lines are model fits. Size composition data are at the right with observations in box plots (aggregated over year; black lines are median, grey box represents 25-75th quantiles, circles are outliers) and colored lines are model fits.

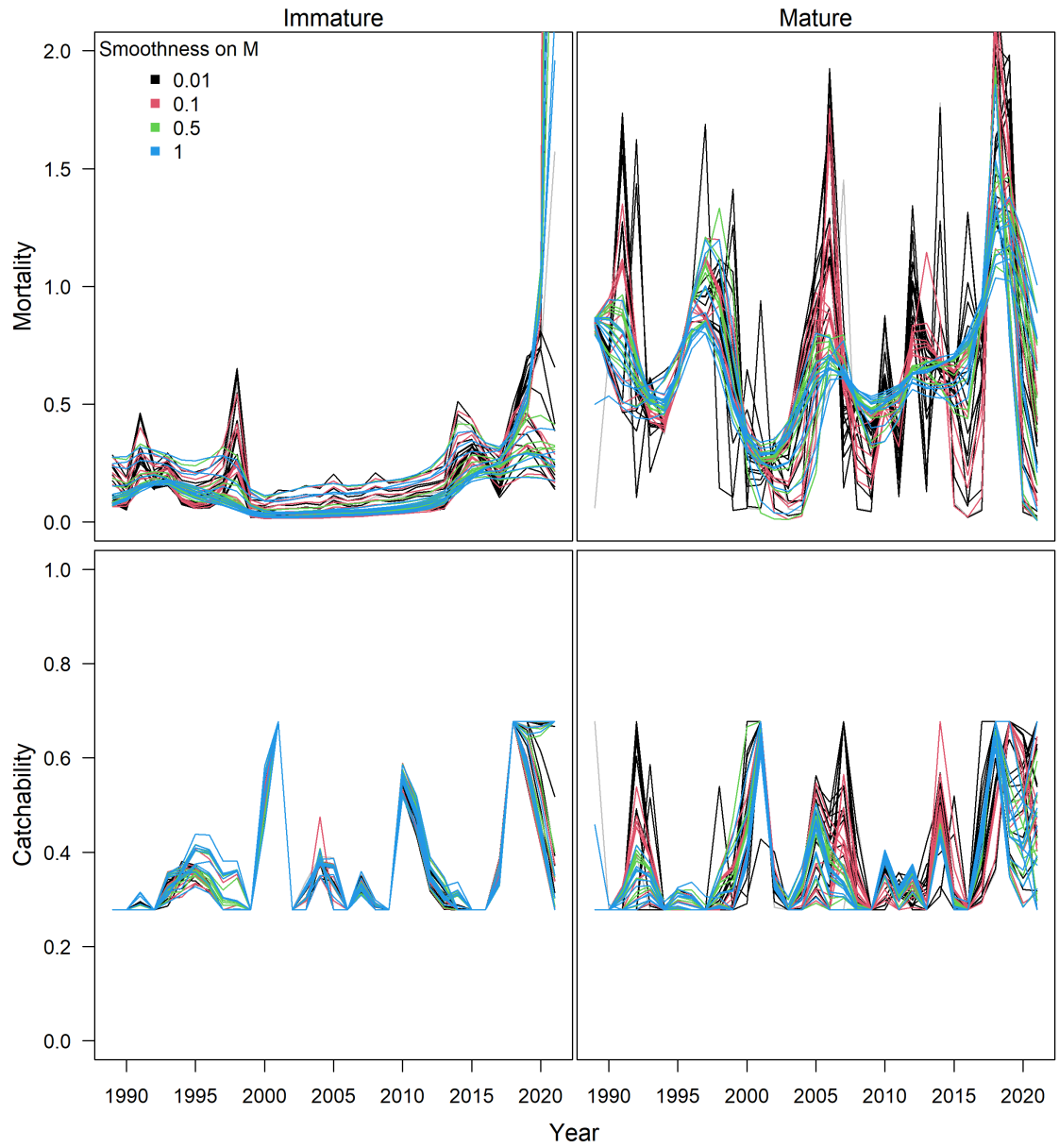


Figure 17: Estimates of mortality and catchability by maturity state over sensitivity runs. Lines are colored based on the smoothness penalty on mortality.

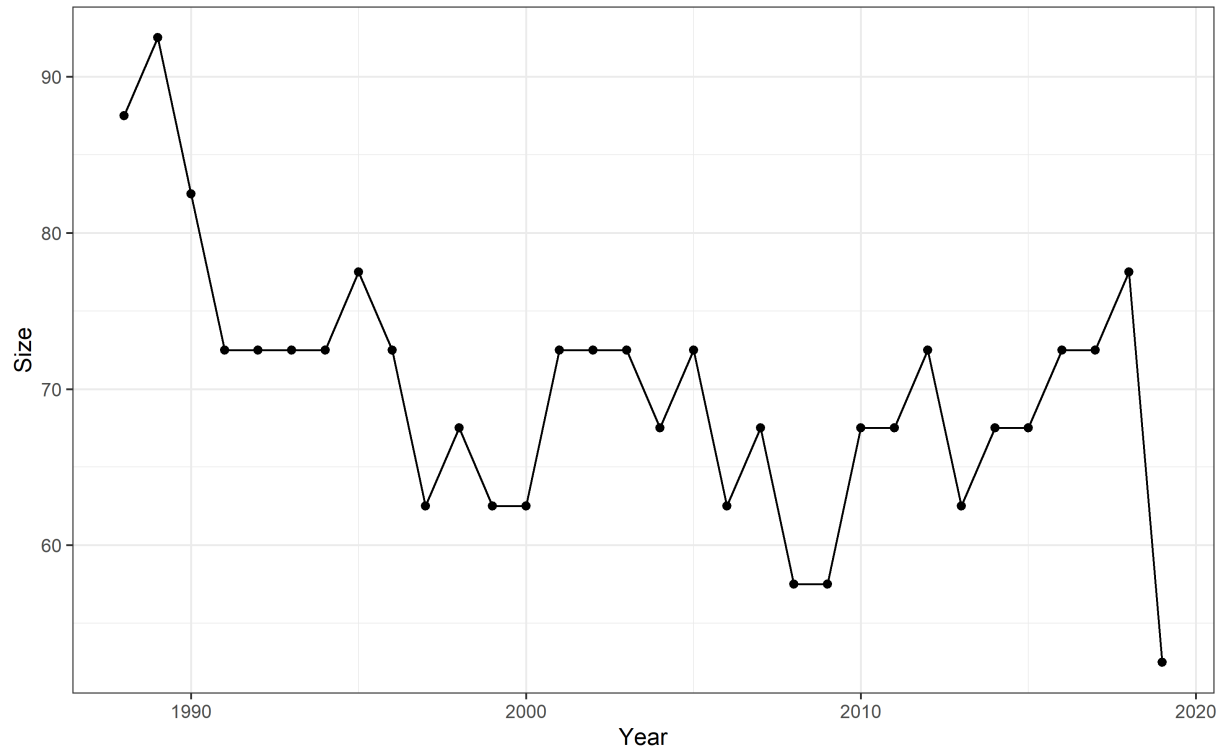


Figure 18: Size at which half of the crab in the population are mature over time (note, this is not the probability of undergoing terminal molt, rather the proportion of the number of mature vs. immature crab at size in the population).

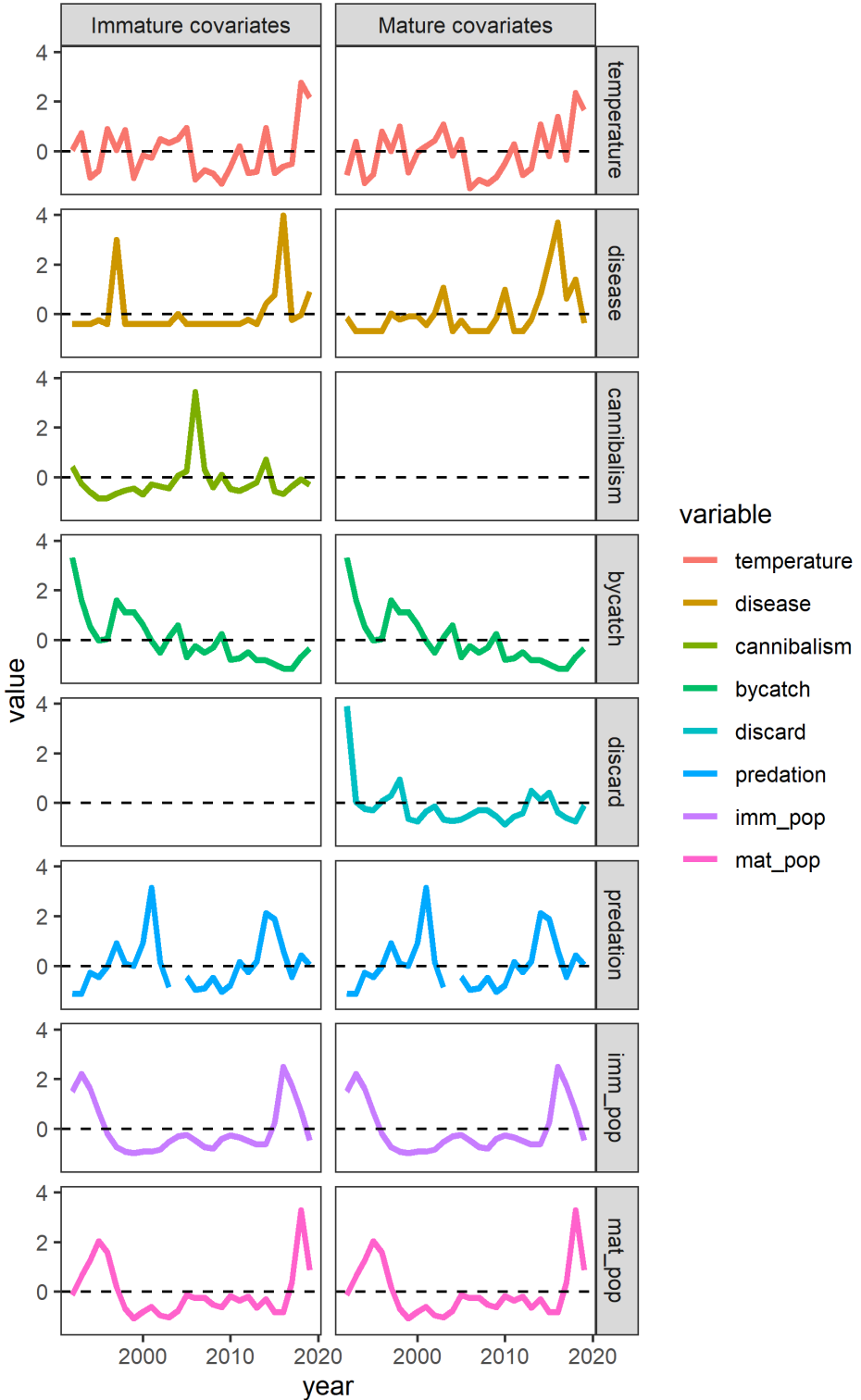


Figure 19: Calculated covariates incorporated into GAMs to relate stressors to estimated mortality. Two covariates (discard and predation) are only relevant for one maturity state based on the critical role size plays in the process (i.e. discards are primarily relatively large crab and predation is primarily smaller crab).

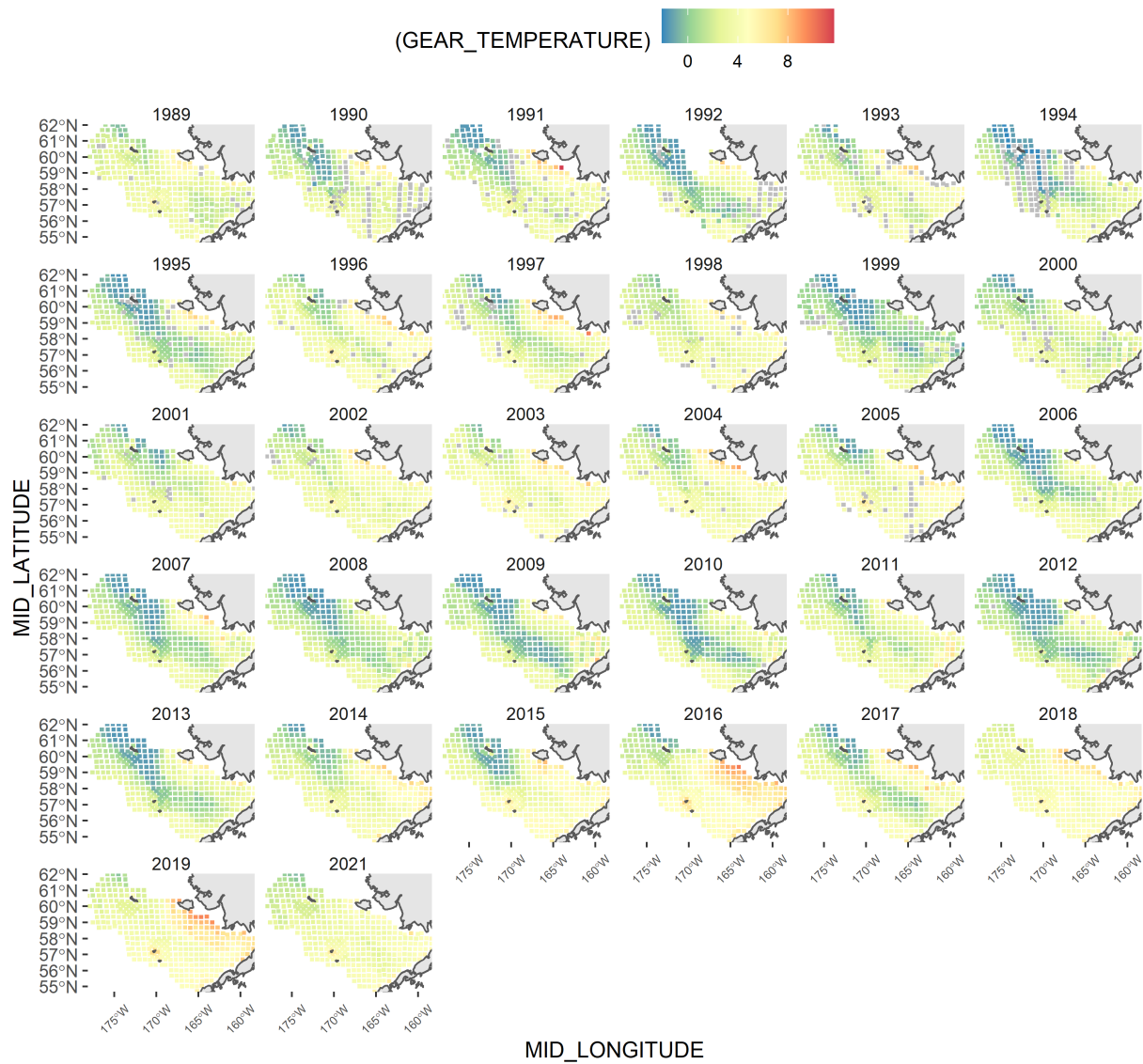


Figure 20: Observed bottom temperature at the time of the NMFS summer survey. Less than 2 degrees C represents the cold pool, seen in green and blue here.

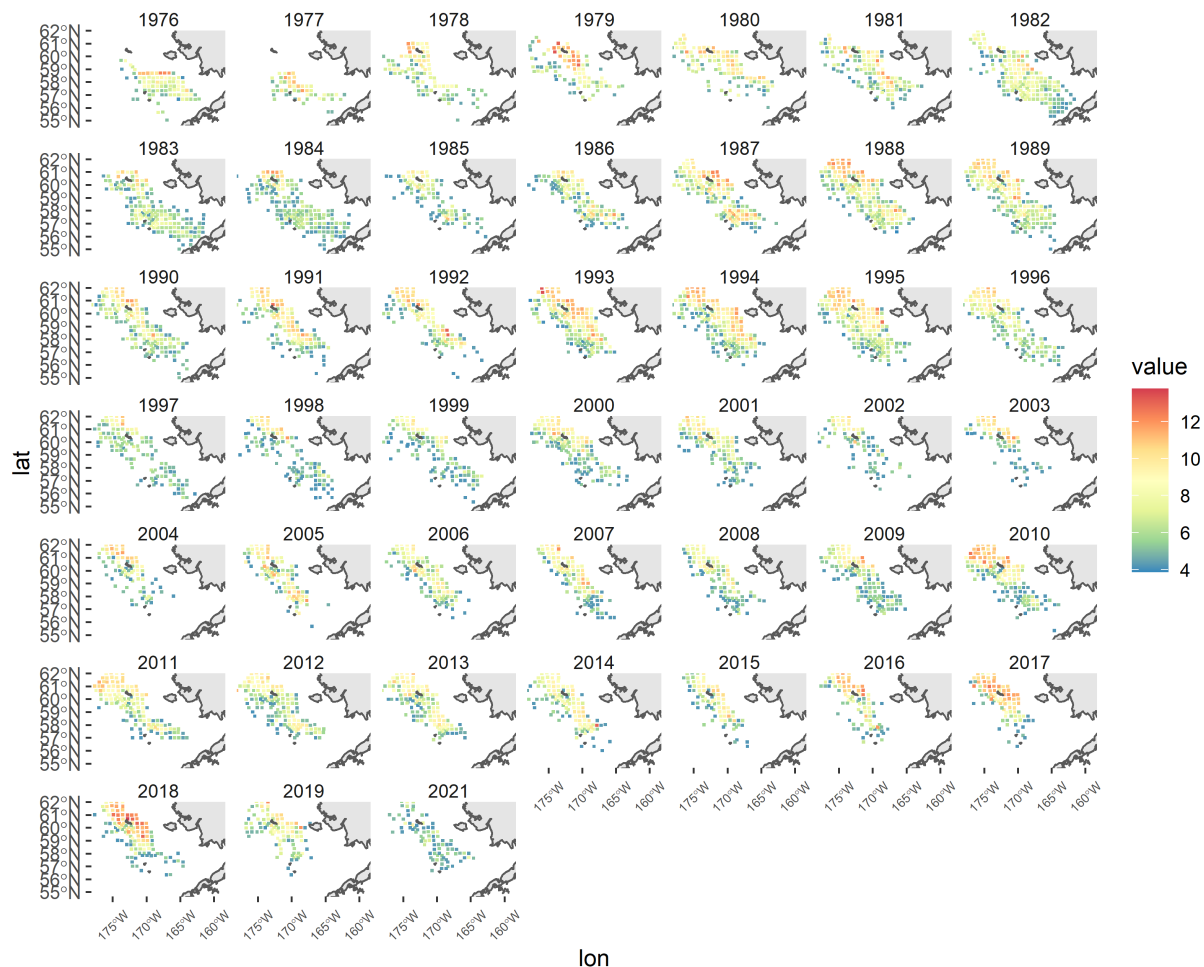


Figure 21: Distribution and intensity of densities (in log numbers) of crab <55 mm carapace width in the NMFS summer survey.

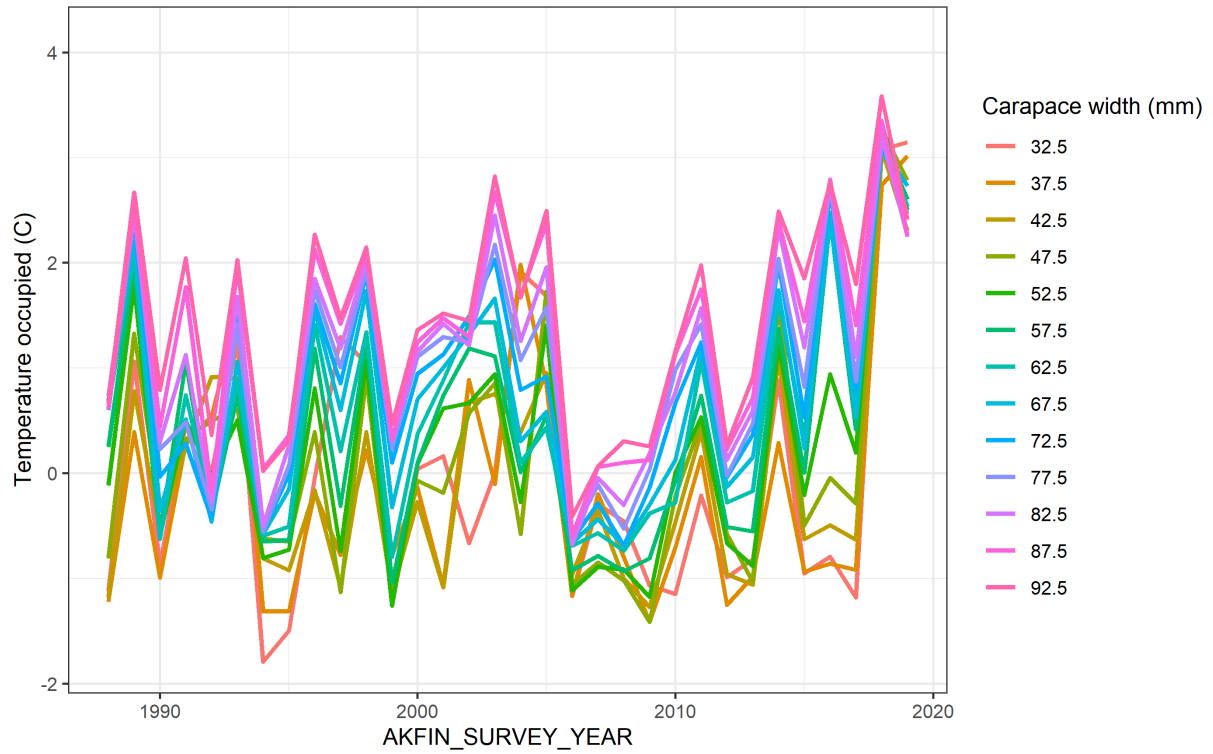


Figure 22: Temperature occupied over time of crab by 5 mm size bin.

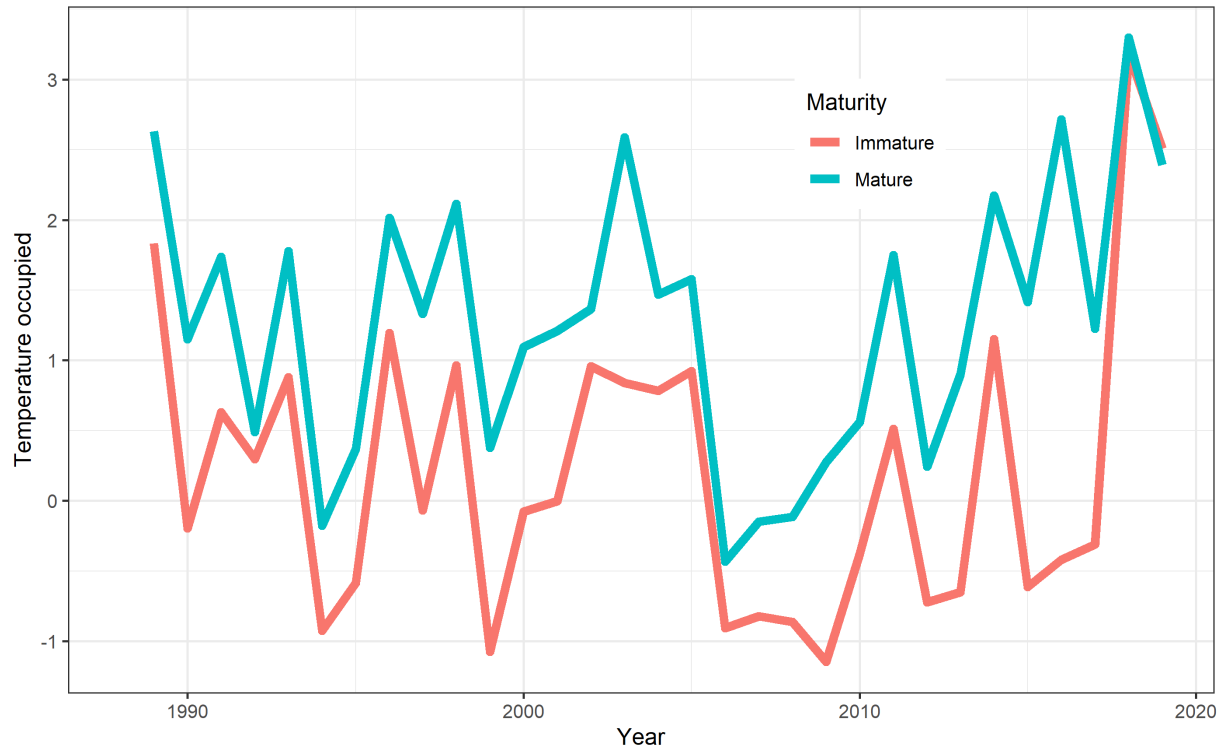


Figure 23: Temperature occupied over time of crab by maturity state defined by the size at which 50% of crab are mature according to chela height.

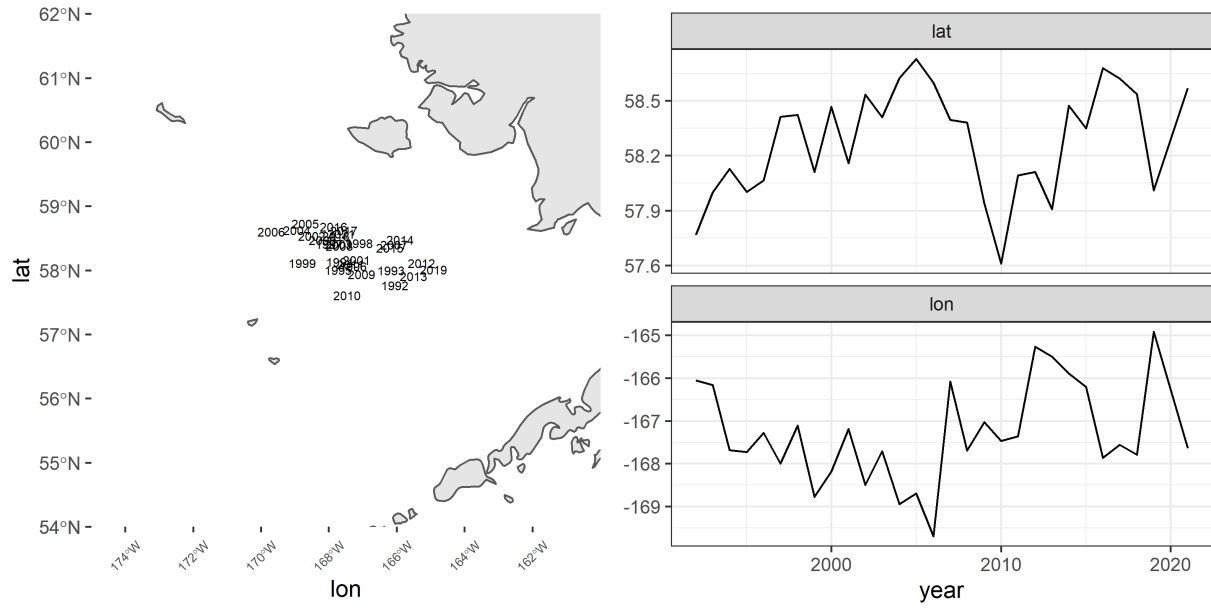


Figure 24: Centroids of abundance for Pacific cod in the Bering Sea over time (left). Right panels show the time series of the centroids broken down by latitudinal and longitudinal components.

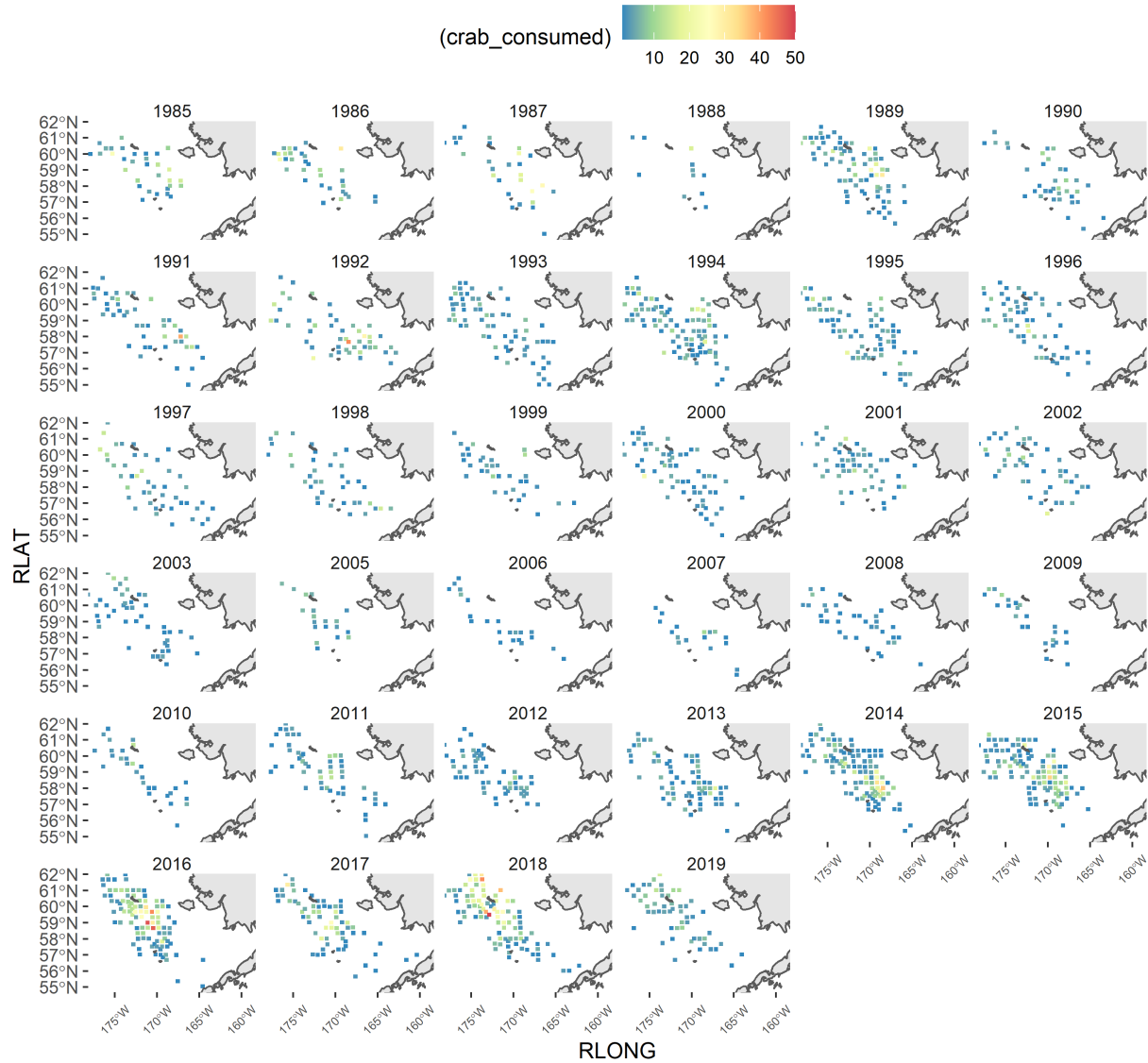


Figure 25: Location and number of crab observed in cod stomachs over time. These are the raw data used to calculate crab consumption by cod and have not been adjusted for sampling effort, but provide background for the spatial distribution of predation over time.

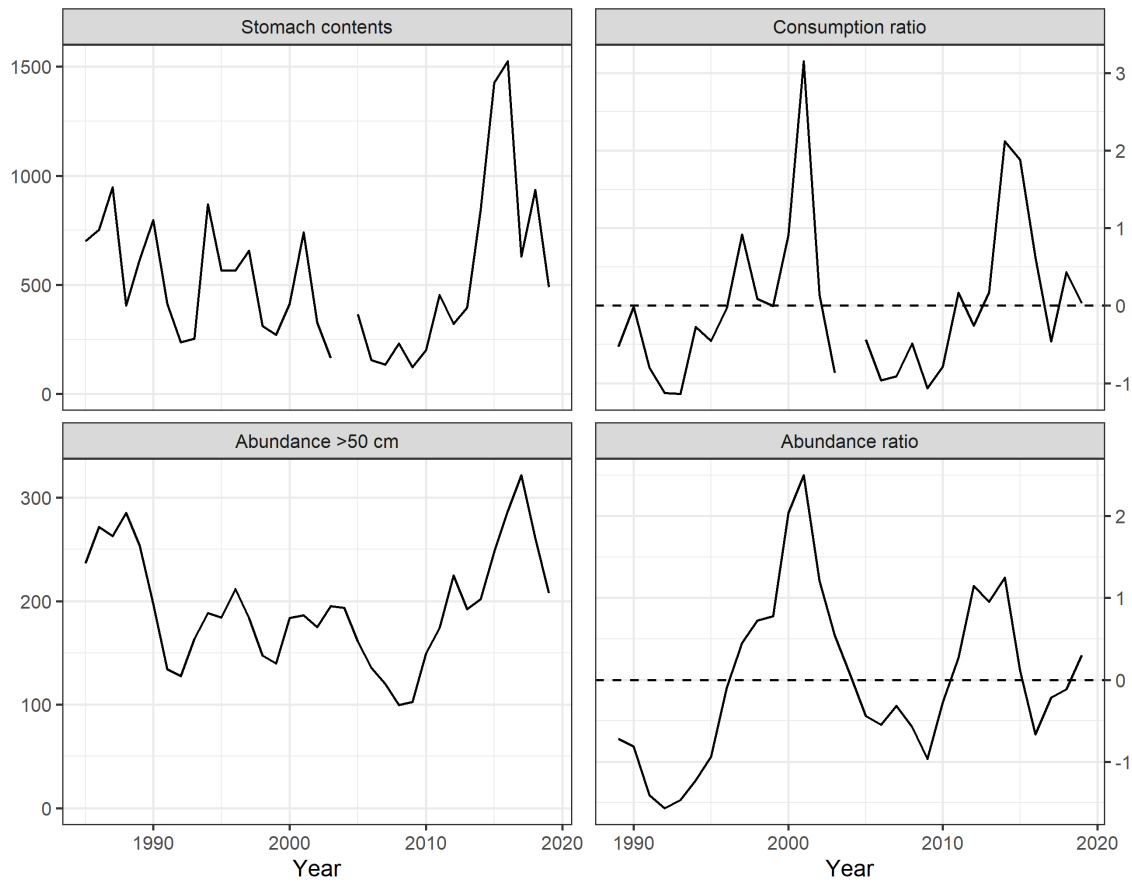


Figure 26: A comparison of indices of cod predation on snow crab. Left column are the calculated consumption of crab by cod (top) and the raw numbers of cod greater than 50 cm. The right column is the left column divided by the estimated number of crab in the eastern Bering Sea.

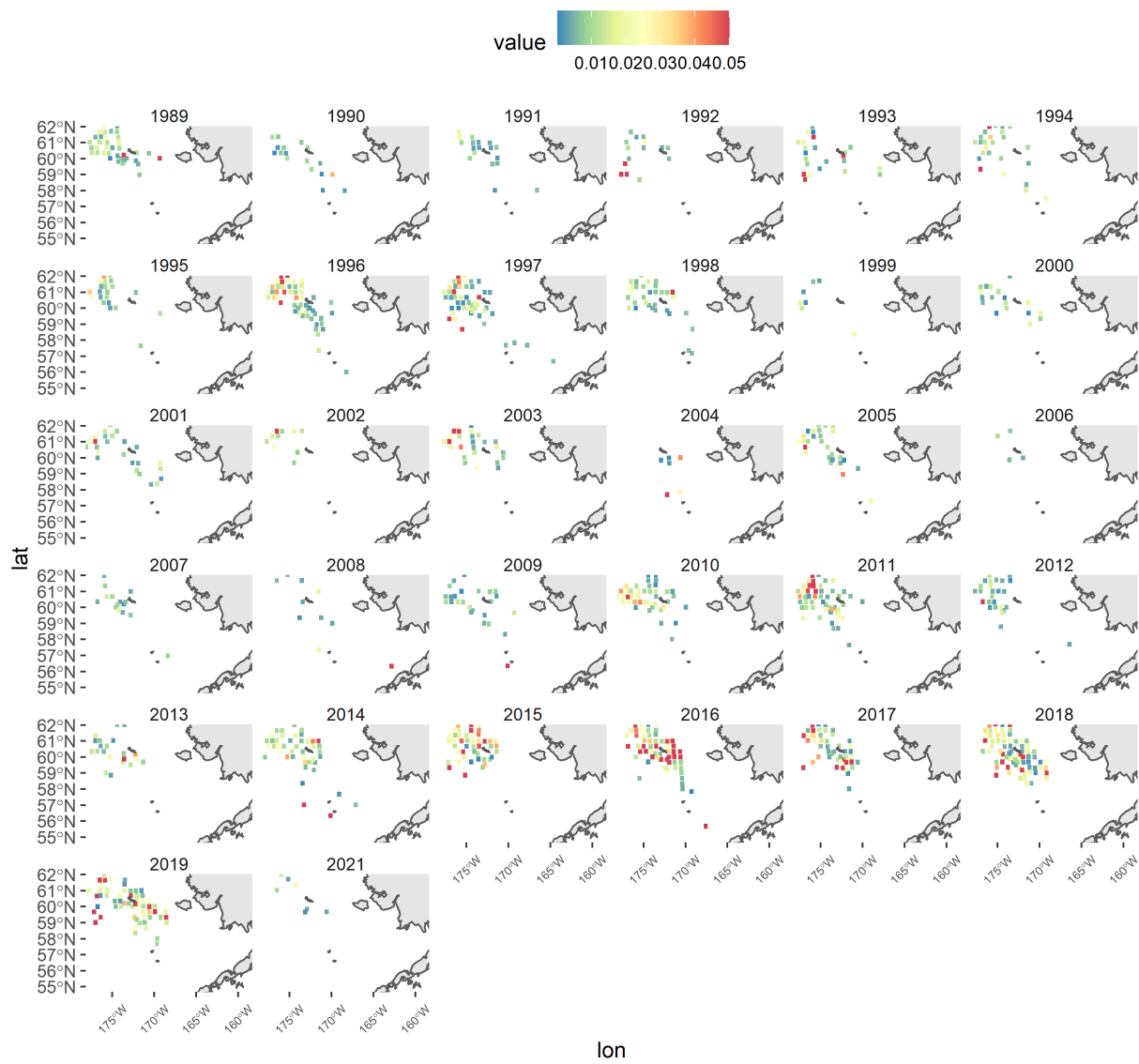


Figure 27: Location and intensity of bitter crab disease over time from visual prevalence observations in the NMFS summer survey.

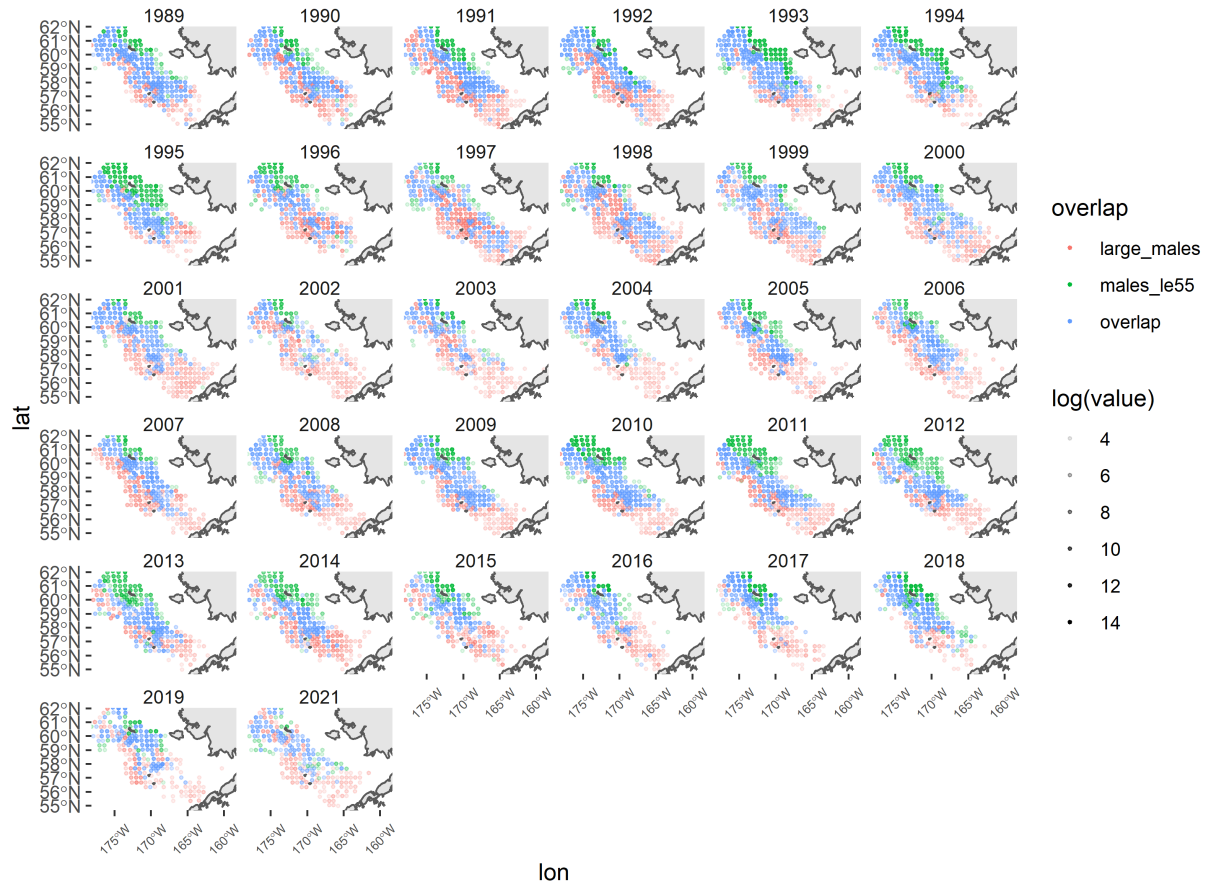


Figure 28: Overlap of large males (>95 mm carapace width) and males smaller than 55 mm carapace width. Opacity of the dot represents the density of crab. Blue represents overlapping distribution. Green and red represent non-overlapping observations of small and large males, respectively.

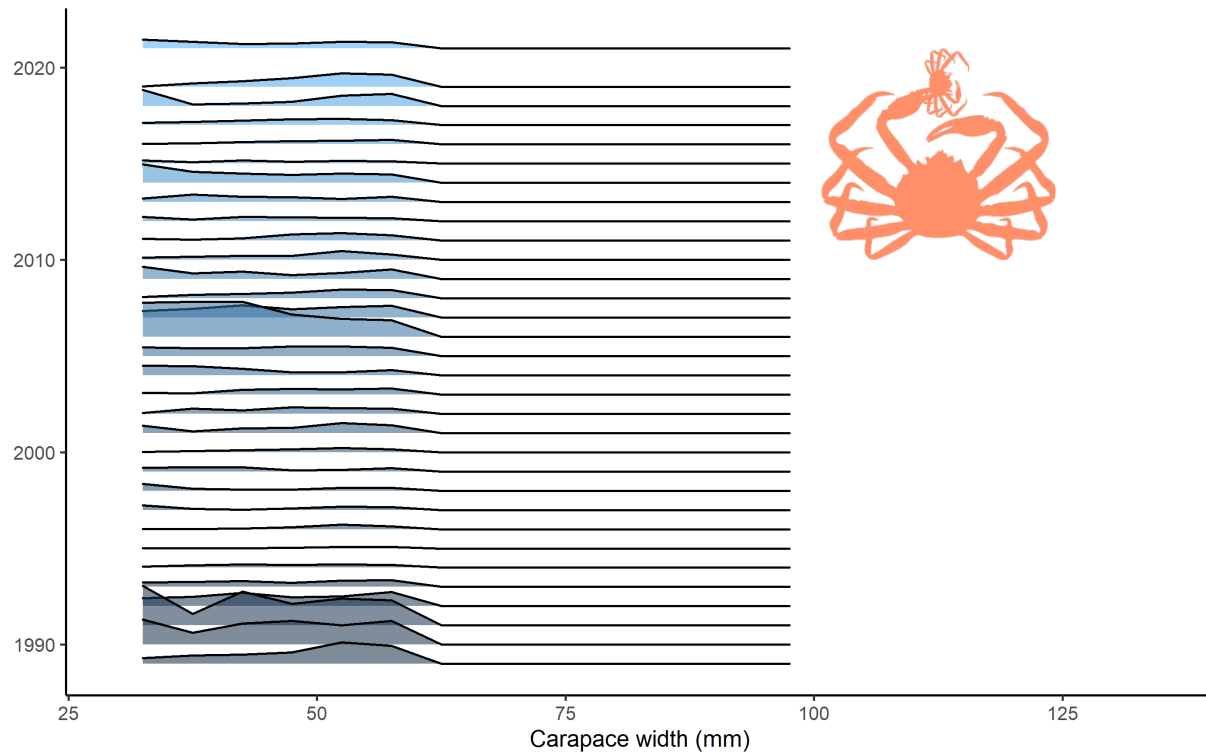


Figure 29: Relative risk at size for cannibalism over time.

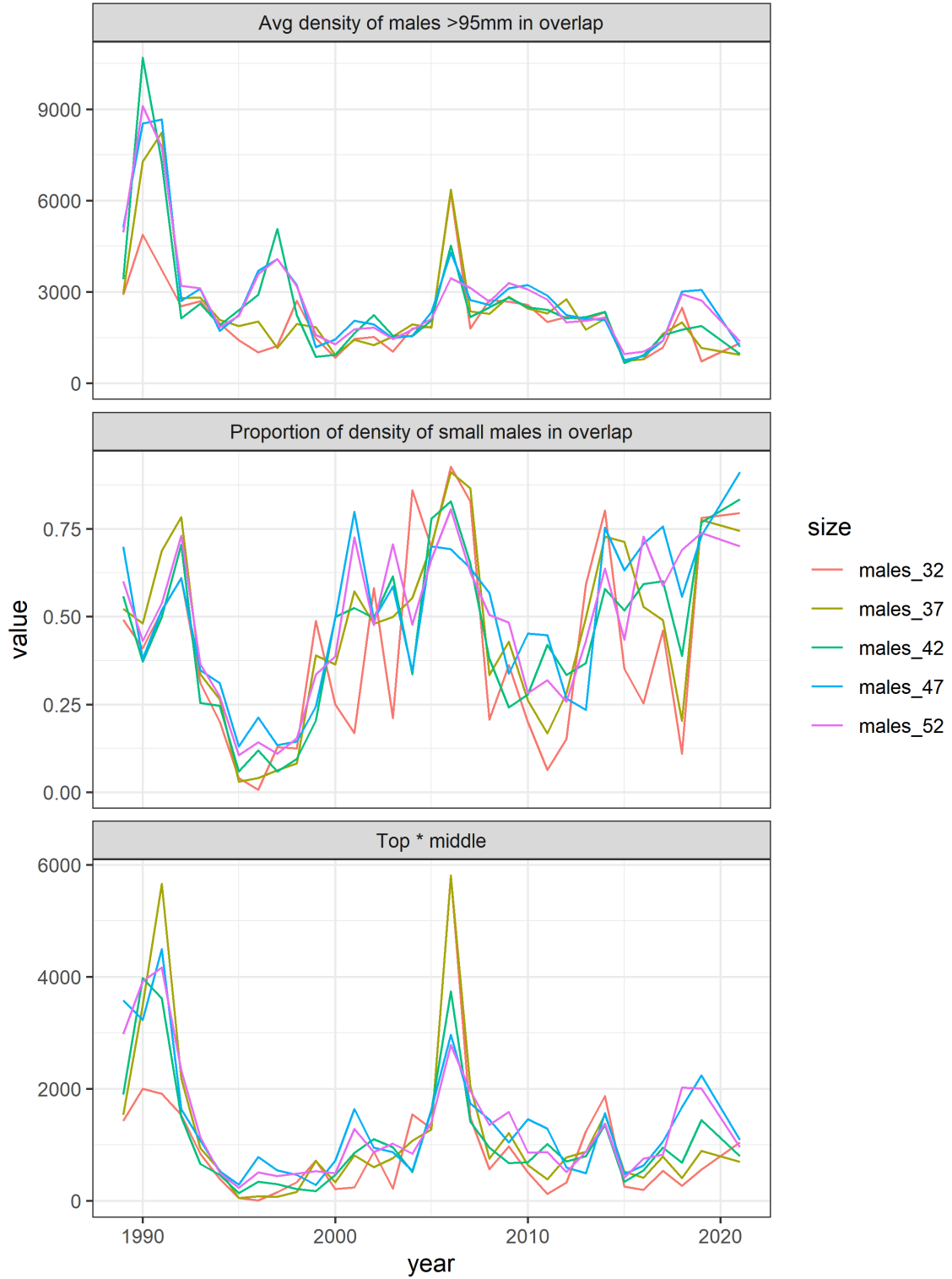


Figure 30: Times series by size of the density of large males in overlapping space (top), the proportion of small males in the overlapping area (middle), and the product of the two (bottom), which is used as an index of cannibalism in the models relating estimated mortality to environmental stressors.

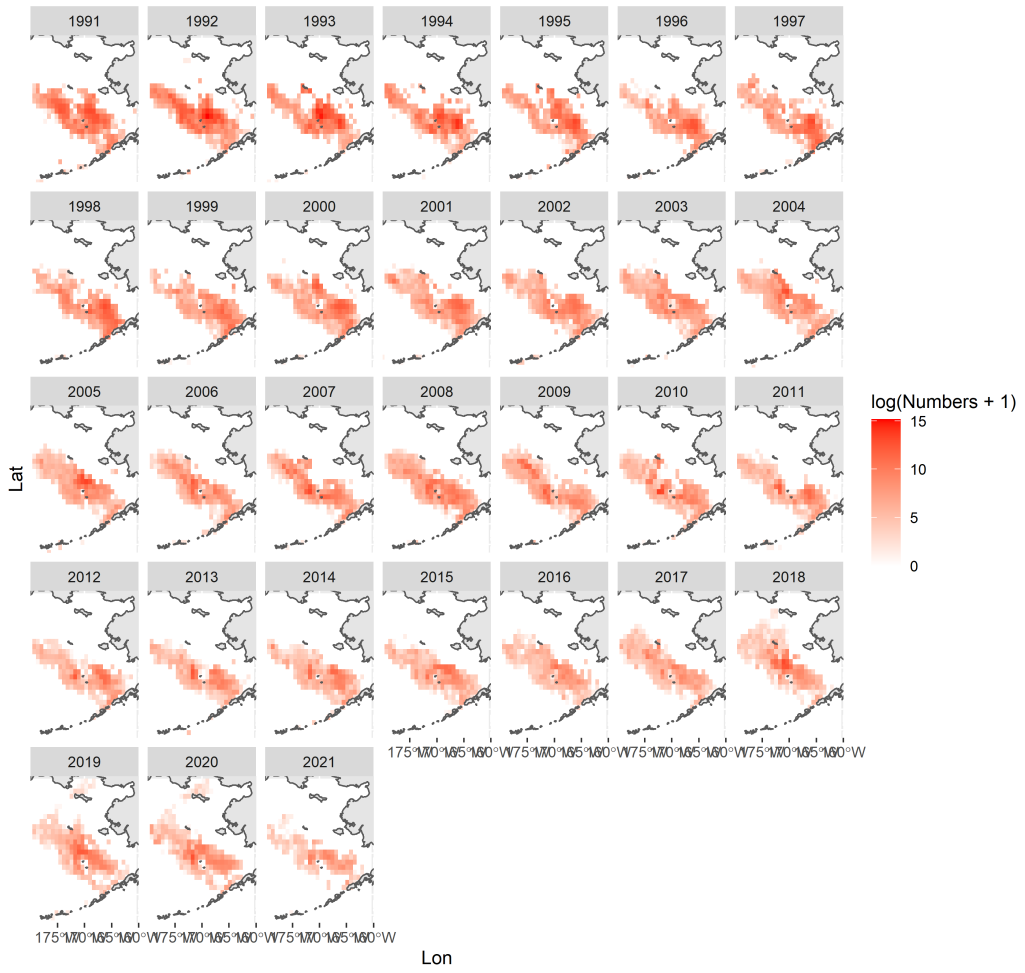


Figure 31: Location and intensity of bycatch of snow crab over time in log space.

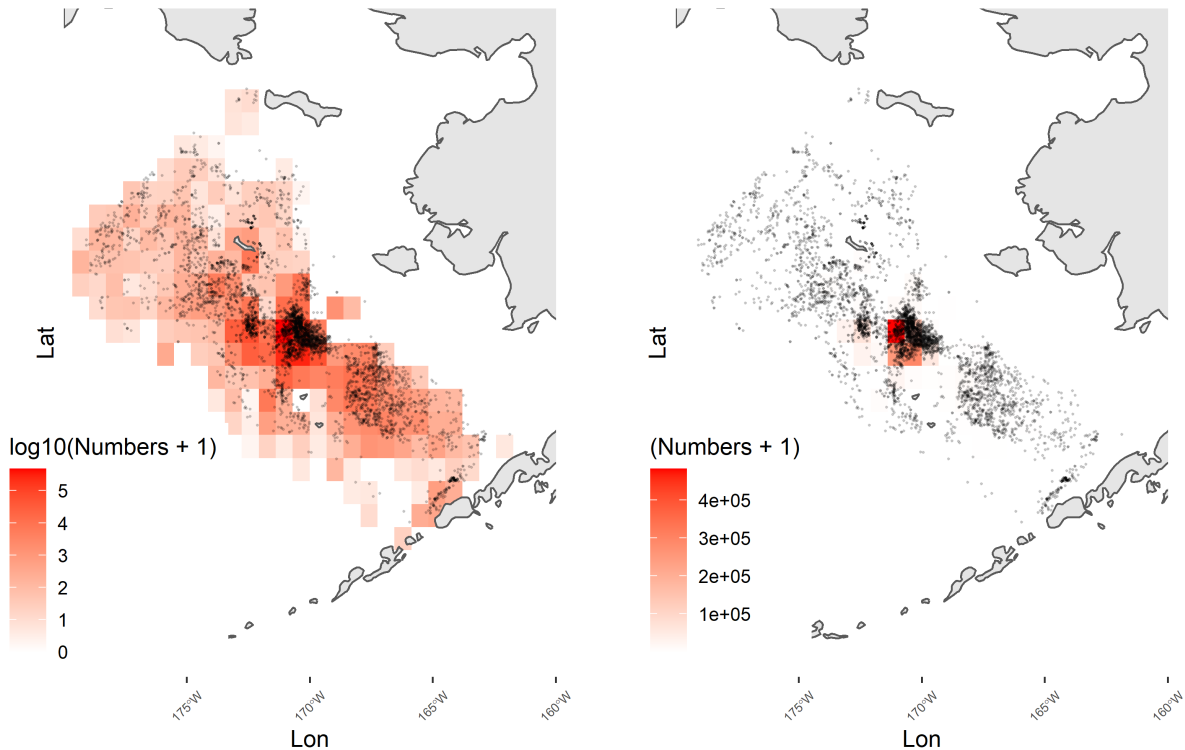


Figure 32: Comparison of location and intensity of bycatch in 2018 for natural and log space.

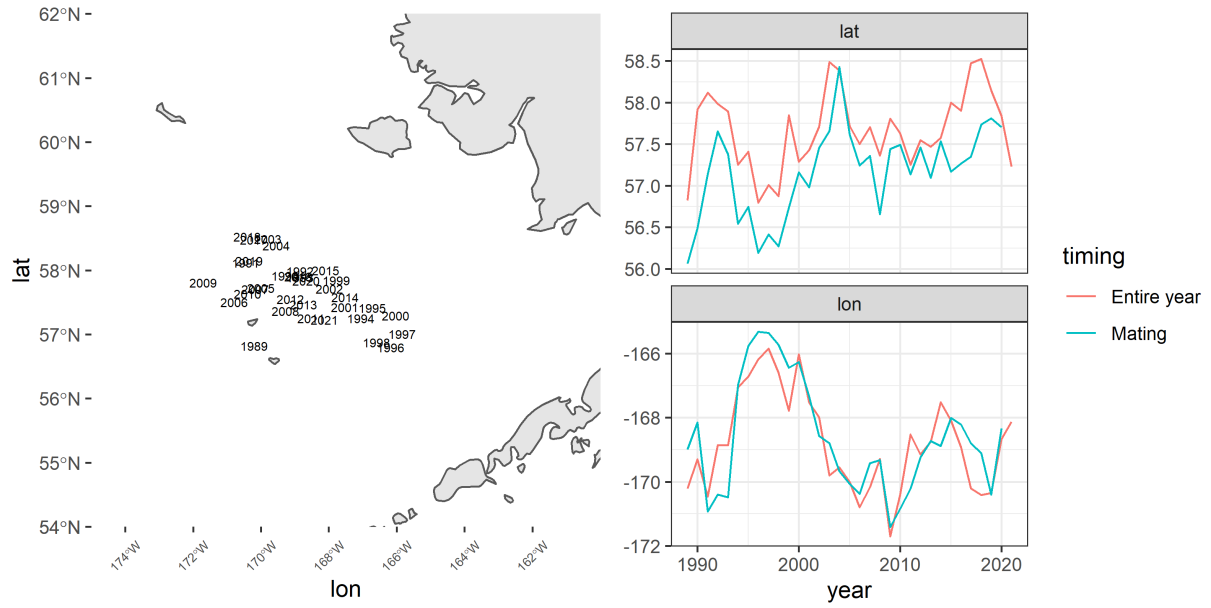


Figure 33: Centroids of bycatch over time calculated over the entire year (left). Centroids broken into time series of latitudinal and longitudinal components calculated over the entire year and during the months December through March which roughly overlap with mating.

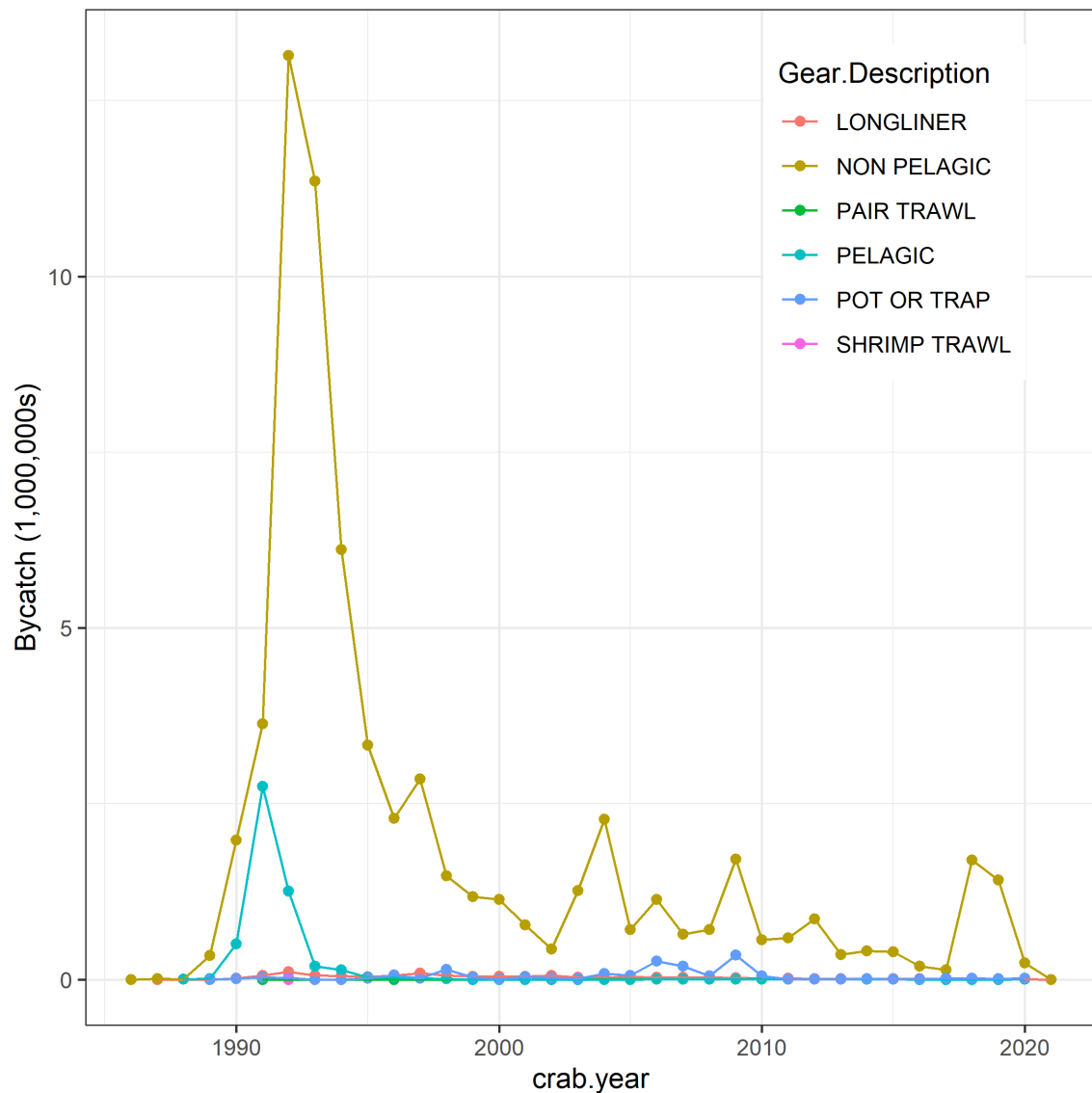


Figure 34: Bycatch in numbers by gear types reported from NMFS observer programs.

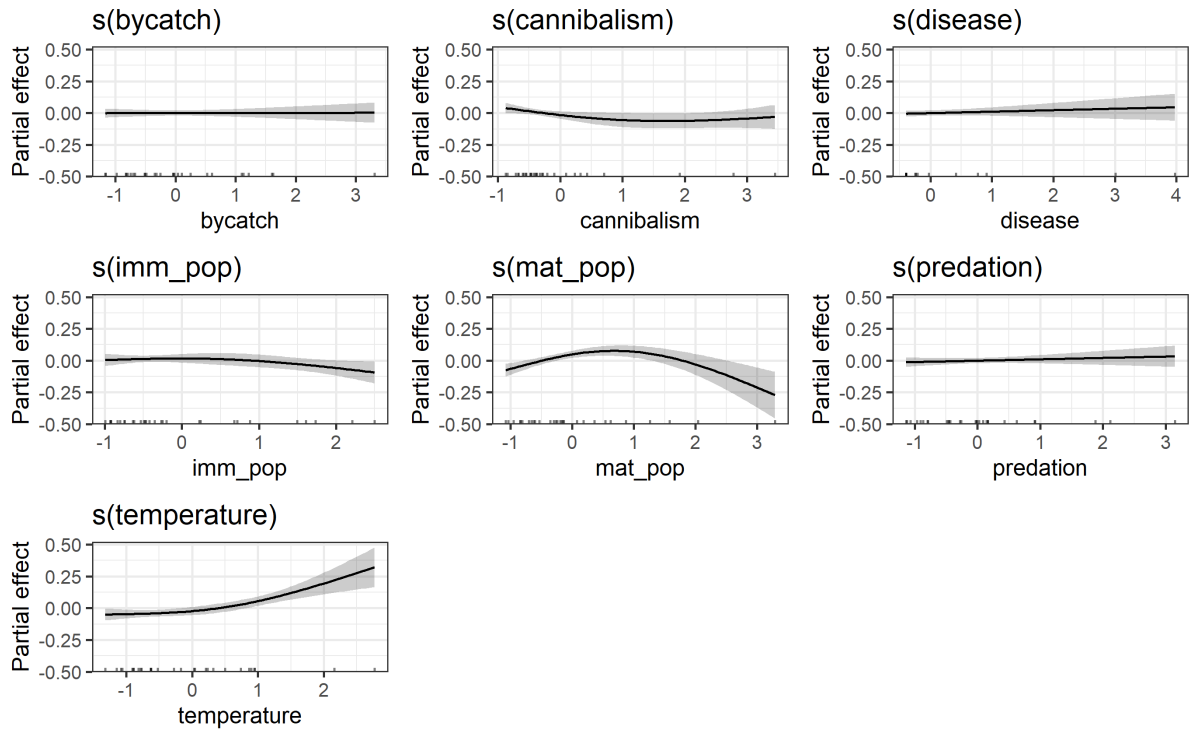


Figure 35: Smooths resulting from the full model estimating the relationship between environmental covariates and immature mortality.

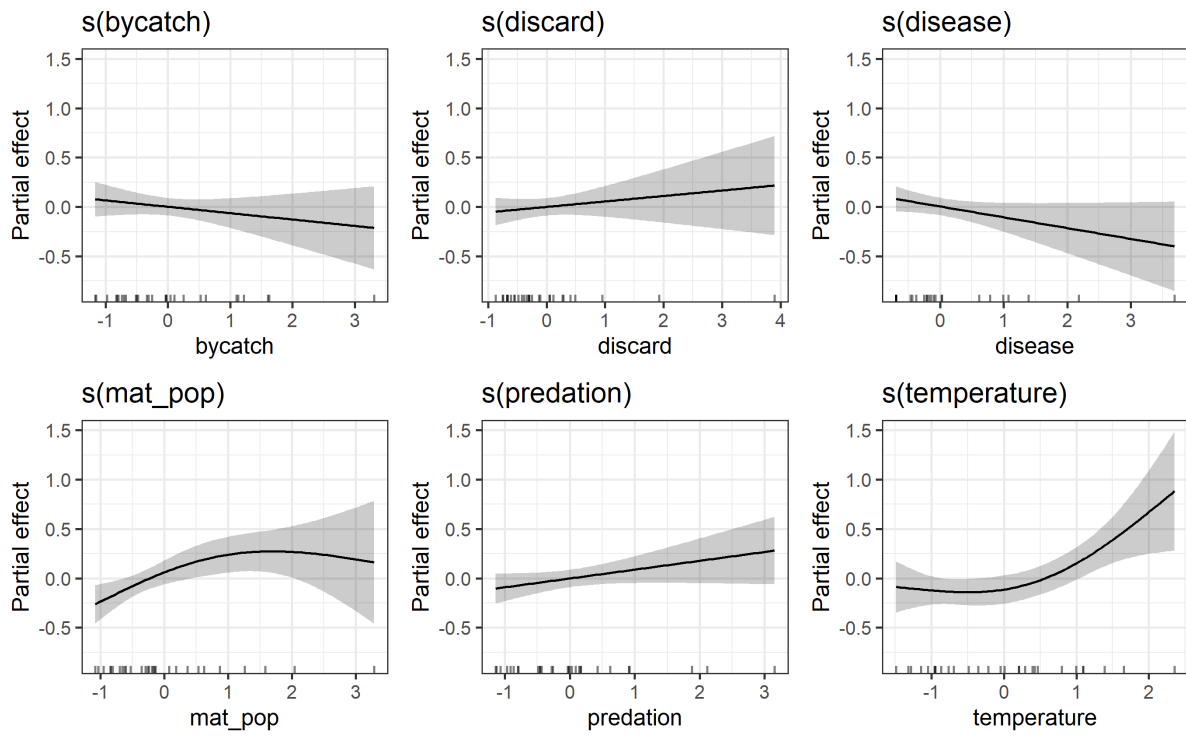


Figure 36: Smooths resulting from the full model estimating the relationship between environmental covariates and mature mortality.

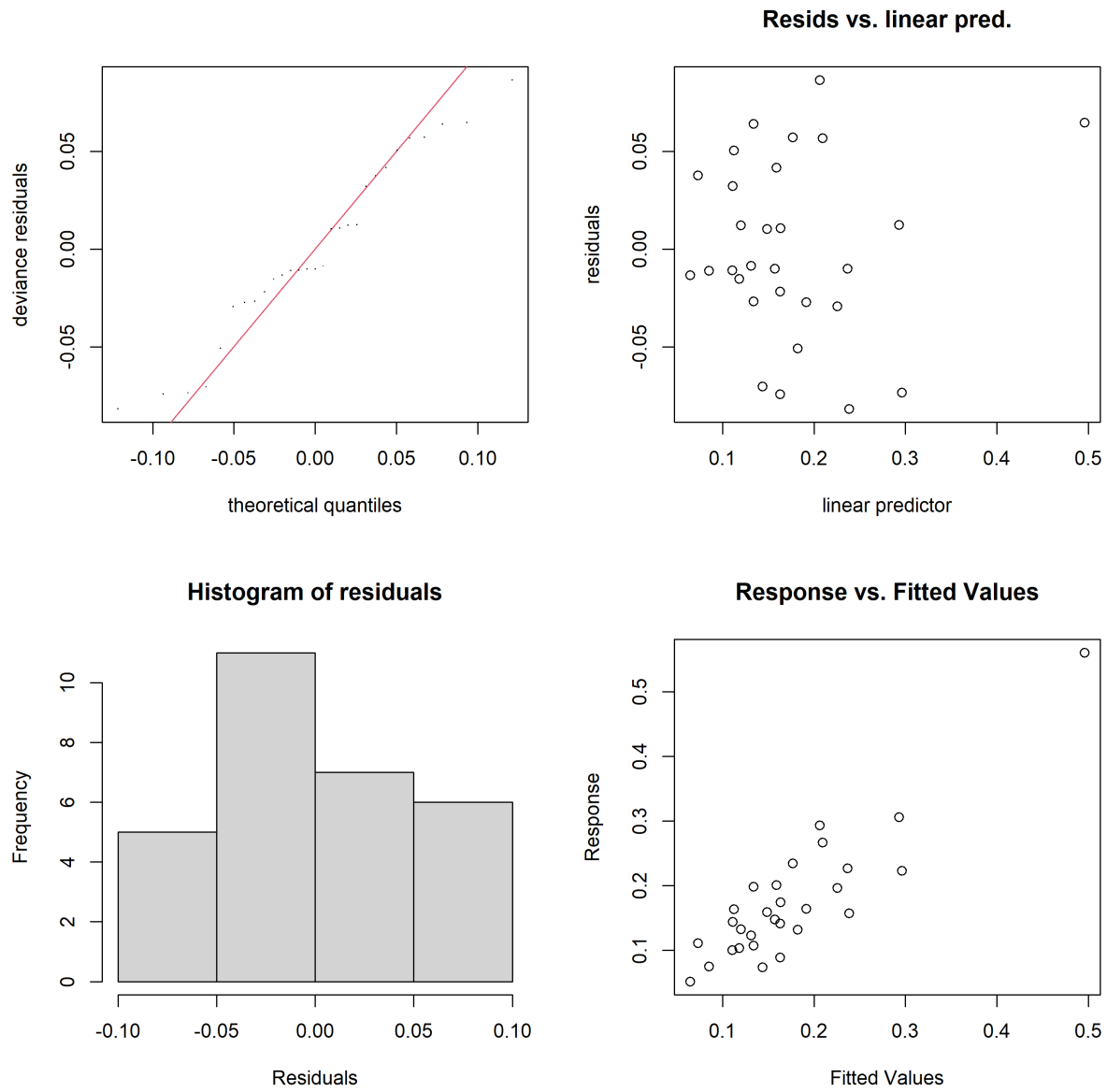


Figure 37: Diagnostic plots for the full model relating immature mortality and environmental stressors.

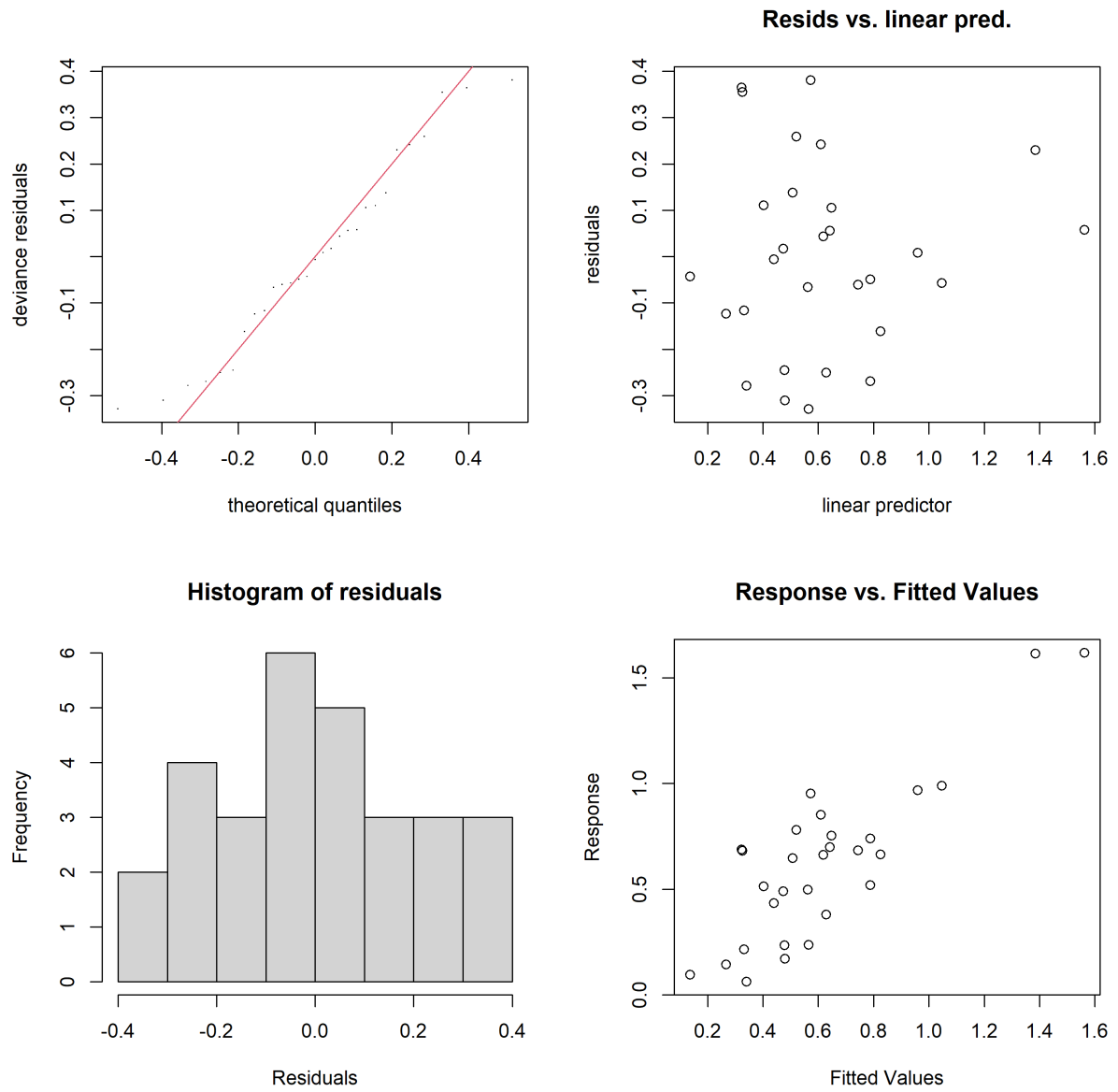


Figure 38: Diagnostic plots for the full model relating mature mortality and environmental stressors

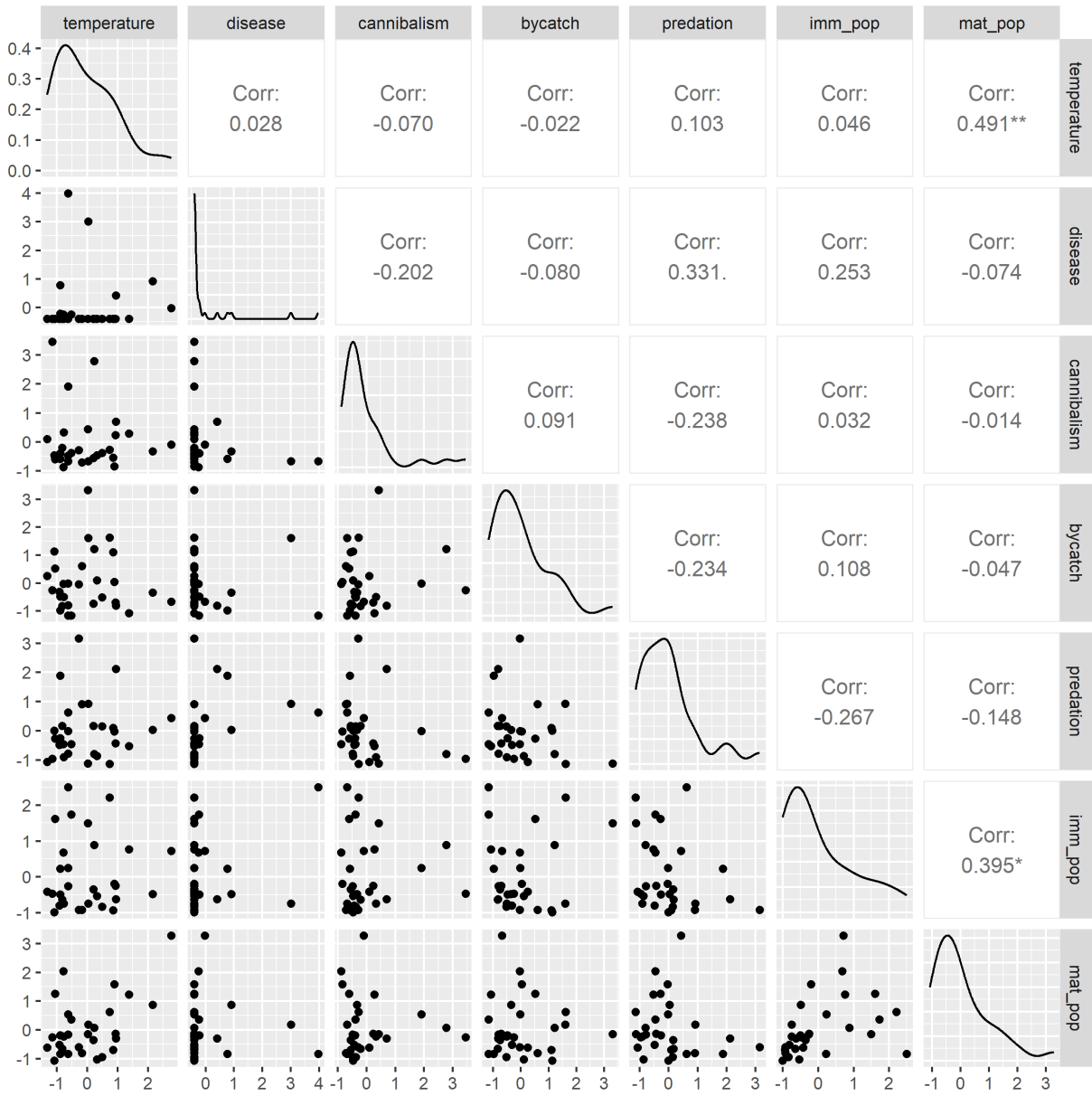


Figure 39: Pairs plots displaying the correlation between covariates for immature crab. Diagonal represents the distribution of a given variable.

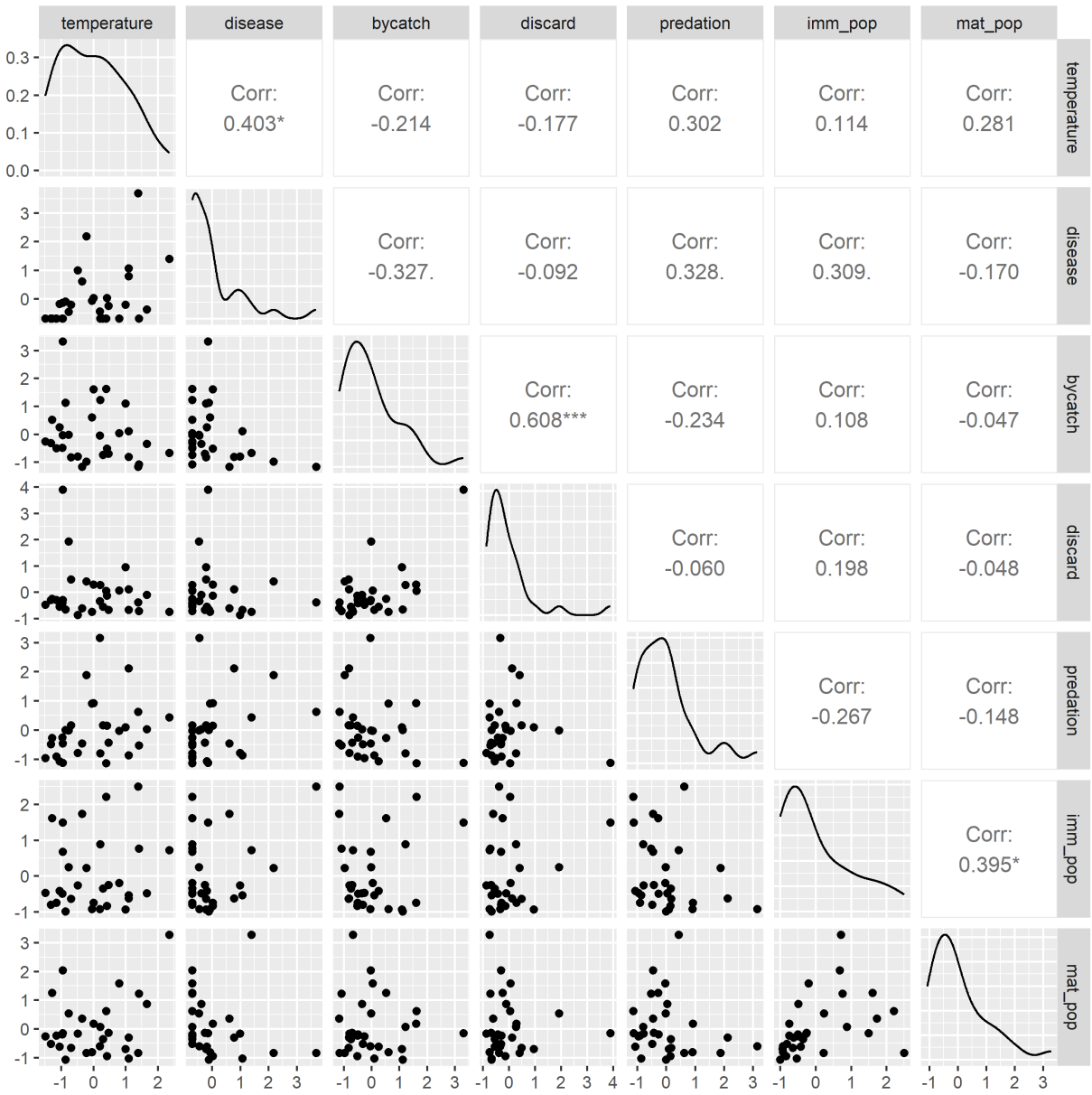


Figure 40: Pairs plots displaying the correlation between covariates for mature crab. Diagonal represents the distribution of a given variable.

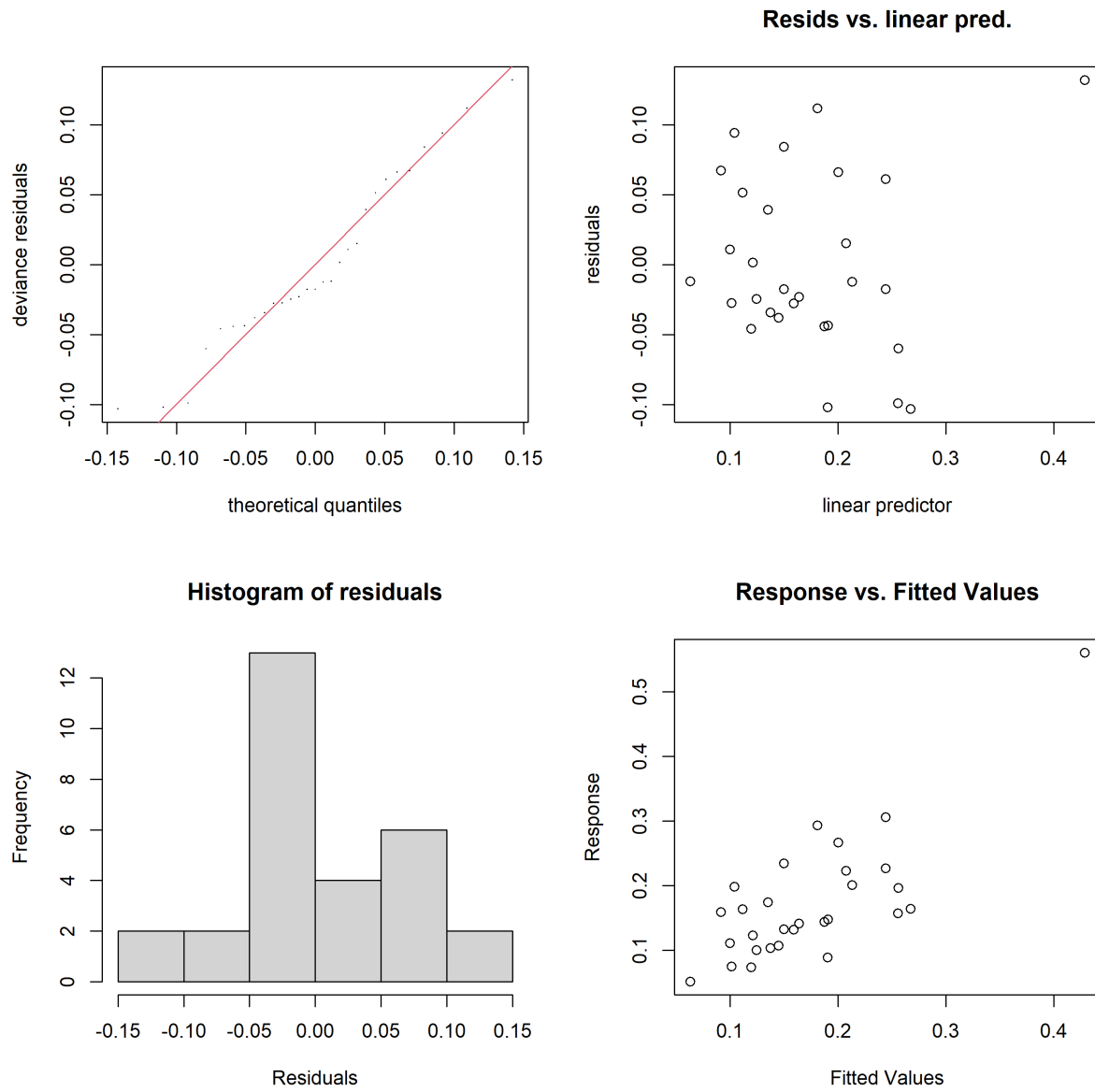


Figure 41: Diagnostic plots for the trimmed model relating immature mortality and environmental stressors.

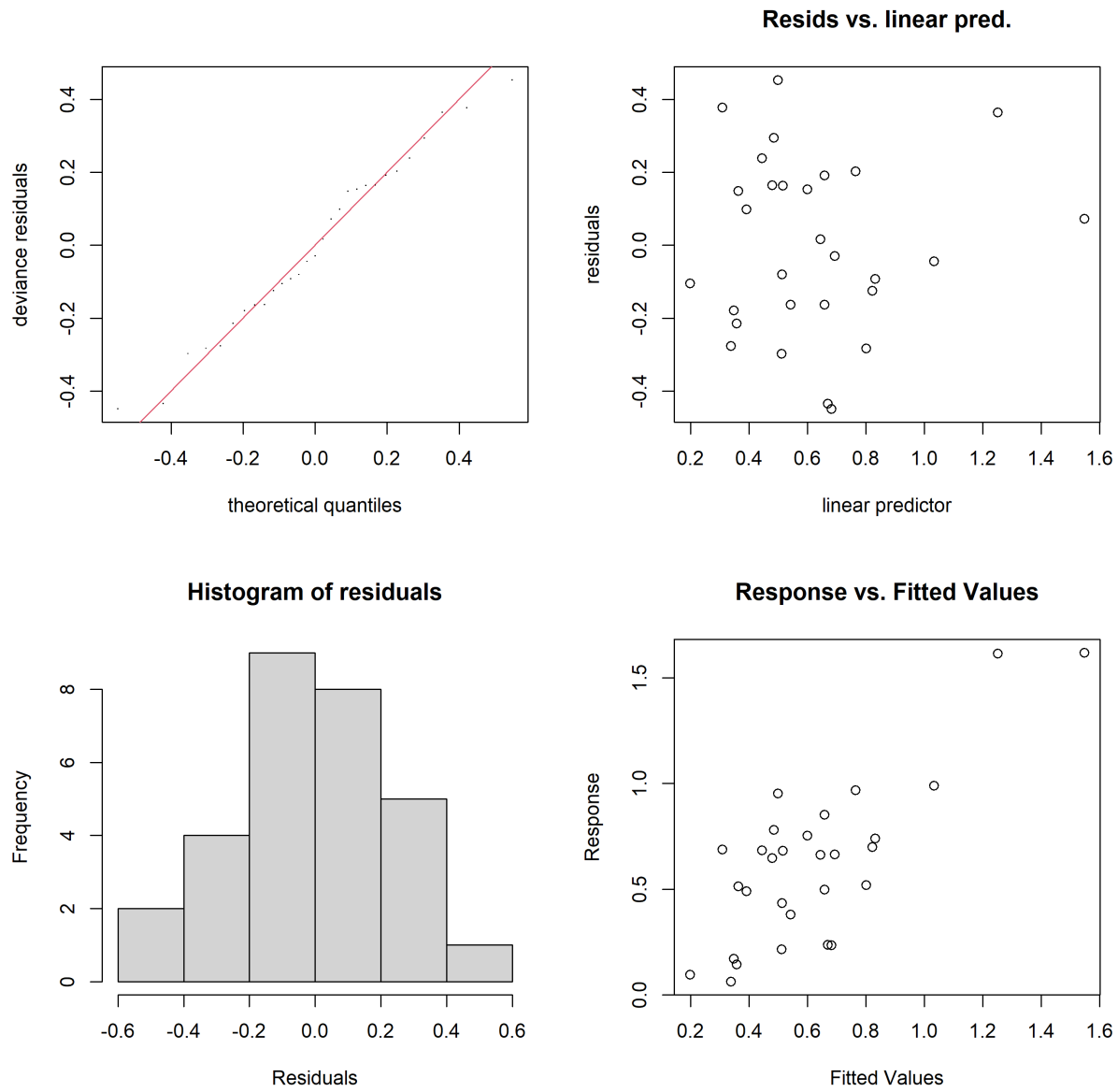


Figure 42: Diagnostic plots for the trimmed model relating mature mortality and environmental stressors.

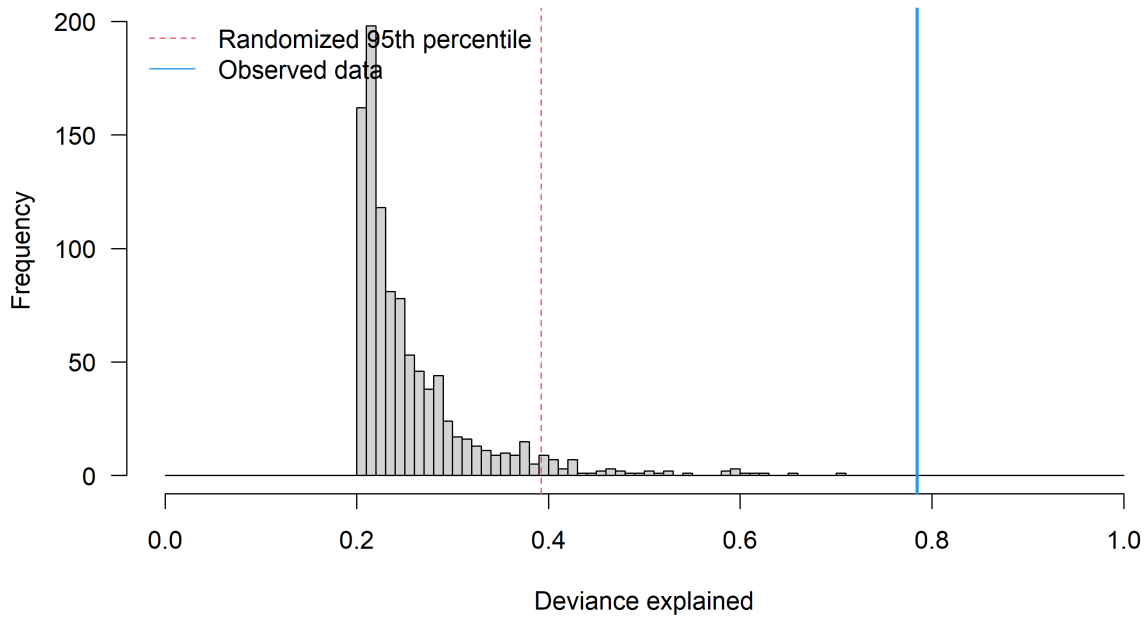


Figure 43: Results of randomization trials for the trimmed model relating estimated immature mortality to environmental stressors. Grey bars represent the number of trials in which the randomized model explained the deviance on the x-axis. Dashed vertical red line represents the 95th quantile of the deviance explained by the randomized trials. Blue line represents the deviance explained with the real data.

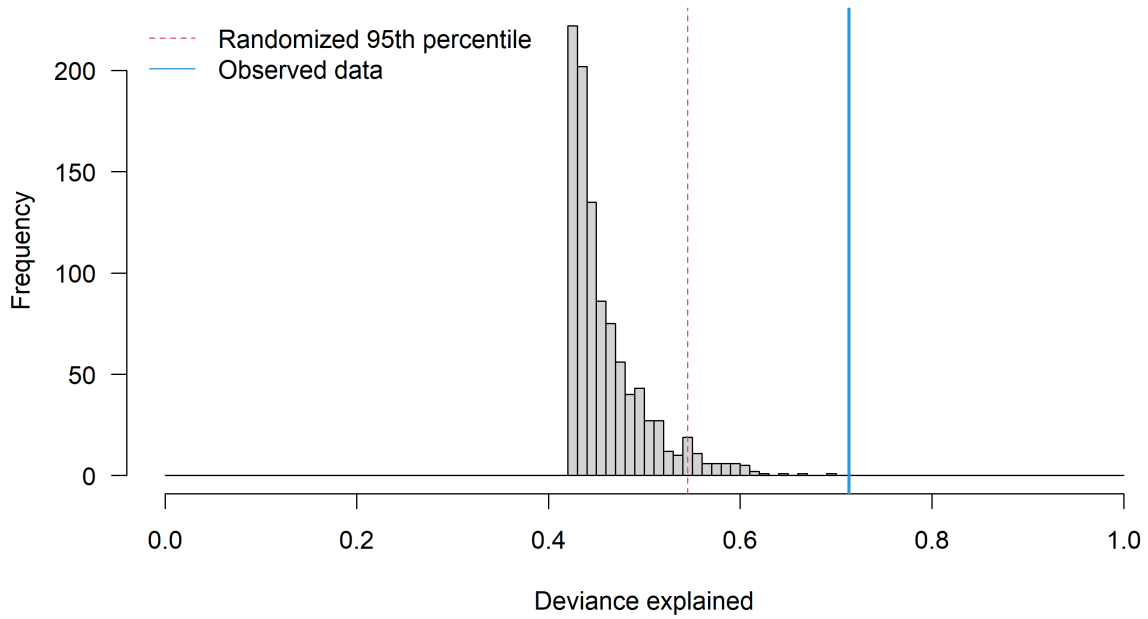


Figure 44: Results of randomization trials for the trimmed models relating estimated immature mortality to environmental stressors. Grey bars represent the number of trials in which the randomized model explained the deviance on the x-axis. Dashed vertical red line represents the 95th quantile of the deviance explained by the randomized trials. Blue line represents the deviance explained with the real data.

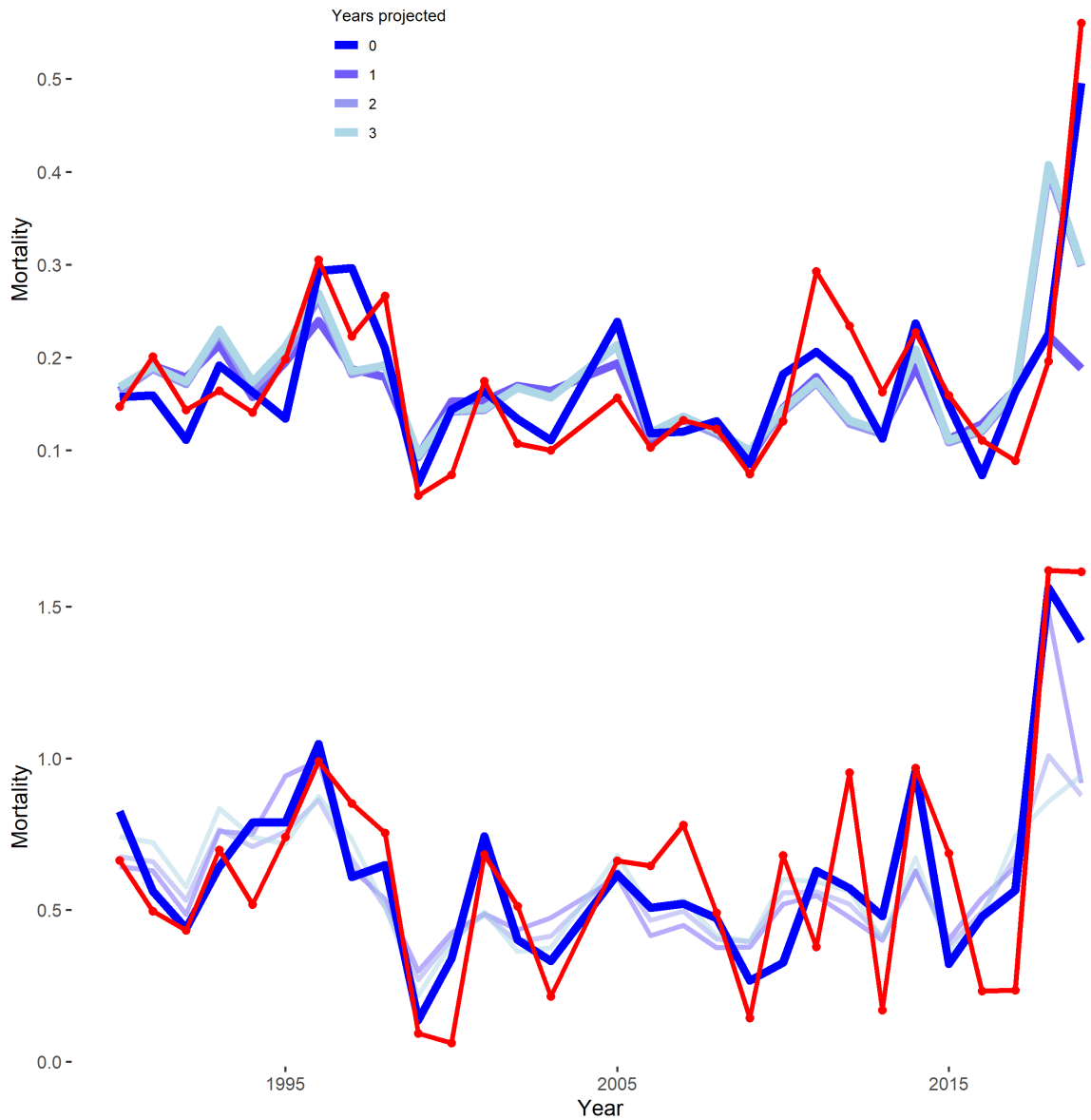


Figure 45: Predictive skill of the GAMs for immature and mature mortality. Reproduced from figure 2 in the main text to provide better detail.

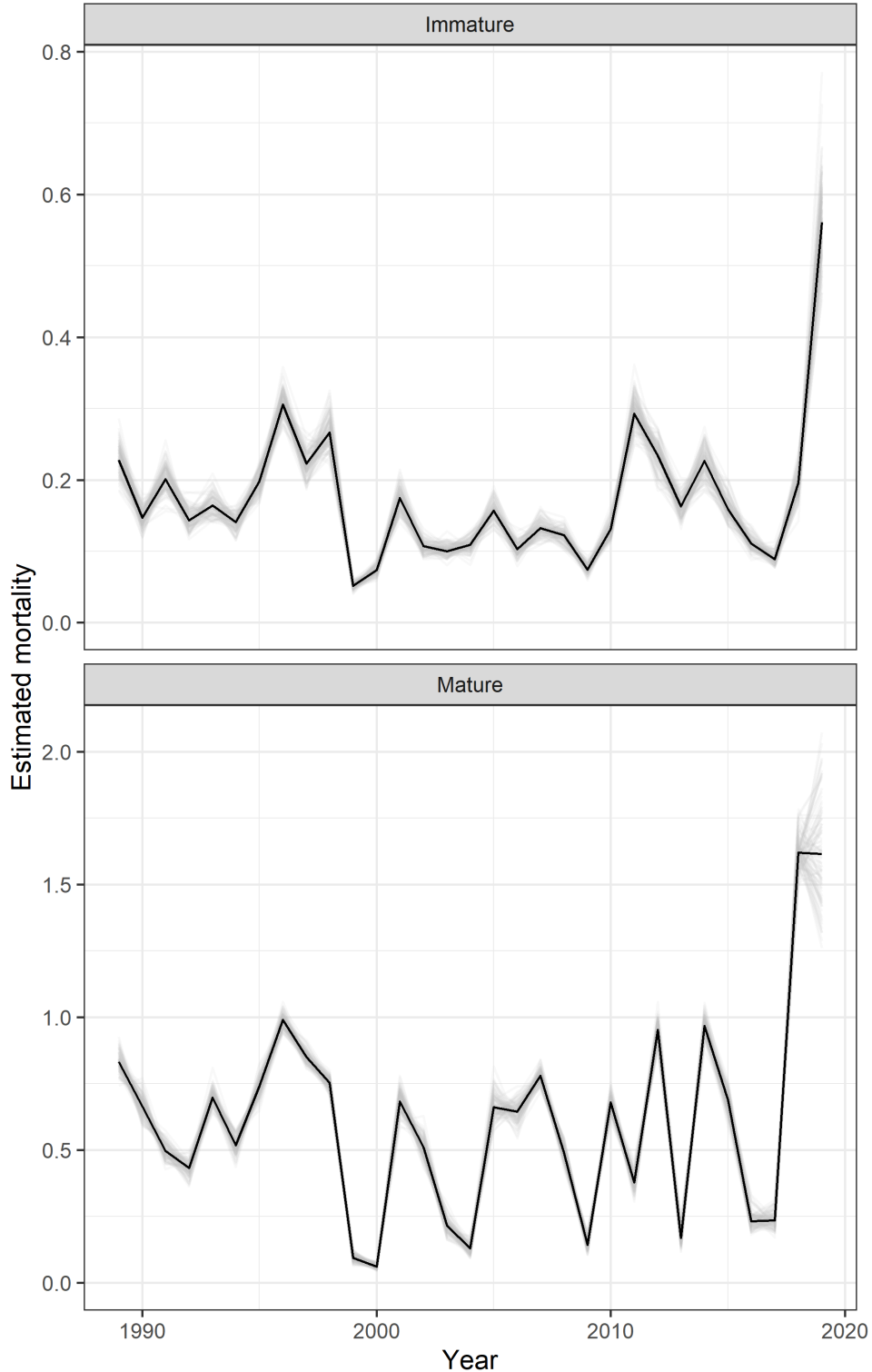


Figure 46: Simulated time series of estimated immature and mature mortality that incorporate the uncertainty associated with the fitting process of the population dynamics model. Each grey line represents one iteration of multiplying the maximum likelihood estimates of the mortality deviations by the covariance matrix. The black line represents the MLE.

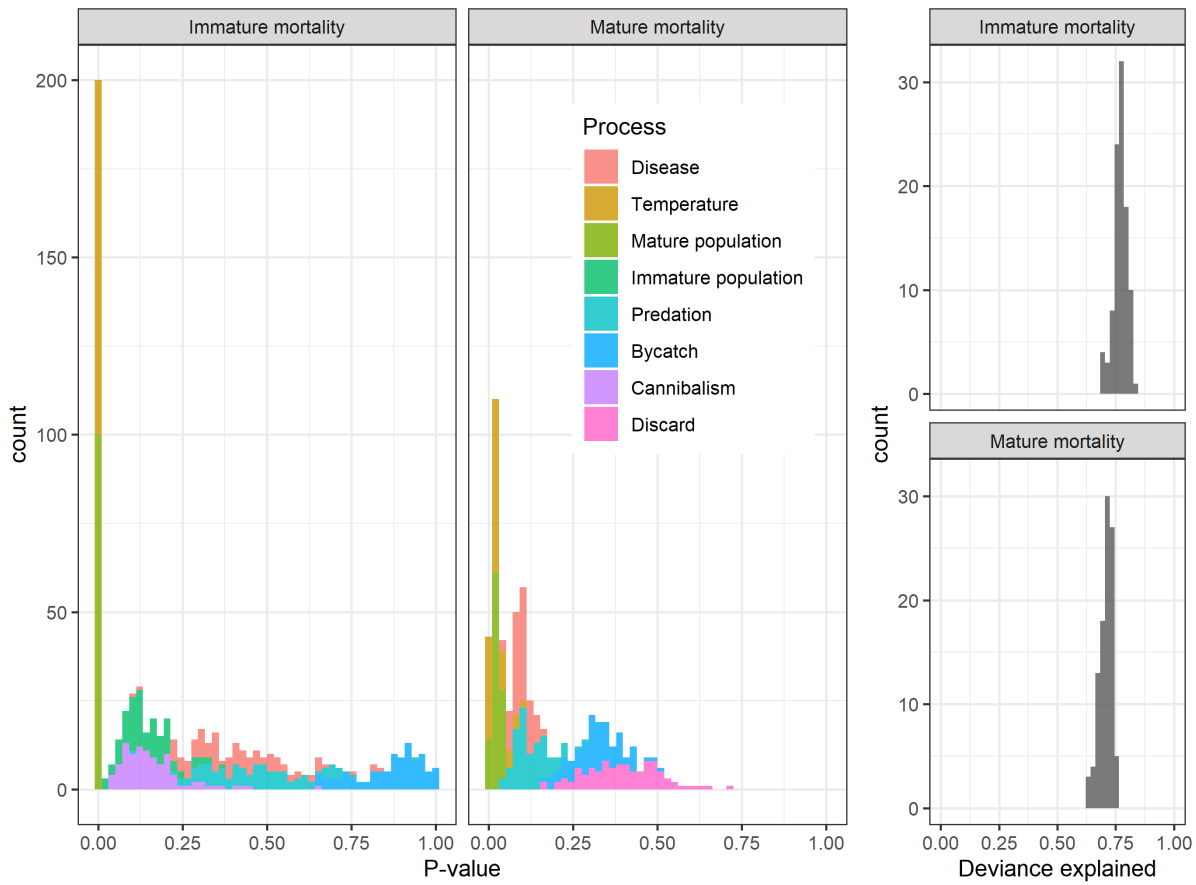


Figure 47: P-values associated with iterations of fitting the GAMs to simulated time series of estimated immature and mature mortality using the covariance matrices estimated in the fitting of the population dynamics model.

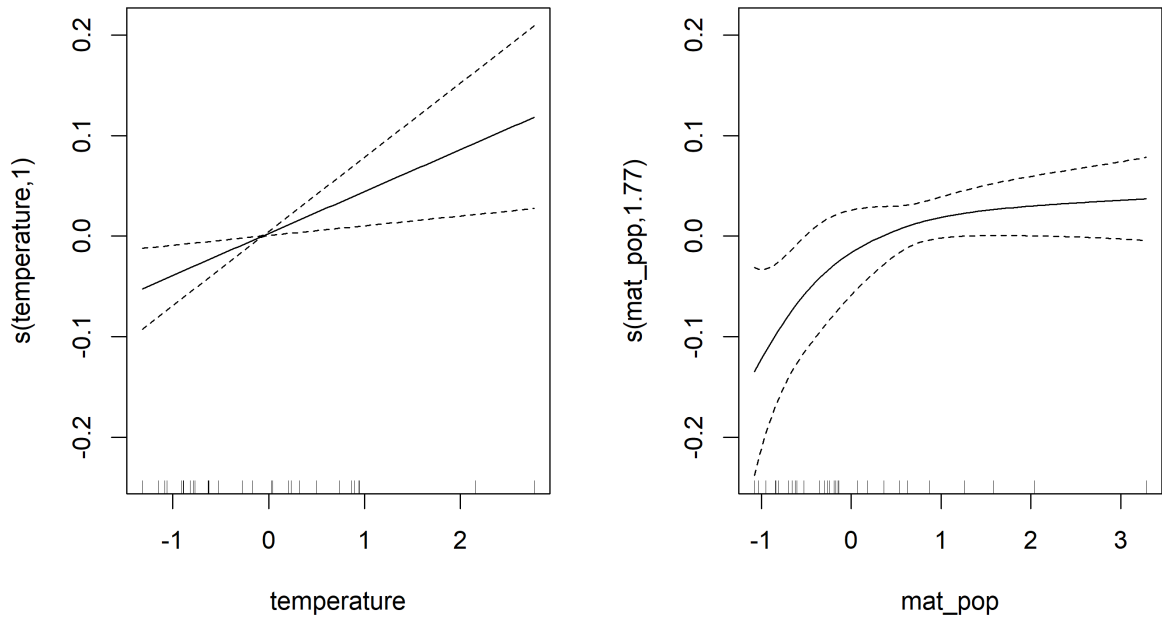


Figure 48: Estimated smooths between immature mortality and temperature occupied and mature population from shape constrained additive models.

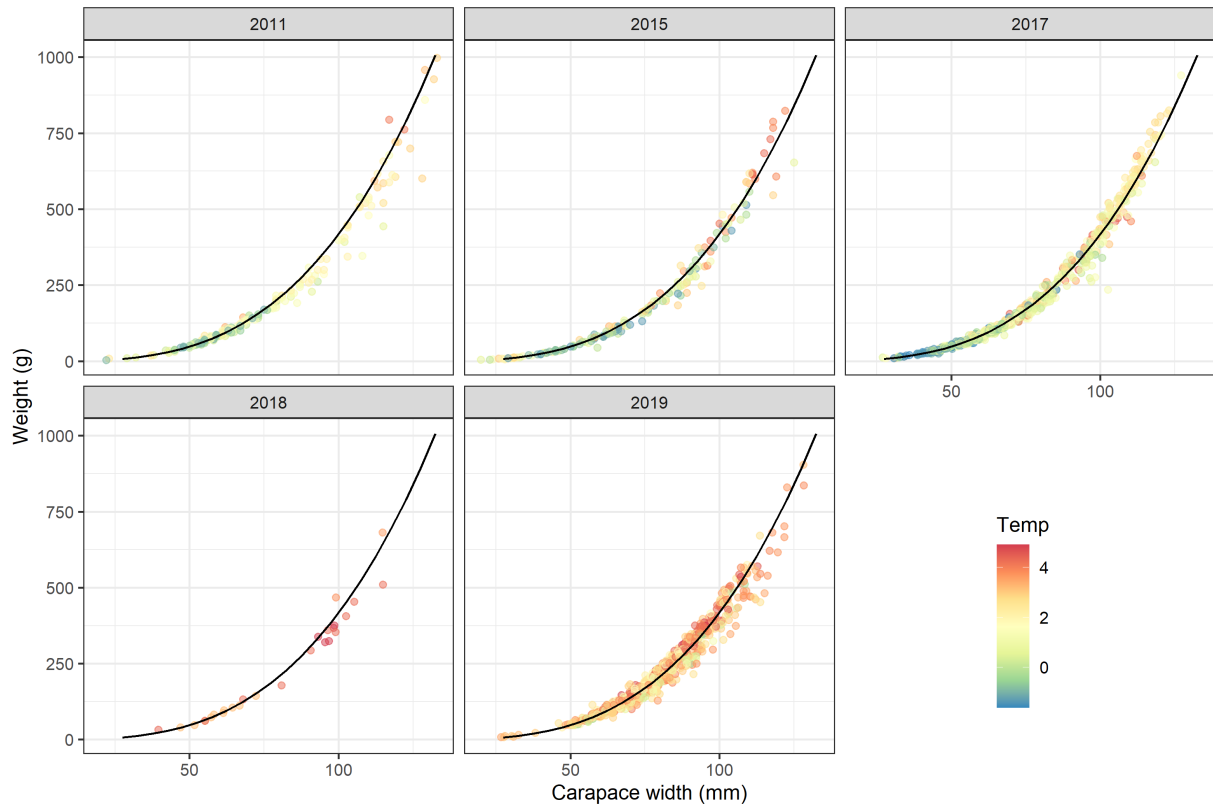


Figure 49: Observed weight at size over time colored by temperature (Celcius) at which the crab was collected.

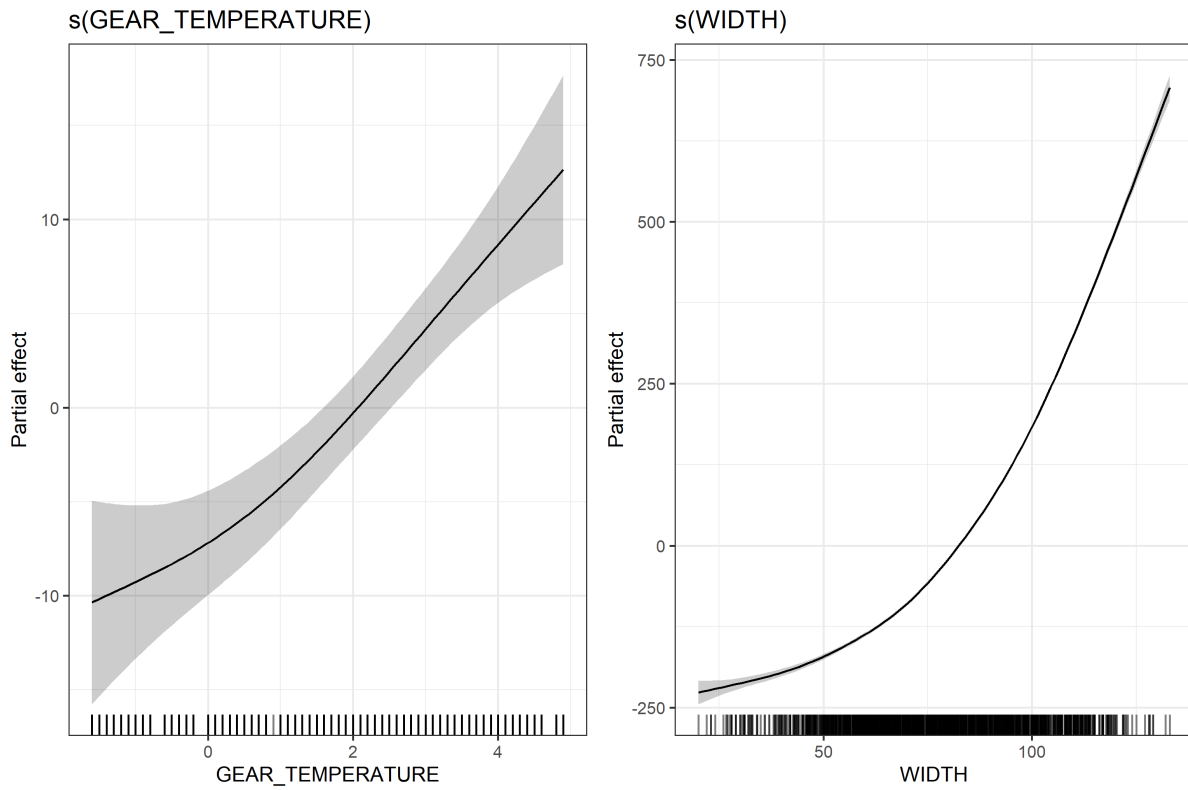


Figure 50: GAM estimated relationships between temperature and carapace width on observed weights of crab.

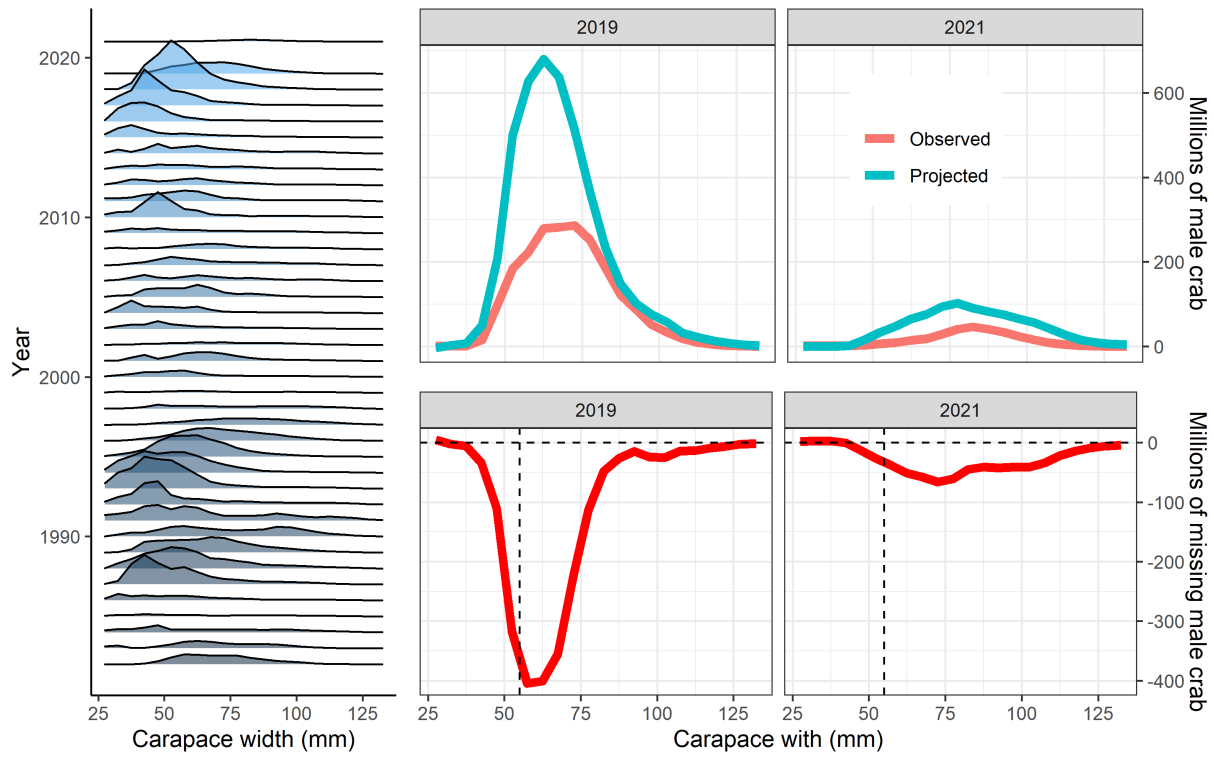


Figure 51: Numbers at size over time of snow crab (left). Observed numbers of crab (red line) in 2019 and 2021 vs. projected numbers of crab from 2018 and 2019 given a mortality equal to 0.27 (the assumed value in the assessment; top left). Numbers of missing crab at size (red line) with the size of crab beneath which cod predate upon (dashed vertical black line).